Study of the exposure of a population to a wireless communication network via dosimetric tools and statistic

Yuanyuan Huang

IMT Atlantique
Bretagne-Pays de la Loire
École Mines-Télécom

UNIVERSITE BRETAGNE LOIRE

THÈSE / IMT Atlantique

sous le sceau de l'Université Bretagne Loire

pour obtenir le grade de

DOCTEUR D'IMT Atlantique

Mention : Sciences et Technologies de l'Information et de la Communication

École Doctorale Sicma

Présentée par

Yuanyuan Huang

Préparée au département Micro-ondes

Laboratoire Labsticc

Étude de l'exposition d'une population à un réseau de communication sans fil via les outils de dosimétrie et de statistique

Thèse soutenue le 13 mars 2017

devant le jury composé de :

Cédric Quendo
Professeur, Université de Bretagne Occidentale / Président

Martine Lienard
Professeur, Université de Lille / Rapporteur

Philippe De Doncker
Professeur, Université Libre de Bruxelles / Rapporteur

Emmanuelle Conil
Ingénieur, Agence Nationale des Fréquences / Examinatrice

Joe Wiart
Directeur d'études, Télécom ParisTech - C2M / ERxaminateur

Christian Person
Professeur, IMT Atlantique / Directeur de thèse

Nadège Varsier Favre
Ingénieur R&D, Orange Labs / Invitée

Acknowledgements

First and foremost, I would like to address my special thanks to Professor Dr. Christian Person, my supervisor from IMT Atlantique Bretagne- Pays de la Loire, for his support and encouragements during these three years. Your advice on both research as well as on my career have been priceless for me and definitively helped me to become a research scientist.

I would like to thank Dr. Joe Wiart for his patience, support, supervision and for providing me the opportunity to work in Orange Labs. Without his help, I would not have been able to complete my thesis.

I would especially like to thank Dr. Nadège Varsier. She has always been willing to help me. The discussions with her really inspired and motivated me towards the end of my Ph.D.

My Ph.D would not have been perfect if I did not receive the support and encouragements from people I have been working with during these 3 years: my dear colleagues from the direction of SRH in Orange Labs, Azeddine Gati, Thierry Sarrebourse, Hamid Hadjem, Mouléro Aniambossou, Fatma Salem, Juilien Voyat, Emmanuelle Conil, Pierric Kersaudy, Anis Krayni. I am also grateful for other colleagues in Orange Labs, Emmanuel de Wailly, Abdoulaye Tall, Zwi Altman, for their kindness to share with me their expertise and for their patience when answering my questions. And also thanks to my colleagues from the Chair C2M of Télécom ParisTech, Yenny, Taghrid, Tarek, Soumaya, Amirreza with whom I spend a wonderful time.

Last but not least, a special thanks to my family for all their love. My dear parents, far away in China, who raised me in a scientific environment and fully supported me in my professional career. And most of all, my loving, encouraging, patient husband, for taking care of me and sharing my happiness and tears.

The journey toward my Ph.D will end but I know that research will never end.

Abstract

This thesis was dedicated to evaluate via dosimetric tools and statistical methods the global exposure of a population to Radio Frequency ElectroMagnetic Fields (EMFs) by taking into account different technologies, usages, environment etc. We analyzed for the first time the average population exposure to third generation network (3G) induced EMFs, from both uplink and downlink radio emissions in different countries, geographical areas, and for different wireless device usages. Results, derived from device usage statistics, show a strong heterogeneity of exposure, both in time and space. Among those results, we show that, contrary to popular belief, exposure to 3G EMFs is dominated by uplink radio emissions, resulting from voice and data traffic, and average population EMF exposure differs from one geographical area to another, as well as from one country to another, due to the different cellular network architectures and variability of mobile usage. Thus the variability and uncertainties linked to these influencing factors were characterized. And a variance-based sensitivity analysis of the global exposure was performed for the purpose of simplifying its evaluation. Finally, a simplified methodology based on advanced statistical tools was proposed to evaluate the day-to-day global LTE induced EMFs exposure of a population taking into account the variability and uncertainties linked to propagation environment, usage, as well as EMFs from personal wireless devices and base stations. Results have highlighted the importance of received power density from base stations to the issue of global exposure induced by a macro LTE network.

Résumé

De nos jours, les équipements de communication sans fil utilisant les radiofréquences (RF) sont utilisés partout et par tous. Comme le montre les études de TNS Sofres [TNS, 2010] la population française utilise de manière massive les moyens de communication sans fils. Plus de 80% des français ont et utilisent un mobile. Des segments tels que celui de plus des 12 ans sont équipés à 100 %. Paradoxalement, si l'utilisation des équipements de communication sans fil est aujourd'hui massive, l'inquiétude du public vis-à-vis des hypothétiques effets sanitaires des ondes RF ne s'est pas atténuée.

Dans la plupart des études caractérisant l'exposition de la population aux champs électromagnétiques (EM) RF, une approche pire cas est souvent adoptée. D'un côté, il existe une grande confusion autour de ces questions et notamment autour de celle liée à la maitrise de l'exposition. L'exposition est souvent perçue comme étant majoritairement induites par les antennes relais. Aujourd'hui de nombreux travaux relatifs à l'exposition ont été menés en «statique» et considèrent séparément l'exposition induite par les mobiles et les stations de bases. On quantifie les niveaux d'exposition en termes de débit d'absorption spécifique maximal aux équipements personnels de communication sans fil et de l'autre les niveaux de champs maximum induits par les stations de base. Cette approche ne permet cependant pas de caractériser l'exposition réelle de la population aux ondes RF.

L'exposition induite par les champs émis par les antennes relais et les mobiles dépend de l'usage (localisation du mobile et type usage – data, voix...), de la «distance» aux points d'accès, de la technologie, des réseaux (e.g., macro cellulaire) et de la gestion de puissance associée (e.g., gestion des handovers en 2G et 3G). La mobilité, la diversité des usages et des technologies font que, pour une personne, l'exposition globale est le résultat de nombreuses configurations qui dépendent des habitudes de cette personne et des capacités offertes par le réseau. L'exposition d'une personne passant du temps dans les transports en commun, travaillant dans une zone dense et habitant en banlieue va recouvrir des configurations différentes de celles rencontrées par une personne habitant une grande ville et ayant la possibilité d'aller travailler à pied.

L'étude de l'exposition d'une population passe donc d'abord par la segmentation des différentes configurations possibles et l'évaluation de l'exposition induite par les réseaux dans ces configurations. De gros efforts ont été menés depuis 20 ans dans les domaines des méthodes numériques pour évaluer l'exposition associée aux ondes EM. Aujourd'hui les progrès des calculateurs, des méthodes numériques, de déformation de structure et les méthodes statistiques permettent d'évaluer l'exposition associée

à ce type de configurations même si des travaux complémentaires sont nécessaires pour bien maitriser les incertitudes associées. L'analyse de l'exposition globale de la population passe ensuite par la pondération de ces différents résultats en fonction des réseaux, des technologies, de la densité de population, de l'urbanisme...

Les travaux réalisés dans cette thèse ont donc été consacrés à construire et valider une nouvelle méthode d'évaluation de l'exposition globale d'une population aux ondes EMF-RF. Cette nouvelle méthode se propose d'explorer les activités journalières des gens dans le but de caractériser l'exposition d'une population, dans une zone géographique donnée, induite par un réseau dans son ensemble, des stations de base aux équipements de communication sans fil, prenant en compte les différentes technologies et les différents usages. Finalement, analyser les paramètres influant pouvant être utilisés pour optimiser l'évaluation de l'exposition globale.

Ces travaux sont complémentaires et en synergie avec le projet FP7 Low Electromagnetic Fields Exposure Network (http://www.lexnet.fr/) dédié à la réduction de l'exposition d'une population induite par les nouveaux réseaux.

Contents

List of Figures

List of Tables

List of Abbreviations

Aeff . . . . . Antenna effective area.
ANOVA . . . . Analysis of Variance.
BTS . . . . . Base station.
CV . . . . . Coefficients of variation.
CDF . . . . . Cumulative Density Function.
EMF . . . . . Electromagnetic Field.
eNB . . . . . E-UTRAN Node B, also known as Evolved Node B.
EI . . . . . Exposure Index.
FDTD . . . . . Finite-Difference Time-Domain.
GSM . . . . . Global System for Mobile Communication.
GEV . . . . . Generalized Extreme Value.
ICNIRP . . . . International Commission on Non-Ionizing Radiation Protection.
ICT . . . . . Information and Communication Technology.
KPI . . . . . Key Performance Indicator.
LTE . . . . . Long Term Evolution.
LEXNET . . . Low Electromagnetic Fields Exposure Network.
LARS . . . . . Least Angle Regression Selection.
LOOCV . . . . Leave-One-Out Cross Validation.
LHS . . . . . Latin Hypercube Sampling.
MRI . . . . . Magnetic Resonance Imaging.
PC . . . . . Polynomial Chaos.
PLE . . . . . Path Loss Exponent.
PDF . . . . . Probability Density Function.
QoS . . . . . Quality of Services.
RF . . . . . Radio Frequency.
RNC . . . . . Radio Network Controller.
SAR . . . . . Specific Absorption Rate.
SAM . . . . . Specific Anthropomorphic Mannequin.
3G . . . . . third generation of mobile telecommunications technology
UMTS . . . . . Universal Mobile Telecommunication System.
UE . . . . . User Equipment.

1 General introduction

Wireless communication technologies, since their introduction, have evolved very quickly and people have been brought in 30 years into a much closer world. Indeed radio signals on the Global System for Mobile Communication (GSM)), Universal Mobile Telecommunication System (UMTS) or Long Term Evolution (LTE) networks are covering our homes, offices, or means of transport. In parallel people are more and more exposed to radiofrequency (RF) electromagnetic fields (EMF). As a consequence, people's attentions around **health risks of exposure to RF EMFs** have grown just as much as their usages of wireless communication technologies.

Exposure characterization to RF EMFs is not a new research domain. Great efforts have been carried out to find the evidence of adverse health effects from the exposure to RF EMFs in recent decades. While according to the World Health Organization, there was no convincing evidence that exposure to RF EMFs shortens the life span of humans. The International Agency for Research on Cancer concluded in 2011 that RF EMFs are possibly carcinogenic to humans [WHO, 2011].

Among the public, there still exists great confusion around the issue of RF EMF exposure. An in-depth survey about the perceived sources of daily RF EMFs exposure has been conducted from April to June 2013 in France, Germany, Portugal, Spain, Romania, Montenegro and Serbia [Freudenstein et al., 2014]. **Results indicated that the public is more concerned about Base station (BTS) than other RF EMF sources (e.g., wireless devices)** as one can see the BTS are high-powered RF transceivers that transmit all day long. In contrast, mobile handsets are low-powered RF transmitters, e.g., in busy mode, a GSM mobile phone emits about 20-50 % of its maximum transmission power (2 W) [Wiart et al., 2000] and a UMTS mobile phone emits a few percent of its maximum transmission power (0.25 W) [Gati et al., 2009]. But as a matter of fact, the value of peak power density radiated by BTS (or access points) is highly dependent on the distance [Kamo et al., 2011]. The study of Thuróczy et al. [Thuróczy et al., 2010] gives an overview of measurement performed in European sites. They have shown that more than 60 % of measured total EMF exposure values were below 0.003 W/m^2, less than 1 % above 0.095 W/m^2 and only less than 0.1 % were above 1 W/m^2 which are all below the recommended exposure limit range (4 – 10 W/m^2) for the public. On the contrary the exposure due to mobile phones should not be underestimated since personal wireless devices are used very close to the human body. In Joseph et al. [Joseph et al., 2010] they have thus shown that the highest RF-EMF exposure might be measured in transport vehicles (i.e. train, car or bus), due to radiation from mobile phones.

The issue of exposure to RF EMFs induced by BTS (downlink) or by mobile devices (uplink) is not a new problematic but attention should be paid here when dealing with **real exposure assessment issue**. The uplink and downlink exposures should not be considered separately. A strong link between the power transmitted by wireless devices and the power received from BTS was observed on the operating wireless network [Gati et al., 2010]. Furthermore, the assessment of real EMF exposure of a population is the result of many exposure configurations due to the diversity of technologies, usages, mobility, people's habits as well as other influencing factors. It was therefore a challenge to assess the RF-EMF exposure of a population by considering all the different parameters that may influence it.

In fact, influencing parameters taken into account in the assessment of the day-to-day EMF exposure are highly variable over time and space.

Thus communication traffics generated by wireless devices are unbalanced among users. Emitted and received powers as well as data rates depend on the load of wireless networks, cellular network architectures as well as usages of devices for voice or data services and plenty of other parameters. Hence, by solving the challenge of how to manage and characterize the uncertainties associated with these influencing parameters, the variability linked to the global EMF exposure could be for the first time assessed. Furthermore, through the approach of uncertainty propagation and sensitivity analysis, the influence of random influencing parameters on the model's output which is the global EMF exposure could be also assessed.

The work carried out in this thesis was therefore dedicated to evaluate via dosimetric tools and statistical methods the global exposure of a population to RF-EMF by taking into account different technologies, usages, environments, etc., considering both uplink and downlink radio emissions. The thesis also involved setting up a new exposure metric that would explore the daily activities and usages of people in order to assess their average EMF exposure induced by a wireless communication network as a whole.

The study performed in the framework of this thesis has partially contributed to the European Seventh Framework Program (FP7) Low Electromagnetic Fields Exposure Network (LEXNET) project (http://www.lexnet.fr/). In 2013, the European Union has specifically expressed the need for low-EMF technologies in FP7, by designating low-EMF system designs as a target outcome. This target was specifying the need for new network topologies and management that would reduce the EMF levels without compromising the user's Quality of Services (QoS). To respond to this need, the LEXNET project has been launched in November 2013. It involved 17 partners from 9 European countries: France, United Kingdom, Spain, Belgium, Germany, Portugal, Romania, Republic of Serbia, and Republic of Montenegro. The main objective was to reduce the exposure of a population induced by the new networks and integrating the issue of exposure to RF-EMF into the heart of the design of wireless networks. The thesis results were specifically used in the work package dedicated to the development of a new RF-EMF exposure metric assessing the global exposure of a population to a network as a whole.

The thesis manuscript is organized as follows:

Chapter 2 introduces the state of the art on existing RF-EMF exposure metrics as well as assessing methods currently used to quantify the human exposure induced by RF EMFs, that is to say, three frequently used exposure metrics dedicated to different exposure conditions and one newly developed metric.

Chapter 3 presents the first thorough study of average population exposure to third generation of mobile telecommunications technology (3G)-induced EMFs, from both uplink and downlink radio emissions in different countries, geographical areas, and for different wireless device usages. First the collected sets of mobile usage data in France and Serbia are introduced and the results of a statistical analysis performed for each set of data to characterize and quantify the differences among mobile device usages are presented. Then different scenarios of macro 3G networks are implemented finally leading to the RF-EMF exposure to 3G networks assessment using device usage statistical data and through the LEXNET approach and metric.

Chapter 4 is dedicated to the variance-based sensitivity analysis of the complex exposure metric, called Exposure Index (EI), developed within the European project LEXNET. To this end, the variability and uncertainties linked to the response

of the system (EI in our case) with multiple random variables (influencing input parameters on EI) were determined, the variability of input parameters being characterized through statistical methods. These statistical methods dedicated to uncertainty propagation and sensitivity analysis are presented in the first place and the main findings and conclusion are given at the end.

Chapter 5 presents finally a simplified methodology based on advanced statistical tools to evaluate the day-to-day global EM field exposure of a population taking into account the variability and uncertainties linked to the propagation environment, information and communication technology usage data, as well as EM fields from personal wireless devices and base stations. A sensitivity analysis was carried out in order to assess the influence of these parameters on EM field exposure.

2

EMF exposure metric

Contents

2.1 Context

RF electromagnetic environment has significantly changed over the last decade. New wireless technologies are exposing us to new RF electromagnetic radiations (Fig. 2.1). Wireless communications play a significant role in people's everyday lives and the extremely rapid technological evolution results in phenomenal changes in the usage of wireless devices.

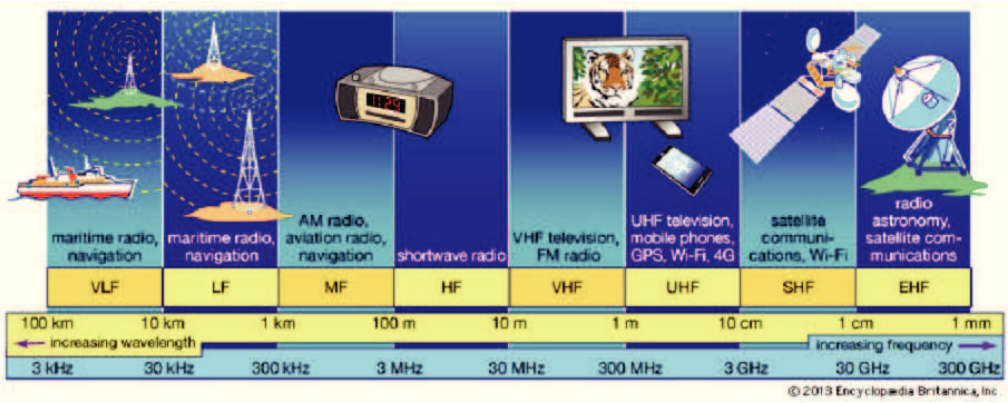

Figure 2.1: Commercially exploited bands of the RF spectrum.

On one hand, new devices and new generations of wireless networks have made many new applications popular. These applications (mainly supported by smartphones) are consuming more and more data as illustrated in Figure 2.2. On the other hand, the number of mobile subscribers increased significantly during the last years. According to a survey carried out in France [TNS, 2010], 82% of those over 12 years old reported using a mobile phone (Fig. 2.3). But paradoxically, along with expansions both in terms of mobile technologies and subscribers, the public concern around EMF health risk has grown just as much.

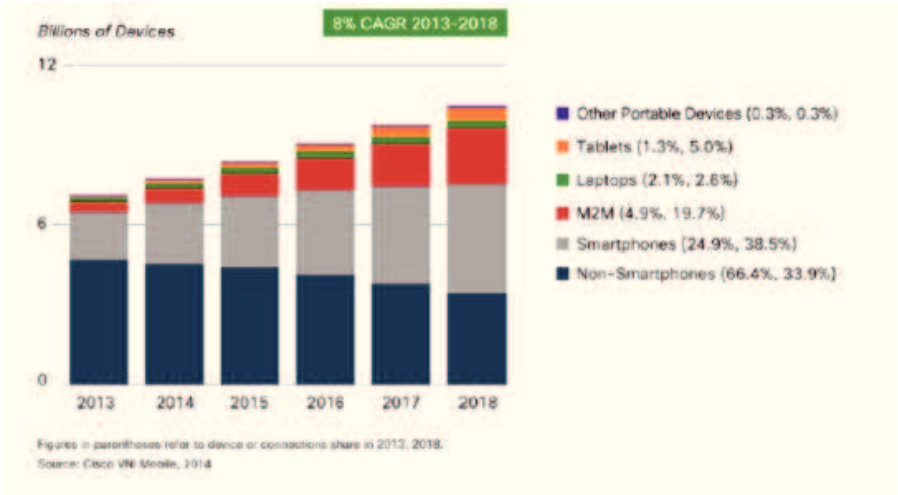

Figure 2.2: Global mobile data per month traffic forecast by type of device. Source: Cisco VPN Mobile Forecast 2014

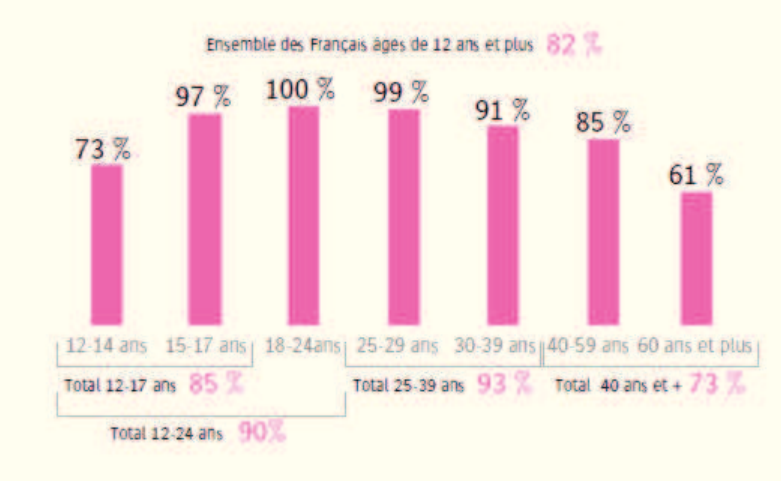

Figure 2.3: Mobile owners (personal or professional)

Facing public's risk perception about possible health effects of RF EMFs, it has become necessary to characterize the human exposure to RF EMFs. To assess RF EMF exposure different approaches are available. Compliance testing and safety standards such as International Commission on Non-Ionizing Radiation Protection (ICNIRP) 1998 [Guideline, 1998], IEEE C95.1 1991 [IEEE Standards Coordinating Committee 28, 19 and Federal Communications Commission 2001 [FCC, 2001] are based on worst-case exposure assessment while epidemiological studies will emphasize the realistic exposure assessment. **The human RF EMF exposure can be characterized using different quantities**. As a matter of fact, the nature of the field and the characteristics of the source (e.g., frequency, intensity, duration of exposure, etc.) differ considerably resulting in a wide variety of quantities which might be used as exposure metrics, for instance:

- Electric field (E) is a vector quantity defined as the electric force per unit charge expressed by volts per meter (V/m).
- Magnetic field (H) is a vector quantity, which, together with the magnetic flux density, specifies a magnetic field at any point in space expressed by amperes per meter (A/m).
- Power density (S) is the appropriate quantity used for very high frequencies, where the depth of penetration in the body is low. It is the radiant incident power perpendicular to a surface, divided by the area of the surface (W/m^2).
- Specific energy Absorption (SA) is the energy absorbed per unit mass of biological tissue expressed in joules per kilogram (J/kg). It is accepted to measure non-thermal effects from pulsed microwave radiation.
- Specific Absorption Rate (SAR) is the rate at which energy is absorbed per unit mass of body tissue and is expressed in watts per kilogram (W/kg).

Among these quantities, **electric, magnetic fields, power density and SAR have been commonly adopted as exposure metrics**. However, different exposure conditions can be present, such as individual- or multiple sources, near- or far-field and short- or long-term exposure. Thus the existing exposure metrics can be classified as follows:

- **Incident field metrics** in terms of power density, electric and magnetic fields.
- **Absorption metrics**, assessing the rate of RF energy absorption in the human body in terms of SAR.
- **Dose metrics** which are the combination of the field or absorption metric and the exposure duration.

In the following sections, these three exposure metrics are respectively presented.

2.2 Incident field metrics

As an electromagnetic wave travels through space, its energy is transferred from the source to receivers. The rate of energy transfer per unit area is expressed as the product of the electric field strength and the magnetic field strength (Equation 2.1).

$$\boldsymbol{S} = \boldsymbol{E} \times \boldsymbol{H} \tag{2.1}$$

where $\boldsymbol{S}$ is the Poynting vector, $\boldsymbol{E}$ is the electric field vector and $\boldsymbol{H}$ is the magnetic field vector. As a result, the exposure induced by radiation originating from incident EMFs can be determined through power density, electric and magnetic fields.

Specifically, when considering far-field [Rappaport et al., 1996], EMFs can be expressed as follows:

$$S = \frac{E^2}{Z_0} = Z_0 \times H^2 \tag{2.2}$$

with S the power density in watts per meters square (W/m^2), E the root-mean-square (RMS) electric field strength in V/m, H the RMS magnetic field strength in A/m and Z_0 the impedance of free space, equal to 377 *ohms*. Thus in the far field of an antenna, it is sufficient to assess exposure to incident EMFs by the incident electric fields or the power density.

In practice, incident electric fields or the power density can be assessed through numerical investigations or by in-situ measurements.

2.2.1 Numerical simulation assessment

Exposure assessment via the approach of numerical simulations allows extracting detailed information about the field strengths distribution. In this case, **three-dimensional ray-based tools** are often used to predict the field strength distribution in a given area, e.g., indoors [Chaigneaud et al., 2001, Lostanlen and Gougeon, 2007, Lai et al., 2011], urban area [Allegretti et al., 2005, Corre and Lostanlen, 2007, Lai et al., 2012] etc.

Ray-based methods are based on geometrical optics that is widely used in high frequency propagation modeling. When accurate building data base is available, they allow calculating the possible rays between a given transmitter and receivers. Depending on the ways of ray construction techniques, ray-based methods involve ray tracing and ray launching approaches [COST Action, 1999].

- Ray tracing produces (Fig. 2.4) precise rays between a transmitter and a receiver. Therefore, when large receiving locations are considered, the ray tracing approach suffers an exhaustive ray path-finding process which leads to large computation time and processing power.

- Ray launching (Fig. 2.5) involves a number of rays launched from the source in all relevant directions. Each ray is traced until it arrives to the receiving location. Finally field strength is summed up at each of the receiving locations. Therefore its computation time is independent of the number of prediction locations. To improve the prediction accuracy, a large set of rays has to be launched, whereas the computation time will increase. This approach was adopted in the thesis for the purpose of modeling the RF waves propagation.

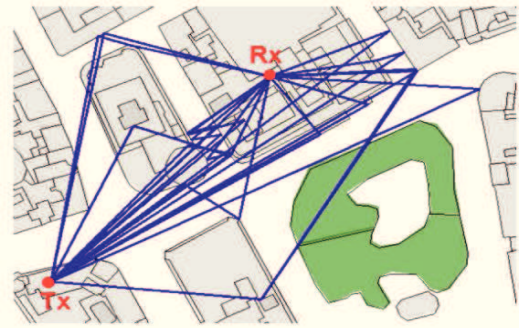

Figure 2.4: Ray tracing approach

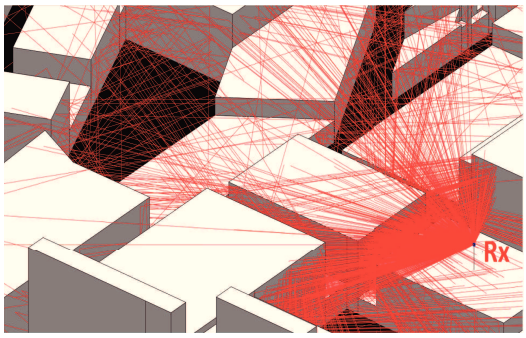

Figure 2.5: Ray launching approach

2.2.2 In-situ measurement assessment

In-situ measurements can be carried out with the help of various field measurement equipments (Fig. 2.6). Wireless communication technologies typically cover the RF range from 700 MHz to 6 GHz and each of them operates in its allocated frequency band. Consequently, when measuring the exposure, we do separate the measurements into two categories, respectively, broadband and frequency-selective (also known as narrow-band).

Figure 2.6: Commercial field measurement equipments: NBM-550 broadband field meter, SRM-3006 selective radiation meter, EME SPY exposimeters (from left to right)

Broadband measurements are performed using a field meter [Website Narda.us, 2016] equipped with a broadband probe, which is a device sensing any signal spanning several GHz at once. Finally, a single exposure value (e.g., a value in V/m, or in W/m^2) is obtained for a whole frequency range. In Alanko et al. study [Alanko et al., 2008], one broadband meter was used to map the field strengths around the antenna at different distances and heights in order to determine the safety zones for workers. Furthermore, many exposure studies [Paniagua et al., 2014, Abdelati, 2015, Gallastegi et al., 2016] carried out in the framework of risk assessment were based on the broadband measurements.

In the meantime, **frequency-selective measurements** for which the measurement system consists of a field antenna and a spectrum analyzer (or a frequency selective receiver) allow monitoring the frequency range of interest. By providing each frequency band with one exposure value, one can identify the importance of a communication technology in the total exposure. In previous studies [Joseph et al., 2006a, Joseph et al., 2012, Gajšek et al., 2015], by performing narrow-band spectrum analyzer measurements, compliance of exposure due to signals from GSM, UMTS, LTE, WiMAX, etc. with safety limits was tested: procedures for measurements in the vicinity of BTS have been developed in [Joseph et al., 2002, Joseph et al., 2006b, CENELEC, 2008]. Moreover, in epidemiological studies [Knafl et al., 2008, Frei et al., 2009, Joseph et al., 2010, Ibrani et al., 2016], another narrow-band device was used: personal exposure meters (PEM) also known as exposimeters (e.g., ESM 140 [Website Maschek.de, 2016], EME Spy [Website Satimo.com, 2016]). Exposimeters are worn by a person and easy to handle in using measurement protocol [Mann, 2010, Röösli et al., 2010], however not suitable for accurate field assessment (e.g., the presence of the human body at the vicinity of the exposimeter compromises its measurement accuracy [Kwate et al., 2016]). Bolte et al. study [Bolte et al., 2011] concluded that measurements performed by exposimeters tend to underestimate the actual exposure. Therefore, it has been proven that a maximum frequency-dependent correction factor of 1.1–1.6 should be applied to the electric field [Bolte et al., 2011]. Furthermore, exposimeters have the drawback of the limitation in detection range (e.g., EME SPY 140 with

measurement range from 0.005 - 10 V/m) which may lead to a part of non-detected through field measurements. However in reality, the probability of measurement below the detection level can be ignored.

It is important to note that **exposure to RF varies across individuals, time and space**. Bornkessel et al. study [Bornkessel et al., 2007] found that a measurement at a certain time or at a fixed location may not be representative for the time or spatially averaged exposure, or for the maximum possible exposure to a base station (BT). In fact, **some standards have already defined the measurement procedures spatially and temporally**. E.g., IEC 62232:2011 [IEC, 2011] defines measurement grids for spatial-averaging measurements. ICNIRP [Guideline, 1998] specifies a 6 minutes time-averaging period for measuring the level of squared RMS field and the power density. Nonetheless, longer periods measurements (i.e., more than 6 minutes) are in practice difficult to execute, and are time-consuming and expensive. In Joseph et al. [Joseph et al., 2009] they investigated how short-period measurements can be related to the actual maximal and average exposure extracted from longer measurement runs, for example performed over a week. Anyhow, in general, **compliance is tested by performing measurements during a short time-period (i.e., less than 6 minutes) and by extrapolating a worst-case measurement (e.g., maximum emitted power) to determine the maximum possible exposure**. Overall, different approaches exist in assessing human exposure via field metric. One has to be selected depending on the objective of exposure assessment.

2.3 Absorption metrics

Another frequently used exposure metrics are absorption metrics in terms of SAR. As we know, RF fields can penetrate tissues in the wide range of 1 MHz to 10 GHz. The lower the frequency is, the deeper the penetration. Meanwhile it also produces heating due to power absorption. The power absorbed by the tissue can be characterized by **SAR**. SAR is the measure of the rate at which power is absorbed by the human body when there is exposure to a RF EMF and is usually averaged over the whole body (so called whole-body exposure) or a small volume like 1 g or 10 g of contiguous tissue (so called localized SAR) and over a certain time period (e.g., 6 minutes according to ICNIRP guidelines). The unit of SAR is expressed in watt per kilogram. In the mathematical formulation as presented below (Equation 2.3), SAR is linked to the electric field (magnetic losses are negligible), to the conductivity as well as the density of the tissue.

$$SAR = \frac{\sigma E^2}{2\rho} \tag{2.3}$$

where σ is the electrical conductivity is S/m, E the peak amplitude of electric field in the tissue, in V/m and ρ the density of the tissue in Kg/m^3.

In addition, studies [Governmental Industrial Hygienists, 1995] have shown that a rise of 1°C in body temperature caused by energy absorption is considered as a dominant factor inducing adverse health effects such as heat exhaustion and stroke. Moreover, if the whole-body exposure is about 4 W/kg during 30

minutes, the body core temperature can increase of 1°C [Shellock and Crues, 1987, Magin et al., 1992, Hirata et al., 2007]. And in the case of localized exposure, cataracts can be induced in rabbits 'eyes when localized SAR is around 100 W/kg for 2-3 hours exposure duration [Guy et al., 1975].

Taking into account these acute established effects, **SAR was adopted as an exposure limit indicator**. The ICNIRP 1998 guidelines considered 4 W/kg (whole-body SAR) and 100 W/kg (localized SAR) as threshold values. Then a safety factor of 50 (resp. 10) was applied to the threshold in order to define the **basic restrictions**[1] of exposure for the public (resp. occupational). Some basic restrictions for time varying electric and magnetic fields for frequencies from 10 MHz to 10 GHz for individuals defined by ICNIRP [Guideline, 1998] are shown in Table 2.1. ICNIRP distinguished between the head and trunk region and the limbs, since most vital organs are located in the head and trunk of the body.

Table 2.1: Basic restrictions for time varying electric and magnetic fields for frequencies from 10MHz up to 10 GHz

	General Public	Occupational
	W/kg	
Whole body average SAR	0.08	0.04
Localized SAR (limbs)	4	20
Localized SAR (head and trunk)	2	10

Averaging time of 6 minutes. Local SAR (Specific Absorption Rate) is determined over the mass of 10 g.

To date, for long-term exposure to low level of EMFs, no adverse health effects were established. But since factors of 50 and 10 were used in order to define the basic restrictions for general public and occupational, we may consider that ICNIRP recommendations cover long-term effects in the frequency range from 10 MHz to 10 GHz as well.

At the same time, as SAR is difficult to measure, **reference levels**[2] were defined related to the basic restrictions for practical exposure assessment purposes. These reference levels were defined in function of frequencies to limit the incident strength fields to levels inducing a whole-body exposure equal to basic restrictions. Figure 2.7 shows the reference levels for EMF strength relative to the frequency.

One should note that measurements of SAR inside the human body are impossible. Therefore, **studies to evaluate SAR values in a human were carried out either by using computational methods or by experimental measurements in phantoms**.

[1] Basic restriction: restrictions on exposure to time-varying electric, magnetic and electromagnetic fields which are based directly on established health effects and biological considerations.

[2] Reference levels: these levels are established in order to limit the exposure below the basic restrictions for practical exposure assessments. The reference levels can be derived from relevant basic restrictions using measurements/ computational techniques.

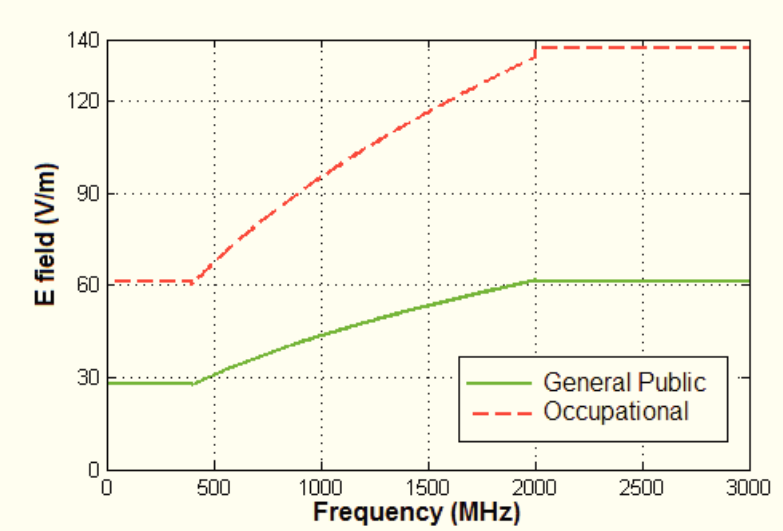

Figure 2.7: Reference levels of EMF strength for general public and occupational
Note: reference values in V/m can be conversed to W/m^2 through Equation 2.2

2.3.1 Computational method assessment

Computational methods, such as the **Finite-Difference Time-Domain (FDTD) method [Hagness and Taflove, 2000], have been largely used over the last decade to assess numerically the EMFs absorbed by the biological tissues**. Such computational method relies on **realistic heterogeneous body models** and **EM sources**.

2.3.1.1 Numerical human body models

Existing heterogeneous body models have been built using large data sets obtained from Magnetic Resonance Imaging (MRI), computer tomography or anatomical images. These heterogeneous body models are represented by voxel images of thin slices of the body, and each voxel corresponds to a particular type of body tissue. Several human models have already been developed. E.g., the widely used Virtual Family (VF) [Christ et al., 2009], which is a family of MRI based models (Fig. 2.8). In the thesis, we used the SAR values calculated for near-field and far-field exposure (near and far-field sources are presented in next section) for two anatomical human body models in the VF, Duke, a 34-year-old male and Eartha, an 8-year-old girl.

Furthermore, dielectric properties (i.e., permittivity and conductivity expressed in Siemens per meter (S/m)) of body tissues for each frequency band [Gabriel et al., 1996] are also required to use computational methods. Peyman et al. study [Peyman and Gabriel, 2010] has shown that some of the dielectric properties of the tissues vary significantly with age. For this reason, the dielectric properties of the tissues were experimentally calculated using different mammals at different ages (e.g., adult sheep, rats aged 30-days, pigs of 10 kg).

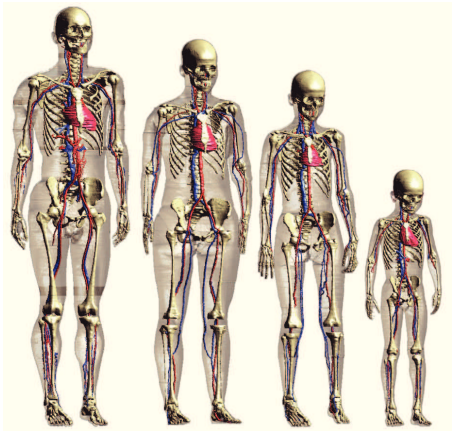

Figure 2.8: The Virtual Family: Duke, Ella, Billie, Thelonious (from left to right)

2.3.1.2 EM sources

The modeling of radiations from EM sources and wave propagations in heterogeneous environments take an important place in computational evaluation of exposure. To complete the exposure configurations, **radiations of EM sources should be defined when they are near or far from the human body**.

Near-field sources (used close to the human body) such as mobile phones, tablets, computers, etc. were modeled on a basis of commercial devices using software simulations (e.g., Matlab). The voxel digital models take into account the characteristics of real devices like the dimensions, the battery, the screen, the Printed Circuit Board and the antenna. One digital model of mobile handset [Pinto et al., 2011] is presented in Figure 2.9. This mobile handset is a Personal Digital Assistant model of dimensions $5.4 \times 1.6 \times 1.5$ cm (with a 2 mm resolution) with a dipole type antenna mounted at the bottom of the mobile phone, operating at 1940 MHz. The localized SAR (i.e., 1 g or 10 g of contiguous tissue, organ-specific[3]) in numerical human body models can be characterized using these near-field sources under different exposure conditions. In previous studies dedicated to exposure induced by a handset phone, the averaged SAR over 10g in the head, over 1g in the brain or in different anatomical brain structures, etc. were estimated, considering age-dependent changes of the anatomy and dielectric tissue properties [Christ et al., 2010], considering different handset phone's positions [Ghanmi et al., 2014] and their usages (e.g., short message service, multimedia messaging service, video, etc.) [Hadjem et al., 2010], even considering the variability of the delivered input power of a handset phone for given propagation conditions [Krayni et al., 2016].

Far-field sources are located at a great distance (varies from meters to kilometers) from the human body. Base stations or access points are, for example, far-field sources. Thus, the EM radiations from BTS can be considered as plane waves, with a specific incidence direction, having a propagation vector $\overrightarrow{K}$ and an amplitude A (V/m). To numerically simulate these radiations in FDTD, the technique known as the Huygens box is used through the principle of equivalence

[3]The organ-specific SAR can only be assessed by computational methods

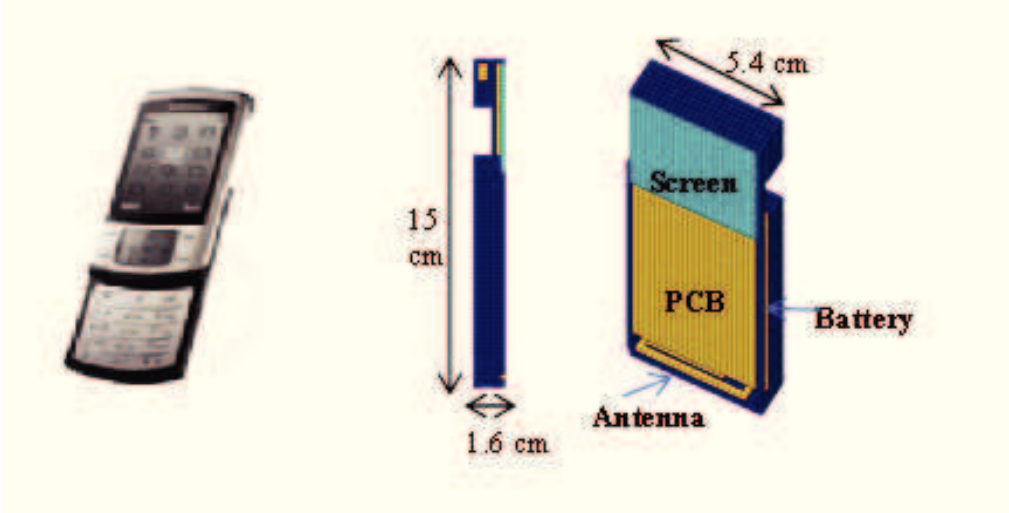

Figure 2.9: Example of digital model of mobile phone

[Merewether et al., 1980, Holland and Williams, 1983, Benkler et al., 2009]. The numerically simulation adapted to FDTD is done by inserting a numerical human model in a virtual box (so called Huygens box) whose dimensions are slightly larger than the human body. And taking into account the description of a plane wave's radiation, the equivalent currents corresponding to the plane wave around Huygens box are computed with a certain resolution (this resolution should be equal to the one used for the human model). Through the approach of equivalence principle, the excitation of equivalent currents allows to evaluate the field induced by such radiations in the entire Huygens box. In this way, whole body or localized SAR of the numerical human model induced by the plane wave can be assessed, for instance, the study presented in [Conil et al., 2008].

2.3.2 Experimental measurement assessment

Using experimental measurement assessment the electric field at various points inside simple phantoms is usually experimentally measured with a dosimetric setup (Fig. 2.10). This dosimetric setup consists of a robotically positioned probe (calibrated for measuring electric fields in tissue-equivalent simulating liquid) and of a SAR phantom filled with tissue-equivalent simulating liquid. The robot is controlled by a computer to move the probe in space (inside the SAR phantom) according to 3 axes. Indeed, the majority of experimental measurements are performed with a SAR phantom, which is an international reference phantom named Specific Anthropomorphic Mannequin (SAM) used in the European Committee for Electrical Standardization [CENELEC, 2001], the International Electrotechnical Commission [IEC, 2001] and IEEE [IEEE, 2003] standards. The head of SAM (Fig. 2.11) looks like a head of male adult and has been internationally standardized to help the definition of regulation on exposure levels.

Finally, the obtained data are then used to determinate the exposure at any points and the peak-spatial average SAR can be calculated. This method is used to evaluate the compliance of wireless mobile devices. It should be noted that during compliance testing, the wireless mobile devices are driven in a test mode and set to a maximum power radiation.

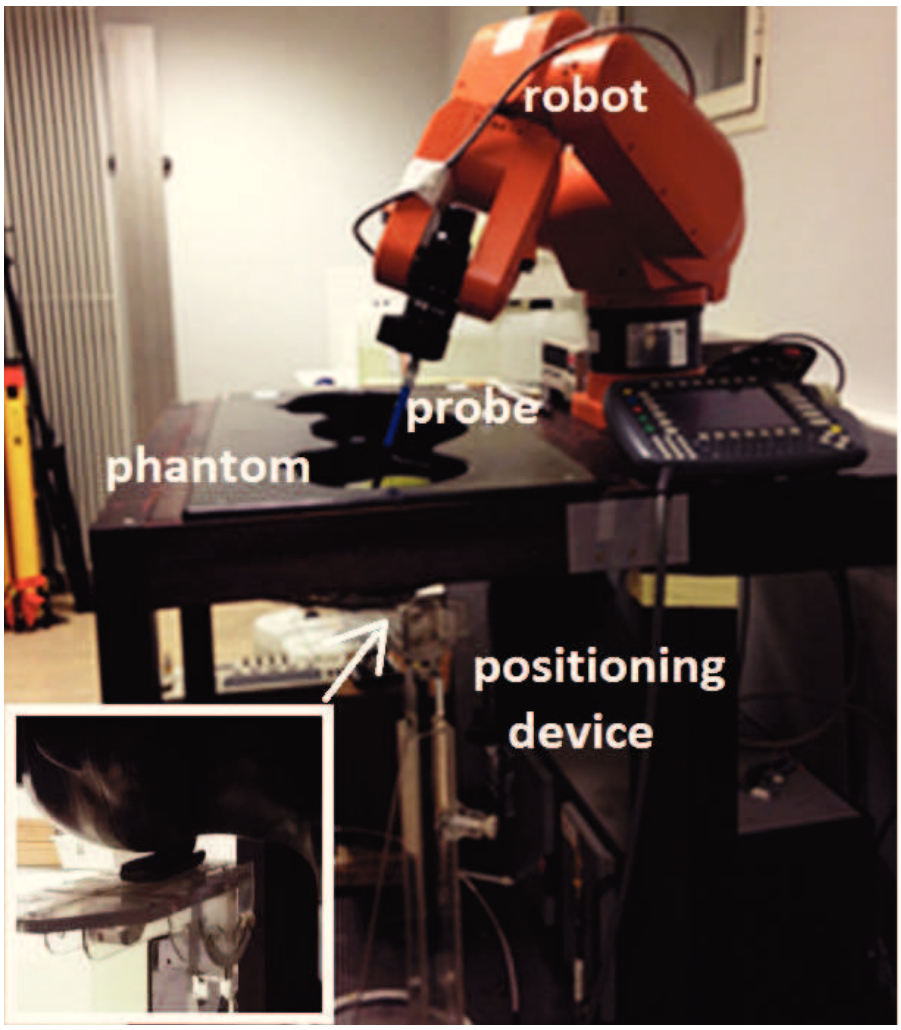

Figure 2.10: Dosimetric measurement setup for SAR measurement

Figure 2.11: International reference phantom:Specific Anthropomorphic Mannequin (SAM)

2.4 Dose metric

We should note here again that the **exposure metrics presented above are assessed during a short time-period (e.g., 6 minutes) or under a worst case assumptions (e.g., maximum level of emitted power)**. However, the trend in assessing real exposure has motivated the need for **a comparative metric combining the exposure duration and the level of exposure (SAR value or field strength)**. Indeed, maximum possible exposure is relevant to the compliance assessment, keeping in mind that maximum emitted power is always adopted in this case. However, when assessing the real exposure, e.g., the radiation power from mobile phone is not always at maximal level but related to the connected BTS, usage... Thus the dose metric is more appropriate.

The fundamental dose metric is the absorbed dose (noted as D), which represents the mean energy $d\bar{\varepsilon}$ imparted to unite mass dm ($D = \frac{d\bar{\varepsilon}}{dm}$). Thus the radiation absorbed in tissue T during a time period τ is expressed as:

$$D_T = \int_0^\tau \overline{D}_T(t)dt \tag{2.4}$$

where $\overline{D}_T(t)$ is the mean absorbed dose in tissue T at time t. Two types of dose metric respectively based on absorbed SAR value and electric field strength will be presented in the following subsections.

2.4.1 Assessment of dose based on SAR value

In [Lauer et al., 2013, Aerts et al., 2014, Plets et al., 2015] studies, **the dose metric has been defined as the combination of SAR and exposure duration**. By multiplying the local- or whole body SAR due to real exposure conditions by the exposure duration, one can get an actual absorbed dose expressed in joules per kilogram (J/kg). However, the dose can be split in two contributions: the dose due to uplink and the one due to downlink exposure. Generally, uplink exposure is induced by EM radiation emitted by mobile devices, while downlink exposure is induced by EM radiation received from BTS or access points.

More specifically, the whole-body SAR due to uplink exposure (SAR_{wb}^{UL}) can be calculated as follows:

$$SAR_{wb}^{UL}\ (W/kg) = \frac{Tx\ power\ (W)}{1\ (W)} \times SAR_{wb,norm}^{UL}\ (W/kg) \tag{2.5}$$

where Tx power is the real power emitted by the mobile device, and $SAR_{wb,norm}^{UL}$ is the normalized whole-body SAR due to exposure induced by uplink signal (i.e., power transmitted by the mobile) with a power of 1 W. Finally, the uplink dose (D_{UL}) can be obtained with the following equation:

$$D_{wb}^{UL}\ (J/kg) = SAR_{wba}^{UL} \times T_{use} \tag{2.6}$$

with T_{use} the duration of use of the mobile device in uplink activity.

Meanwhile, the whole-body SAR due to downlink exposure (SAR_{wb}^{DL}) can be evaluated as follows:

$$SAR_{wb}^{DL}\ (W/kg) = \frac{S_{inc}\ (W/m^2)}{1\ (W/m^2)} \times SAR_{wb,norm}^{DL}\ (W/kg) \tag{2.7}$$

where S_{inc} is the incident spectral power density in real conditions exposure and $SAR_{wb,norm}^{DL}$ is an estimation of the whole-body SAR induced by the specific downlink signal (i.e., a frontal plane wave) with a power density of 1 W/m^2. The downlink dose (D_{DL}) is then:

$$D_{wb}^{DL}\ (J/kg) = SAR_{wb}^{DL} \times T_{exp} \tag{2.8}$$

with T_{exp} the exposure duration to the downlink signal. Finally, the whole-body-averaged dose (D_{wb}) is:

$$D_{wb} = D_{wb}^{UL} + D_{wb}^{DL} \tag{2.9}$$

In the same way, the local body dose can also be obtained by applying local SAR in real conditions of use. E.g., the dose due to uplink radiation of mobile device (D_{loc}^{UL}) can be calculated as follows:

$$D_{loc}^{UL}\ (J/kg) = \frac{Tx\ power\ (W)}{P_{max}^{UL}\ (W)} \times SAR_{loc}^{UL} \times T_{use} \tag{2.10}$$

Where, to assess local SAR in real conditions of use, the local-body-averaged SAR due to uplink exposure (SAR_{loc}^{UL}) is weighted by the ratio between the power transmitted by the mobile device (Tx power) in real use conditions and the maximum allowed power emitted by the mobile device (P_{max}^{UL}).

2.4.2 Assessment of dose based on E field

Dose metric can be based on E field as well. By multiplying the E-field value by the exposure duration, the dose can be expressed in $V/m \cdot h$. This approach was implemented in previous studies for assessing exposure induced by, e.g., medium-frequency broadcast stations [Bortkiewicz et al., 1996], RF with frequencies around 27 MHz [Wilen et al., 2004] or high-frequency antennas [Baste et al., 2010].

2.5 The Exposure Index (EI) from LEXNET project

The existing metrics are well suited to evaluate compliance with some standards under the worst-case condition which presents limit in evaluating the EMF exposure for real life quantification. The actual EMF exposure according to real exposure conditions was characterized through experimental or computational measurements, but in most cases, dealing separately with the uplink and downlink exposures.

To the end of covering day-to-day exposure of a population in a given area incurred by a wireless network as a whole from BTS to personal devices, a global exposure metric called EI was developed under the banner of LEXNET project (Fig. 2.12). The project LEXNET was established to respond to the need of the

European Union for designing low-EMF networks in its Seventh Framework Program (FP7). The FP7 LEXNET project has been launched in 2013 (2013 – 2015) by 17 leading telecommunications operators, vendors, research centers and academic institutions. The object aimed to investigate and propose new network topologies and management that reduce the EMF levels without compromising the user's QoS. To meet this objective, the project has focused early work on determining the actual levels of exposure by proposing the EI metric.

Through approach of EI metric, when dealing with exposure issues, uplink and downlink exposures are treated all together. The concept of EI is structured around the dose metric. Different from a single dose, EI aims at filling the hole of evaluating the real day-to-day EMF exposure of an entire population rather than those of an individual, considering both the uplink and downlink exposure contributions. EI is an everyday everywhere metric which quantifies a global exposure averaged over time by considering a given time frame and averaged over space in a given geographical area.

In the definition of EI [Varsier et al., 2015a, Varsier et al., 2015b], many factors influencing this exposure should be taken into account, e.g., technology, environment, usage, posture, mobility, etc (Fig. 2.13). Different technologies like GSM, UMTS, etc. can generate different levels of exposure [Wiart et al., 2000, Gati et al., 2010]. Indoor environments can lead up to about 10 dB increase of the emitted (Tx) power by the devices compared to outdoor environments [Gati et al., 2010]. Wireless device usages (e.g. voice-calling, data sending) as well as their usage positions are also significant parameters to take into account for RF exposure assessment [Hadjem et al., 2010, Ghanmi et al., 2014]. The duration of usages, distance to access point, etc. can have as well a great impact on the exposure. Thus the EI is expressed by summing all the scenarios according to these different influencing parameters. And the general expression of EI transforms a highly complex set of data from all these scenarios and averaging over time, into a simple value expressed in W/kg which can be easily understood, accepted and used by all the stakeholders (Equation 2.11).

$$EI^{SAR} = \frac{1}{T} \sum_{t}^{N_T} \sum_{p}^{N_P} \sum_{e}^{N_E} \sum_{r}^{N_R} \sum_{c}^{N_C} \sum_{l}^{N_L} \sum_{pos}^{N_{pos}} f_{t,p,e,r,c,l,pos} \left[\sum_{u}^{N_U} (d^{UL} \times \bar{P}_{Tx}) + d^{DL} \times \bar{S}_{Rx} \right] (\frac{W}{kg}) \tag{2.11}$$

where:
- N_T is the number of considered periods within the considered time frame T (e.g., a single day).
- N_P is the number of considered Population categories.
- N_E is the number of considered Environments.
- N_R is the number of considered Radio Access Technologies (RAT).
- N_C is the number of considered Cell types.
- N_L is the number of considered user Load profiles.
- N_{pos} is the number of considered Postures.
- N_U is the number of considered Usages with devices.
- $\bar{P}_{TX}$ is the mean Tx power transmitted by the users' devices during the period t, in usage mode u, connected to RAT r, in environment e. A map of Tx power values

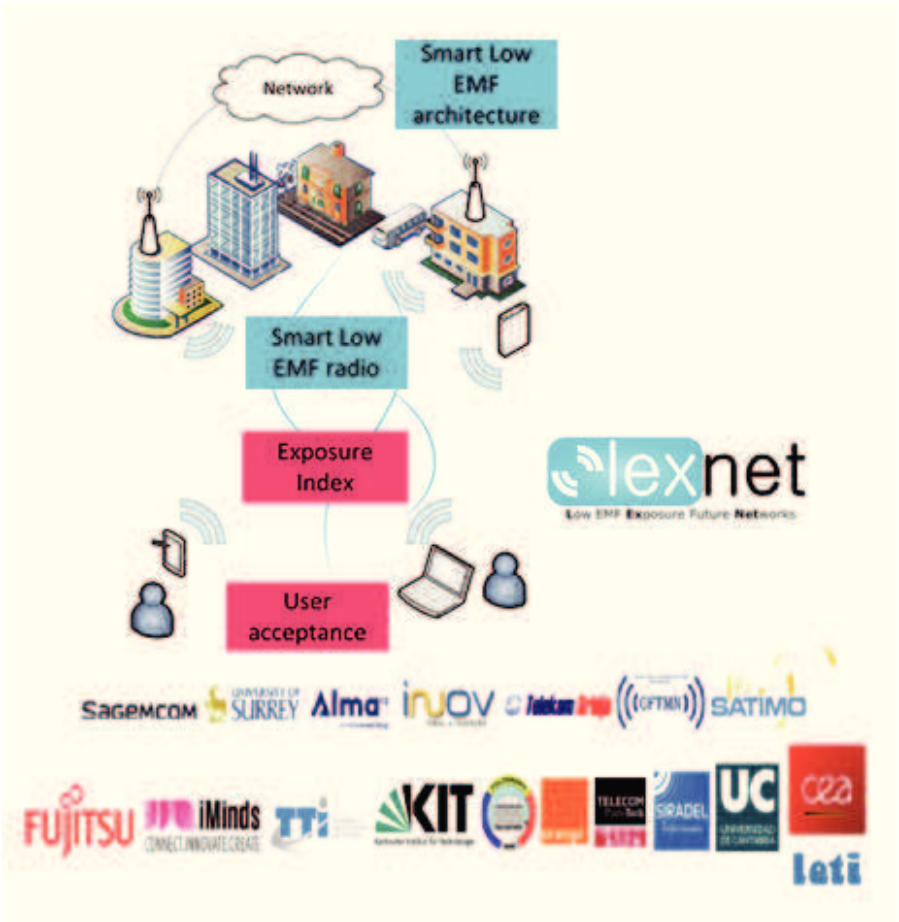

Figure 2.12: Low EMF Exposure Future Networks

Figure 2.13: Influencing parameters in exposure evaluation

is given for the whole considered geographical area and the average value is taken into account for the EI evaluation.
• $\bar{S}_{Rx}$ is the mean incident power density on the human body during the period t, induced by RAT r, in environment e. A distribution of the incident power density for the whole considered geographical area is considered and the average value over this area is taken into account for the EI evaluation.
• $d^{UL} and d^{UL}$ are the normalized raw dose values for the uplink from the mobile devices, and downlink from BTS and access points, respectively, all multiplied by the time spent in the configuration.
• $f_{t,p,e,r,c,l,pos}$ is the fraction of the total population that corresponds to population category p, the user load profile l, in posture pos, connected to RAT r, for a cell type c, in environment e, during the time period t.

2.6 Conclusion

This chapter presents a current state of existing metrics to evaluate the exposure induced by RF-EMF sources. However, most of these existing metrics are well suited to evaluate compliance with some standards under worst-case conditions or to assess real-life exposure for individuals and in most cases, dealing with the uplink and downlink exposures separately, no metric before the EI was available to represent the day-to-day global exposure of a population.

The EI was proposed in the framework of LEXNET project for the assessment of real day-to-day population exposure. In the concept of EI, many factors influencing this exposure are taken into account, e.g., technology, environment, usage, posture, etc. The global population exposure is the results of many configurations which depend on people's habits and capabilities offered by the network. **The exposure of a person spending time in public transport, working in a very dense area and living in the suburbs will cover different configurations from those living in a dense city, going to work by foot**. It is therefore the challenges to assess the population exposure. **The segmentation of various possible configurations according to the influencing exposure parameters and the evaluation of the exposure induced by wireless networks and wireless devices in these configurations are imperative**.

One should note that the number of influencing exposure parameters considered in the EI function increases the difficulty, since the challenge was not to define the EI concept but how to **transform this concept to something which is calculable** in order to assess a global average exposure value for an entire population. That is why the first part of the thesis was dedicated to **identify and characterize all the parameters influencing the EMF exposure**.

3

Assessment of average global exposure of population to EMF by using deterministic network traffic planning tool

Contents

3.1 Context

To assess the global exposure generated by both the uplink and downlink transmissions, a new exposure metric EI was developed in the framework of the LEXNET project. The EI quantifies the whole or partial body (a localized area of the body, e.g., specific organs/tissue) global exposure, averaged over time and an entire population in a given geographical area. The concept of EI metric is based on dose, aggregating the exposure duration as well as the exposure induced by both the near-field and the far-field.

Varsier et al. [Varsier et al., 2015b] study has analyzed an EI for a scenario involving an urban LTE network, or for a specific configuration (indoor, train) of GSM and UMTS networks. However, **environments and cellular networks have a strong influence on the power emitted and received by wireless devices**, which will directly impact the EI. Moreover, the **proximity of the device to the head in case of voice services is significant for RF exposure assessments** [Sadetzki et al., 2014, Ghanmi et al., 2014]. Today the 3G is intensively used for voice and data services in many countries. **Therefore in this chapter we aimed at evaluating the EI induced by such networks for both voice and data usages of mobiles and comparing the population EMF exposure in different geographical areas and different countries**. To achieve this objective, 3G cellular network architectures and statistics about information and Information and Communication Technology (ICT) usages were derived from mobile network operator data.

Briefly, we focused, using device usage statistics from analysis of data collected from operational mobile 3G networks in France and Serbia and through the LEXNET approach and metric, on assessing the level of human exposure to EMF in view of existing 3G networks.

To achieve this objective, two sets of ICT usage data were anonymously collected in two European countries, France and Serbia, partners in the European LEXNET project. A statistical analysis was then performed, detailed in Section 3.2, in order to get valuable information for analyzing EMF exposure. Section 3.3 illustrates the implementation of the EI in order to evaluate the average global exposure of the considered population to a 3G macro network. Discussion and conclusion are presented in the last section.

3.2 Statistical analysis of a population ICT usages

3.2.1 Collected ICT usage data

ICT usage data sets in France were collected by Orange (one of the four telecommunication operators in France). These ICT usage data were obtained through measurement probes installed at the Radio Network Controller (RNC) level in 3G Orange network (Fig. 3.1). Three areas were monitored: one urban area in the district of Paris, one suburban area in the region of Clermont-Ferrand and one rural area in the region of Nancy. Hourly mobile phone usage (e.g., voice call

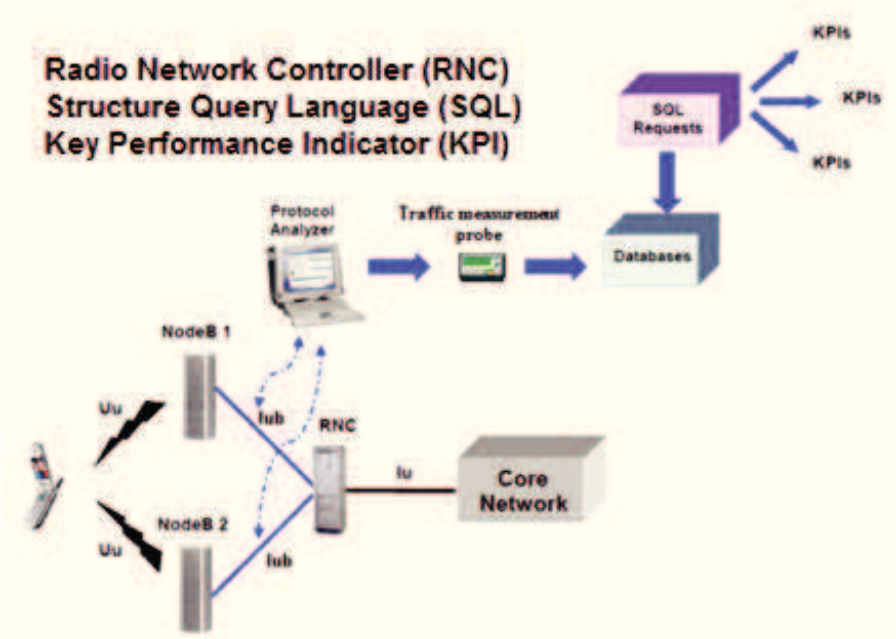

Figure 3.1: Illustration of traffic measurement probe

duration, uplink and downlink traffic volumes) were recorded from these monitored geographical areas for 1 week (including weekend) in November 2013. Each user was distinguished by his/her International Mobile Subscriber Identity number.

In Serbia, similar data were collected by Telekom Srbija from their customer analysis system and were based on users' billing data which were used to discover users in the monitored cells. These ICT usage data were based on the monitored macro cells (2G and 3G) in urban, suburban and rural areas. Data reflected hourly mobile phone usage (voice outgoing calls duration, total data traffic volume etc...) during the whole month of January 2014 for all subscribers generating any traffic in that period.

3.2.2 Comparison of 3G Mobile Usage Between France and Serbia

Based on collected data, differences of 3G ICT usage among the two countries were analyzed statistically. Figure 3.2 depicts mean voice call duration and the mean volume of data exchanged per hour and per user, in 3G network in different areas in the two considered countries by averaging over all the users who made any traffic during that hour. It was clearly observed that **users usually made fewer calls but long duration calls during the night** from 6 p.m. to 8 a.m. (Fig. 3.2a). The average **day-to-night user ratio**, equal to 2, was calculated by dividing the total phone call number during day period by the total phone call number during night period. In addition, data volumes generated per hour, per user in the two countries (Fig. 3.2b) follow the same trend despite some minor differences. E.g., a peak appears around 11:00 a.m. only in the urban area of Serbia.

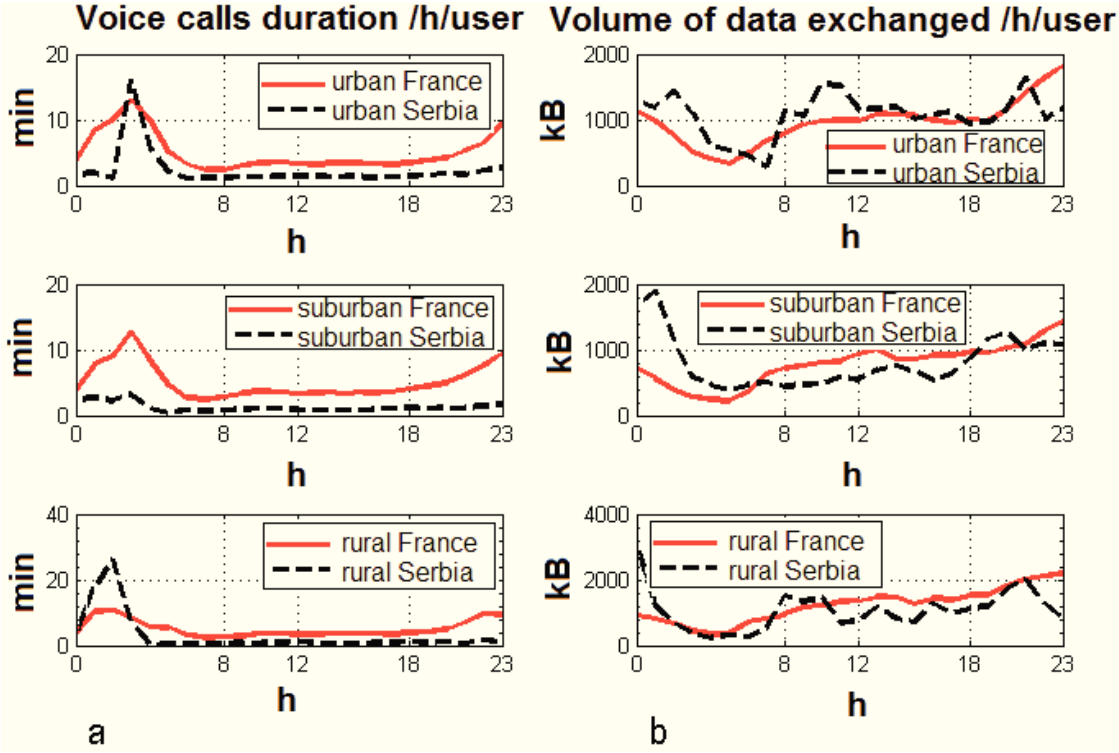

Figure 3.2: (a):Mean voice call duration per hour per user and (b) mean volume of data exchanged per hour per user in 3G network in urban, suburban, and rural areas in France and Serbia.

Hourly traffic distributions were derived in order to see the repartition of voice communications and data traffic per user in France and Serbia, as well as in different geographical areas over 24 h. Figure 3.3a and b give results extracted respectively from voice and data traffic in 3G network in Orange France. It was observed that 60% of mobile phone voice calls (respectively 51% of data traffic) occurred during daytime from 8 a.m. to 6 p.m. **Suburban users generated more traffic for both voice and data services than urban and rural users**. In Serbia, the trend of traffic repartition was similar to the trend in France (Fig. 2c and d). The analysis shows that 63% of mobile phone voice calls and 48% of data traffic occurred during daytime. As the traffic distribution in Serbia is based on data recorded on both 2G and 3G networks, the average daily traffic generation per user was higher than the one observed in France. Meanwhile, in Serbia, when considering voice service (Fig. 3.3c), it was observed that urban users generated the highest traffic among Serbian users. Concerning data service, generated traffic was found equivalent for urban and suburban users while higher than the traffic generated by rural users (Fig. 3.3d).

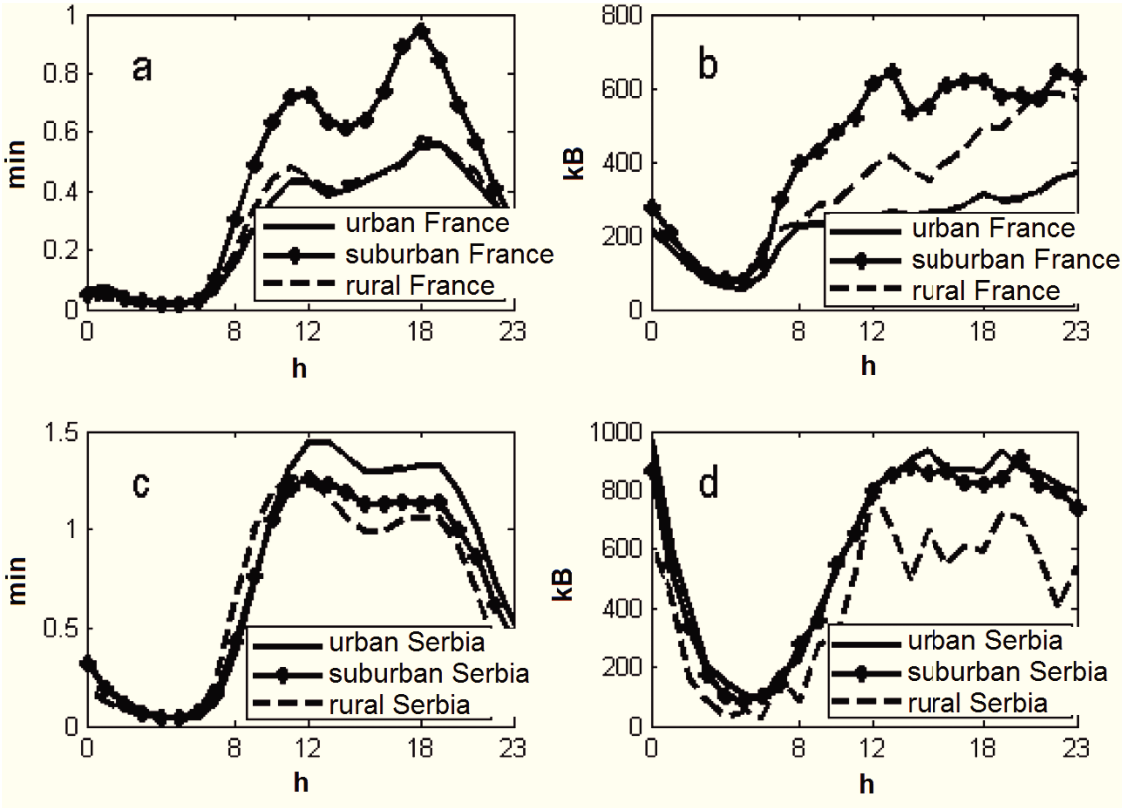

Figure 3.3: (a): Time variations of mean voice usage and (b) data usage per user over 24 h in macro 3G network of Orange France; (c) variation of mean voice usage and (d) data usage per user over a day in macro 2G and 3G network of Telekom Srbija.

Daily average voice communication durations and volumes of data traffic exchanged for all the voice and data traffic users in different area types in the three different countries were calculated. By modeling the Probability Density Function (PDF) of these users' traffic usages, the uncertainty was quantified. The Probability Density Function of daily voice calls duration (the step of histogram is 1 minute) for users in urban, suburban and rural areas of France is illustrated in Figure 3.4 and of Serbia in Figure 3.5. As shown in Figure 3.4, it was found that the PDF of daily voice call duration for French users in urban and rural areas were very similar. The probabilities of short voice calls duration (less than 1 minute) for urban and rural users were about 0.4 which was much larger compared to the one for suburban users (about 0.25). However, in case of Serbian users, the density curve was quite flat for all areas (Fig. 3.5). In addition, the probabilities of short voice calls duration were smaller than those for French users represented in Figure 3.4.

Figure 3.6 illustrates the PDF of daily data traffic exchanged for users in different areas of France (the step of histogram is 1 MB). The figure was truncated at 20 MB. It was observed that the probability of daily data traffic after 20 MB was very small. Daily data traffic consumptions for majority of users were less than 1 MB. Same conclusion can be drawn from the PDF of daily data traffic exchanged for Serbian users (see Figure 3.7). In addition, the PDF of daily data volumes for Serbian users in urban and suburban areas are very similar.

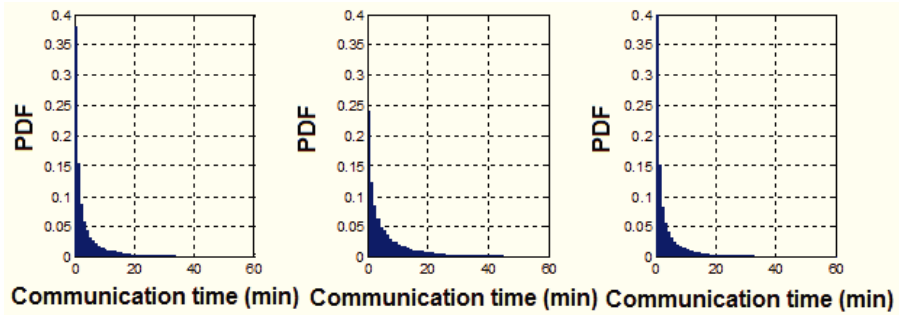

Figure 3.4: Probability density function of daily voice duration (truncated at 60 minutes) for users in urban (left), suburban (middle) and rural (right) areas (France)

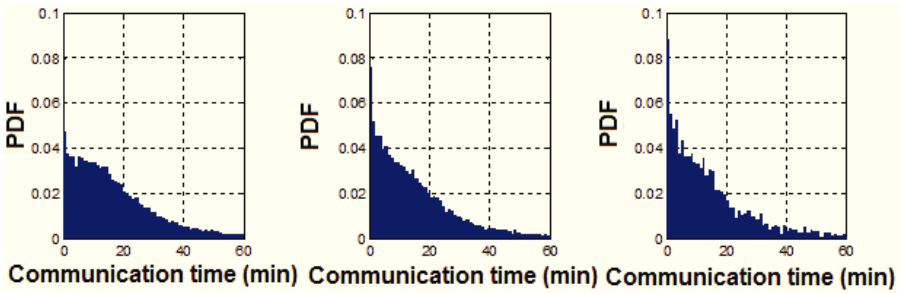

Figure 3.5: Probability density function of daily voice duration (truncated at 60 minutes) for users in urban (left), suburban (middle) and rural (right) areas (Serbia))

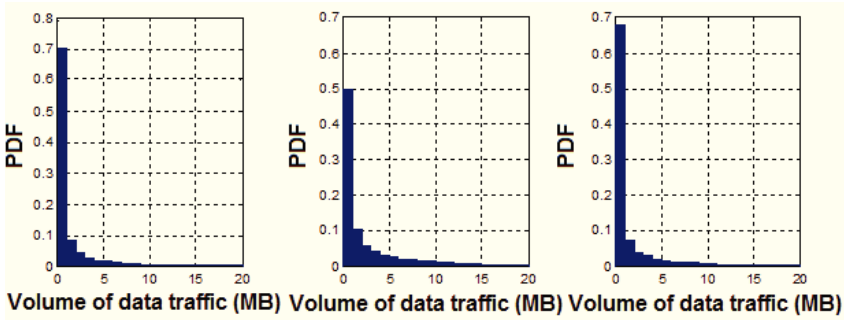

Figure 3.6: Probability density function of daily data traffic exchanged (truncated at 20000 KB) for users in urban (left), suburban (middle) and rural (right) areas (France)

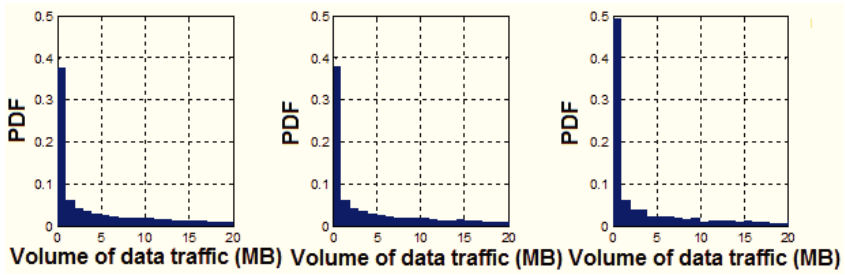

Figure 3.7: Probability density function of daily data traffic exchanged (truncated at 20 MB) for users in urban (left), suburban (middle) and rural (right) areas (Serbia)

3.2.3 User profile

In-depth statistical analysis enabled to identify different profiles of users depending on the type of geographical area. As shown in Figure 3.8, **a small part of users generated a large part of traffic and, as a consequence, usage is completely unbalanced among all users**. Considering this unbalanced usage, users were classified into three different ICT user profiles: heavy, moderate, and light. Figure 3.8 corresponds to the classification for French users. Heavy users are those consuming 80% of the total amount of data traffic (for both voice and data traffic). As Figure 3 shows, whereas they just accounted for only a small percentage of the total voice or data users, they generated most of the total traffic. Moderate users and light users are those generating, respectively, 15% and 5% of the total amount of data traffic. Volumes of data traffic and duration of voice communications per user profile recorded on the 3G Orange network were analyzed. As shown in Table 3.1, there are no large differences among user profiles in urban, suburban, and rural areas in France.

Figure 3.9 presents the classification carried out for Serbian users by applying the same rules as for French users. As stated previously, usage data obtained from Telekom Srbija were extracted for both 2G and 3G networks. Therefore, cell statistics data were gathered from RNC and BTS controller network elements within collection periods for the purpose of deriving 2G versus 3G traffic ratios, as well as uplink versus downlink data traffic ratios. The carried-out analysis shows that 72% of voice communications occurred through Telekom Srbija's 2G network while 28% occurred through Telekom Srbija's 3G network, and 91% of the data traffic was assigned to 3G while 9% to 2G. Therefore, average voice call durations supported by 3G network were shorter in Serbia than in France (Tables 3.1 and 3.2). Concerning data traffic, large differences between 3G heavy users of Orange France and those of Telekom Srbija were observed (Tables 3.1 and 3.2). Average daily volumes of data generated by heavy Telekom Srbija 3G users were approximately 40 MB, while they were between 70 and 100MB for heavy users of Orange France. However, the trend is the opposite for moderate and light users.

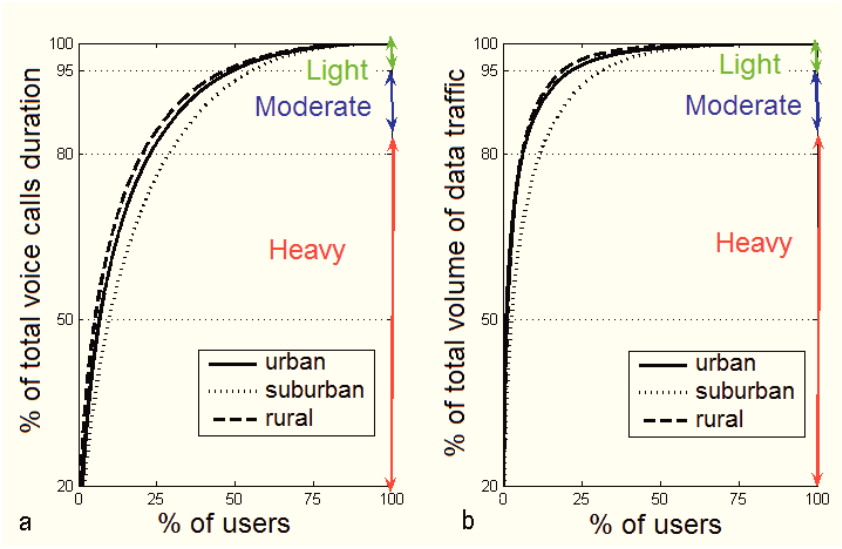

Figure 3.8: (a): Percentages of total communication time and (b) total volume of data traffic versus percentages of users defining three user profiles in urban, suburban, and rural areas in France.

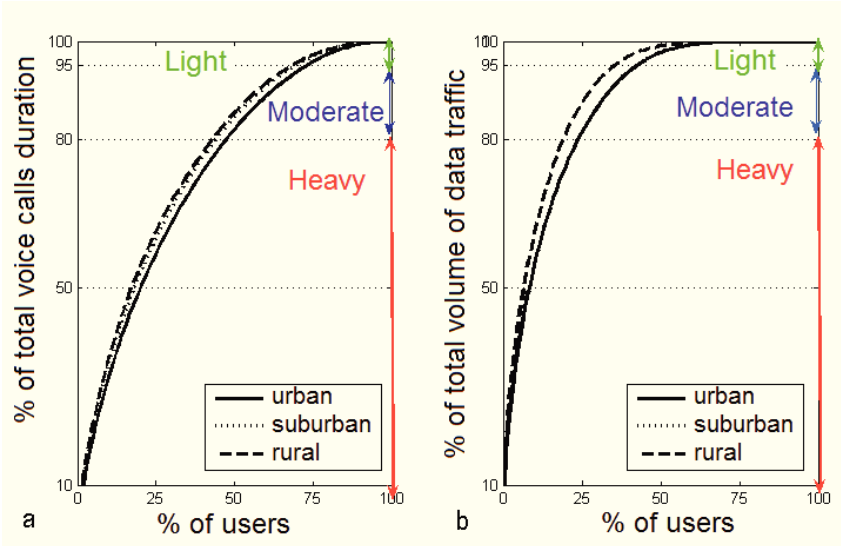

Figure 3.9: (a): Percentages of total communication time and (b) total volume of data traffic versus percentages of users defining three user profiles in urban, suburban, and rural areas in Serbia.

3.3 Global exposure of population to EMF induced by a macro 3G network

To achieve the evaluation of average population exposure to 3G-induced EMFs through approach of EI metric from both uplink and downlink radio emissions

Table 3.1: User Profiles Defined in Urban, Suburban, and Urban Areas in France for 3G Network

	Orange France 3G network											
	Urban				Suburban				Rural			
	Voice[a]		Data[b] (MB[g])		Voice		Data (MB)		Voice		Data (MB)	
User profiles	D[c]	N[d]	D	N	D	N	D	N	D	N	D	N
Heavy	14 min[e]	11 min	30	38	18 min	12 min	36	35	15 min	12 min	44	60
Moderate	2.5 min	1.4 min	2.9	2.4	4 min	2 min	4.7	3.2	2.7 min	1.4 min	4.5	4.8
Light	26 s[f]	16 s	0.2	0.2	49 s	22 s	0.5	0.3	28 s	14 s	0.3	0.2

[a]Voice, daily communication time.
[b]Data, daily volumes of data traffic.
[c]D, during day time from 8 a.m. to 6 p.m.
[d]N, during night time from 6 p.m. to 8 a.m.
[e]min, minutes.
[f]s, seconds.
[g]MB, megabyte.

Table 3.2: User Profiles Defined in Urban, Suburban, and Urban Areas in Serbia for 3G Network

	Telekom Srbija 3G network											
	Urban				Suburban				Rural			
	Voice[a]		Data[b] (MB[g])		Voice		Data (MB)		Voice		Data (MB)	
User profiles	D[c]	N[d]	D	N	D	N	D	N	D	N	D	N
Heavy	4 min[e]	2.4 min	2.1×10^4	22	3.6 min	2 min	20	22	3.5 min	2 min	17	19
Moderate	33 s[f]	20 s	5	5.4	21 s	13 s	4.9	5.3	19 s	11 s	2.1	2.3
Light	5 s	3 s	0.5	0.6	3 s	2 s	0.5	0.6	2 s	1 s	0.3	0.4

[a]Voice, daily communication time.
[b]Data, daily volumes of data traffic.
[c]D, during day time from 8 a.m. to 6 p.m.
[d]N, during night time from 6 p.m. to 8 a.m.
[e]min, minutes.
[f]s, seconds.
[g]MB, megabyte.

in different countries, geographical areas, and for different wireless device usages, many parameters (e.g., age, usage, technology, environment) influencing the EI should be taken into account. The global exposure of a population is the results of many scenarios which depend on people's habits and capabilities offered by the network. Therefore, various possible scenarios have to be built according to influencing exposure parameters (Table 3.3). These parameters can be divided into 4 groups (Fig. 3.10): **life segmentation values, reference SAR values, ICT usage data and averaged emitted power, average received power density**. Finally, the average population EMF exposure can be assessed by cross-matching these four data groups aggregated over time by using the EI metric. **The EI was evaluated over 24 h for macro 3G scenarios in dense urban and suburban areas in order to assess and compare the average global exposure of a population in France and Serbia, with respect to their different usage of wireless devices**.

Table 3.3: Segmentation of influencing exposure parameters

RAT	Cell type	Time	Environment
3G	Macro	Day	Indoors
		Night	Outdoors
Population	**User profile**	**Posture**	**Usage**
Children	Heavy	Standing	Data, mobile
Young people	Moderate	Sitting	Voice, mobile
Adults	Light		
Seniors	Non-user		

Figure 3.10: Cross-match of four data groups to build the EI

3.3.1 Description of macro 3G urban and suburban network scenarios

3.3.1.1 Propagation model

In order to assess a global EMF exposure from both uplink and downlink radio emissions, it is essential to accurately predict radio-propagation behavior through an adopted propagation model. Briefly, existing propagation models can be divided mainly in the following two types:

- Statistical models also known as empirical models (e.g., Okumura model, Hata model, COST-231 model) which are based on measurement data.

- Deterministic models also known as site-specific models (e.g., Ray-tracing, Ray-launching) which are very accurate radio-propagation prediction models.

Okumura model [Okumura et al., 1968] was designed from the data measured in the city of Tokyo and is widely used for propagation in urban areas. Hata model [Hata, 1980] is a developed version of Okumura model. It incorporates the graphical data from Okumura model, but covers the range of frequencies from 150 to 1500 MHz. Further, COST-231 model extends the frequency range in the 1500-2000 MHz. It should be noted that all these statistical models are easy to implement by providing few parameters (e.g., the operating frequency, effective heights of the BTS and the mobile, etc.), while they are less sensitive to environment geometries and limited to certain frequency bands.

The deterministic model is a mathematical simulation of a physical phenomenon between two points and strongly dependent on detailed building and terrain data base. AIRCOM's MYRIAD model was adopted in our study for its ability of automatically adapt itself to all engineering (i.e. micro, mini, small and macro cells), to all environments (i.e. dense urban, urban, suburban, mountainous, maritime, open), and to all systems (i.e. GSM, GPRS, UMTS, WIFI, WIMAX) in a frequency range starting from 400MHz to 5GHz. MYRIAD relies on very realistic modeling of the channel, 2 phenomena are considered in calculation of the propagation loss: the free-space loss LOS and Non LOS (the diffraction, reflection (e.g., walls, water), penetration (e.g., inside a building)) (Figure 3.11).

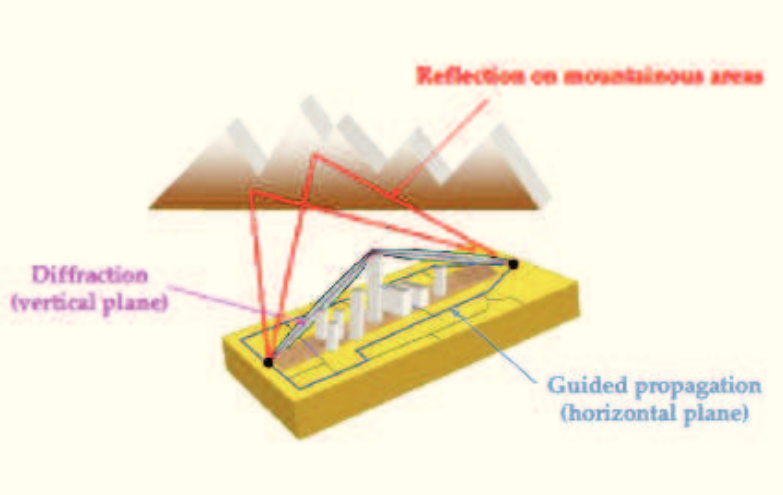

Figure 3.11: Reflection + diffraction + guided propagation = the MYRIAD Model trilogy

3.3.1.2 Macro 3G network environment

In order to evaluate the EMF exposure of a population in different geographical areas (respectively urban and suburban), the corresponding macro 3G network environments have to be defined. The dense urban and suburban environments defined in this study are located respectively in a typical European urban area (10369 hab/km^2, 14 km^2) in the center of Lyon in France, and in a typical European suburban area (5404 hab/km^2, 80 km^2), Cergy, which is in the northwestern suburb of Paris. In the context of macro 3G networks, two network models representative of dense urban and suburban macro cell deployments were conceived based on data collected from Orange in Lyon and Cergy (Fig. 3.12). The network configuration data (i.e., site locations, antenna specifications, power settings of BTS, etc.) were extracted from 53 Orange 3G network sites (154 macro cells) in the urban area and 31 sites (90 macro cells) in the suburban area. All the parameters such as antenna information and user equipment transmit powers etc. are detailed in Table 3.4. Moreover, meshed geographical data (25 × 25 m) describing the altitude above ground, height above surface, and topology (e.g., buildings, forests, rivers) were used as inputs to calculate the attenuation of EM waves propagation. A through-the-wall signal penetration loss of 10 dB and an inside-building loss of 0.66 dB/m were taken into consideration. Traffic distribution data with a resolution of 25 m were built on the studied area (except for forest and river zones) according to a uniform distribution.

3.3.2 Evaluation of EI

3.3.2.1 Life segmentation data

Two time periods, respectively daytime from 8 a.m. to 6 p.m. and nighttime from 6 p.m. to 8 a.m. were considered for all scenarios.

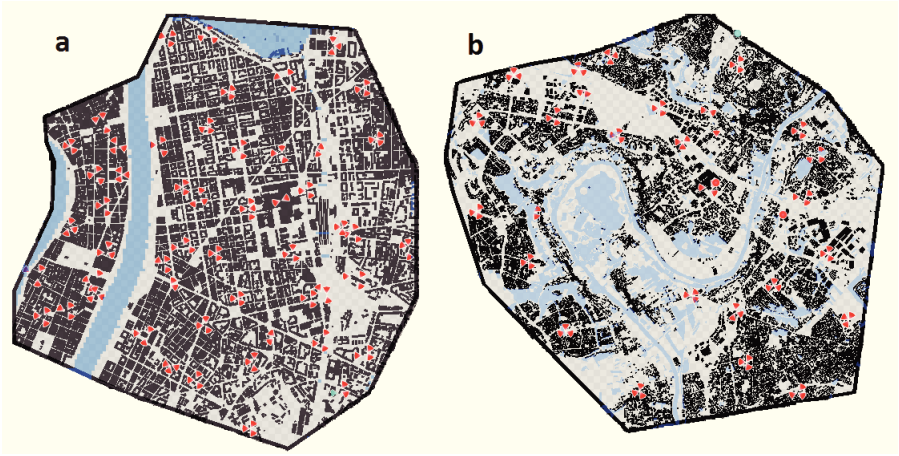

Figure 3.12: Network models of macro cell deployments: macro 3G network in urban (a) and suburban (b) area

Table 3.4: Network parameters for the 3G network in urban and suburban areas

Environment	Typical European dense urban/ suburban environment Radio access technology 3G	
System	Cell type	Macro
	Carrier	FDD10
	Central frequency	2100 MHz
	Max Antenna EIRP	60 dBm
	Antenna	Gain 17.4 dBi, 6° Elec. Downtilt 2 or 3 antennas/sector.
	Power limits	Min/Max DL power per connection: -60 dBm/ 43 dBm
	Noise figure	5 dB
User equipment	Max/Min transmit power	24 (data), 21 (voice) dBm / -39 dBm
	Antenna	Omni-directional with 0 dBi gain 2 antennas/user device Antenna height: 1.7 m above ground
	Body loss	8 dB
	Through-the-wall signal penetration loss for indoor users	10 dB (outside⟷inside), 0.66 dB/m (inside⟶inside)
User traffic	Average active user density	Depends on periods, environments and user profiles
	Distribution	Uniform spatial distribution within the simulation area. Single floor (at 1.7 m height). No user mobility.

To represent differences in mobile phone usage over age, the population was segmented into four categories: children (below 15 years), young (between 15 and 29 years), adults (between 30 and 59 years) and seniors (over 60 years).

The distributions of categories into the population depending on area types and countries (Table 3.5). The categories repartitions in Lyon (urban, France) as well as in Cergy (suburban, France) were derived from [Website Cartesfrance.fr, 2015a]. And the categories repartitions for the urban area (respectively suburban area) in Serbia were evaluated by averaging over all the urban (respectively suburban) municipalities in Belgrade according to Statistical Office of the Republic of Serbia [Vukmirovic, 2012]. All the municipalities can be found in [Website Beograd.rs, 2015].

Time spent indoor or outdoor for each category of population was derived from several European time use surveys [Aliaga, 2006, INSEE, 2011], averaging over 1 year on a daily basis (Table 3.6). The hypothesis that 70% of mobile phone usage occurs indoor and 30% outdoor was taken.

3.3.2.2 Reference SAR data

Two types of network usage were considered: voice and data traffic usage, considering two different postures, sitting posture in indoor environment and standing posture in outdoor environment (as illustrated in Figure 3.13). Normalized whole-body SAR induced by 3G mobiles and by macro 3G BTS for adult and child, for different usage (voice and data), and different postures (sitting and standing) were derived from numerical dosimetric simulations, as part of LEXNET project. It is important to note that the entire population is exposed to downlink EM radiation from BTS everywhere and all day long. While the mobile users receive uplink EM radiation from their devices only during voice communication time or uplink data traffic emissions.

Table 3.5: Repartition of the population in urban and suburban areas of France and Serbia

	France		Serbia	
Population type	Urban	Suburban	Urban	Suburban
Children	13.9%	22.2%	13.5%	14.7%
Young	32.8%	31.4%	18.4%	18.6%
Adults	38.2%	39.1%	43.6%	42%
Seniors	15.1%	7.3%	24.5%	24.7%

Table 3.6: Daily life time segmentation

	Day		Night	
Population type	Indoor	Outdoor	Indoor	Outdoor
Children	8 h 15 min	1 h 45 min	13 h 45 min	15 min
Young	8 h 20 min	1 h 40 min	13 h 10 min	50 min
Adults	8 h 15 min	1 h 45 min	13 h 05 min	55 min
Seniors	7 h 35 min	2 h 25 min	13 h 05 min	55 min

Figure 3.13: Illustration of mobiles' usages: voice and data usage of mobiles in sitting or standing posture

3.3.2.3 ICT usage data

Three user profiles depending on the considered geographical area type and considered country were defined (Table 3.1 and 3.2). Furthermore, in both countries, some hypotheses on repartitions of user profiles among each population category were taken (Table 3.7).

Table 3.7: Repartition of user profiles for Orange and Telekom Srbija 3G usages for each population category

	% Heavy[a]		% Moderate[b]		% Light[c]	
	Orange	Srbija	Orange	Srbija	Orange	Srbija
Population type			Voice communication			
Children	20%	25%	30%	50%	50%	25%
Young	50%	47%	30%	25%	20%	28%
Adult	20%	47%	30%	25%	50%	28%
Seniors	20%	47%	30%	25%	50%	28%
			Data traffic			
Children	50%	60%	40%	20%	10%	20%
Young	50%	60%	40%	20%	10%	20%
Adult	10%	24%	40%	18%	70%	58%
Seniors	5%	5%	40%	25%	70%	70%

[a]% Heavy, percentage of repartition of heavy user profile.
[b]% Moderate, percentage of repartition of moderate user profile.
[c]% Light, percentage of repartition of light user profile.

For each population category, proportions of users and non-users of mobile phones were derived from [Bigot et al., 2013] (Table 3.8).

There are four telecom operators in France (respectively three telecom operators in Serbia), and 35% of the population in France (respectively 44.8% of the population in Serbia) use the Orange (respectively Telekom Srbija) network [Website Journaldunet.com, 2015, Website Worldlibrary.org, 2015]. As presented in Cisco [Cisco, 2016], in 2015 3G connections represented nearly 40% of total connections. Then, the percentage of 3G Orange or Telekom Srbija voice or data users was calculated as market penetration% × 3G connections% × user/non-user%.

Table 3.8: Proportions of users and non-users of mobile phones per population category

Mobile phone user	Children	Young	Adults	Seniros
	Voice communication			
Non-user	10%	4%	5%	30%
User	90%	96%	95%	70%
	Data traffic			
Non-user	45%	33%	59%	90%
User	55%	67%	41%	10%

3.3.2.4 Average transmitted power, average received power density

Network traffic planning tool Several wireless network planning tools are available, for example Volcano Suite by Siradel, WHIPP tool by IMinds, etc. A 3G radio network planning tool, described in [Nouir et al., 2006, Nouir et al., 2007, Nouir et al., 2008] was used to predict received and transmitted powers. This tool is usually used by network providers to predict Radio Access Network performance and to guide operators during deployment and optimization of a mobile network. The main inputs of this tool are the network configuration data, path loss calculation performed by MYRIAD based on network and terrain database, and predetermined traffic configurations (Figure 3.14 –3.16). The MYRIAD propagation model was installed in ASSET (Figure 3.17) (ASSET AirCom International) in order to calculate the loss of propagation. Outputs of this tool consist of uplink transmitted power for voice and data usage as well as downlink received power over all the covered geographical area.

Three user profiles were considered in the traffic configuration with different repartitions depending on usage (voice, data), area types (urban, suburban), and countries (France, Serbia). For each user profile, the average communication time and data volume during day and night times were obtained through statistical analyses of ICT usage data. The traffic was uniformly distributed within the simulation area without considering users' mobility. The mobile terminal Antenna effective area (Aeff) equals to $A_{eff} = \frac{G \times (c/f)^2}{4\pi}$, where $G = 1$, $c = 3 \times 10^8 m/s$, $f = 2100 MHz$. The A_{eff} value leads to quantify the corresponding received power density.

Figure 3.18 illustrates the average emitted power by the Orange data users calculated over the urban area during the day time. Figure 3.19 illustrates the corresponding average received power. Simulation results (Table 3.9) showed a difference of 8–11 dB between received power densities in indoor and outdoor areas and an average difference of 3 dB between received power densities in urban and suburban areas. Furthermore, it revealed a maximum of 7 dB difference between emitted power by mobiles in data and voice services. Indeed, the emitted power highly depends on mobile usage and network architecture.

Finally, the average population EMF exposure could be assessed by cross-matching all the described above input parameters (which means life segmentation values, reference whole-body SAR values, ICT usage data, average transmitted power, and average received power density) aggregated over 24 h by using the EI metric. The average global exposure of the population in a typical dense urban

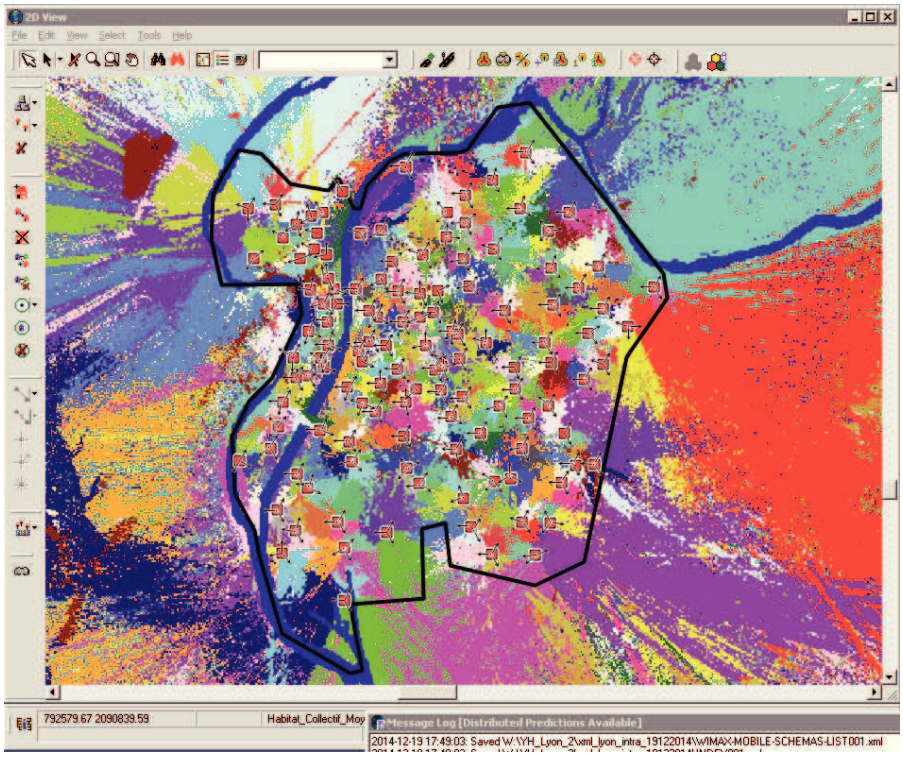

Figure 3.14: 3G network environment

Figure 3.15: High resolution map data

Figure 3.16: Traffic raster data with resolution 25 meters

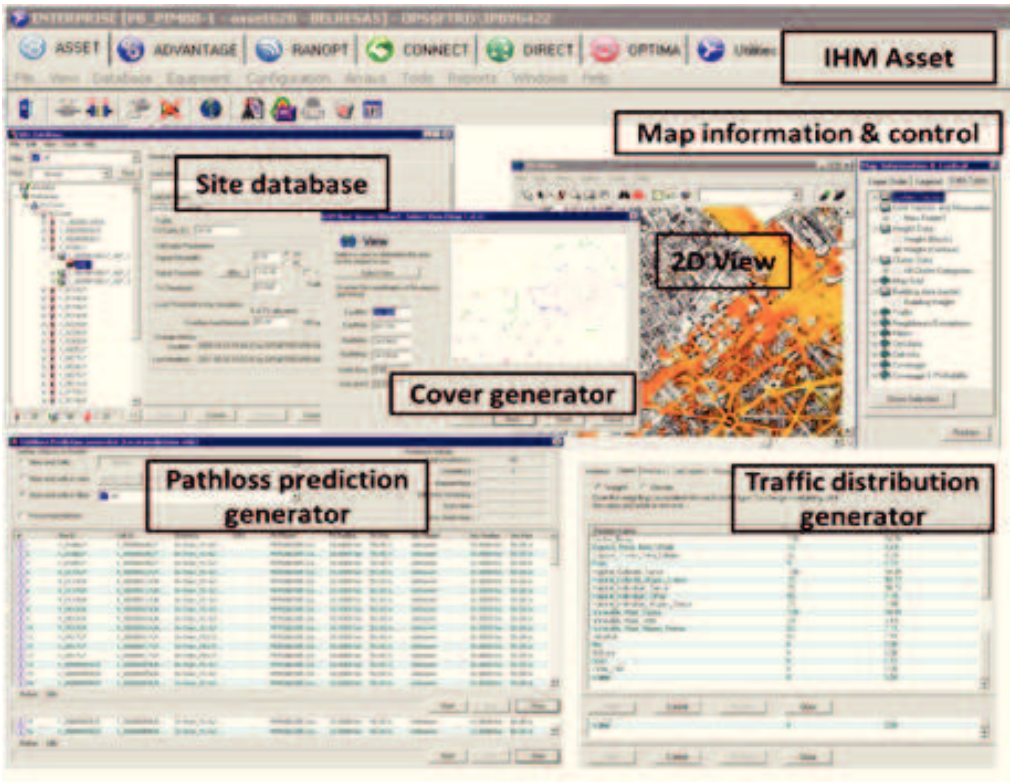

Figure 3.17: Overview of ASSET

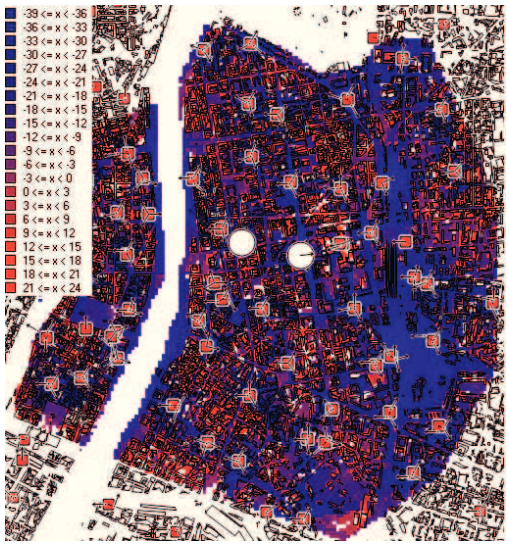

Figure 3.18: Emitted power (Tx) in dBm by the Orange 3G mobile data users calculated over the dense urban area during the day time

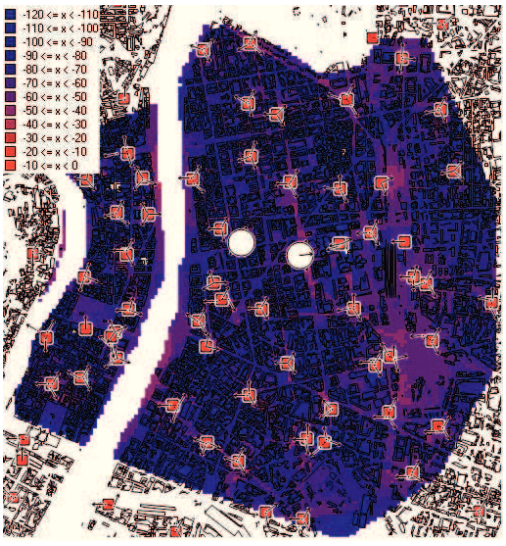

Figure 3.19: Received power (Rx) in dBm calculated over the dense urban area during the day time

Table 3.9: Average received power densities and emitted powers for different traffic configurations

		Day		Night	
		Indoor	Outdoor	Indoor	Outdoor
			France		
Urban	Mean DL[a] power density ($\mu W/m^2$)	1.6453	12.133	0.85417	6.2342
	Mean UL[b] transmitted power (W)				
	Voice	0.0207	0.0013	0.0170	6.5164×10^{-4}
	Data	0.1078	0.0050	0.0853	0.0025
	Mean UL throughput (kbps)	94	126	98	128
Suburban	Mean DL power density ($\mu W/m^2$)	0.49581	7.1564	0.38524	5.6415
	Mean UL transmitted power (W)				
	Voice	0.0264	0.0012	0.0194	5.4574×10^{-4}
	Data	0.1095	0.0029	0.0675	0.0013
	Mean UL throughput (kbps)	93	128	95	127
			Serbia		
Urban	Mean DL power density ($\mu W/m^2$)	1.5553	10.732	0.47493	3.8228
	Mean UL transmitted power (W)				
	Voice	0.0203	0.0013	0.0209	0.0015
	Data	0.1065	0.0049	0.1129	0.0059
	Mean UL throughput (kbps)	72	107	81	116
Suburban	Mean DL power density ($\mu W/m^2$)	0.43354	6.3844	0.21013	3.1255
	Mean UL transmitted power (W)				
	Voice	0.0202	5.6677×10^{-4}	0.0260	0.0012
	Data	0.0809	0.0014	0.1121	0.0029
	Mean UL throughput (kbps)	83	127	84	127

[a]DL, downlink.
[b]UL, uplink.

area induced by a macro 3G network was estimated to 1.92 $\times 10^{-7}$ W/kg in France and 1.28×10^{-7} W/kg in Serbia. And the average global exposure of the population induced by a macro 3G network in a typical suburban area was found to be equal to 2.17×10^{-7} W/kg in France and 1.22×10^{-7} W/kg in Serbia.

3.4 Discussion and conclusion

The results presented in this chapter allow assessing EMF exposure using EI metric. The EI metric was introduced by the LEXNET European project [Tesanovic et al., 2014, Varsier et al., 2015b] with the objective to develop a realistic and global Key Performance Indicator (KPI) allowing optimization of operating networks in terms of EMF exposure. This approach differs from the usual approaches dedicated to compliance testing. Indeed, previous approaches dealing with EMF exposure generally focused on devices or BTS individual exposure, while the EI gives a global view of an entire population's EMF exposure covering both the uplink and the downlink. This section presents results of the first comprehensive analysis in which both uplink and downlink exposures are considered, and where parameters for network configurations, traffic, and ICT usage statistics as well as user profiles are obtained from live mobile network.

The results have shown that, **in France, population exposure to EMFs induced by a 3G network in a suburban area was 1.1 times higher than what was calculated in a dense urban area**. On the contrary, **in Serbia, population exposure was found slightly higher in the urban than in suburban area**. In the studied network environment, the density of urban BTS was 1.7 times higher than the density of suburban BTS. As a consequence, average downlink exposure in a dense urban area was found almost twice as much as what was calculated in a suburban area. However, **downlink exposure was found to have a limited influence on global EMF exposure to 3G networks**. The global exposure in France for suburban population was dominated by uplink exposure due to the great amount of data generated by 3G users.

Investigating differences between the average exposure of a population located indoor and outdoor, it was observed that **the ratio of indoor to outdoor exposure is greater than 20**. This is due to the hypothesis of 70% of the total traffic generated indoor, as well as higher emitted power by mobile phones indoor compared to outdoor.

We also investigated differences between **exposure induced by data traffic and what was induced by voice traffic**. In France, uplink exposure induced by mobiles in data traffic was found to be almost twice the exposure induced by mobiles in voice traffic, while in Serbia, uplink exposure from data traffic was found to be about 7 times higher than exposure due to voice traffic because of users' low voice communication duration through 3G network of Telekom Srbija.

As a matter of fact, the global exposure assessment carried out in this section is associated with only **one operator**. Therefore, to perform a fair comparison between global exposures in the two countries, **it was important to normalize the obtained results by percentage of mobile operators' market penetration and number of operators**. To achieve this objective, the uplink exposure was divided by the percentage of operators' market penetration, and the downlink

exposure was multiplied by the number of operators in a given country. As a result, **the EI to 3G networks in France were found to be roughly 2 times higher than in Serbia** (Table 3). **Results also highlighted the importance of uplink exposure to global exposure**. Uplink exposure (noted as UL%) accounts for more than 90% of global exposure as shown in Table 3.10. The UL% highly depends on uplink usage, keeping in mind that **the higher the uplink usage, the higher the uplink exposure**. Finally, it is important to note that obtained EI values are far below international standard limits for human exposure, even if our purpose was not to test any compliance to the limits. We are aware that presented results are highly dependent on collected data used to identify network architecture and mobile usage, which is why exposure values should always be linked to the time period when data were collected and are likely to evolve in coming years.

Table 3.10: Average Global Exposure in France and in Serbia to 3G Macro Networks

	France		Serbia	
	Urban	Suburban	Urban	Suburban
EI[a], W/kg	5.61×10^{-7}	6.28×10^{-7}	2.93×10^{-7}	2.77×10^{-7}
UL%[b]	95%	97%	93%	96%

[a]EI, global exposure index.
[b]UL%, proportion of uplink exposure to the global exposure.

In conclusion, results derived from device usage statistics collected in France and Serbia, have shown a **strong heterogeneity of exposure, both in time and space**. In fact, average EMF exposure can significantly differ from one geographical area to another as well as from one country to another due to the impact of network architecture and ICT usage differences. Furthermore, as can be seen the LEXNET EI is complex to evaluate, many input parameters should be taken into account. We considered, in this chapter, the average values of input parameters to evaluate the EI. **However, input parameters on EI (e.g., emitted and received powers and ICT usage data) are not constant but highly varied among mobile users**. Therefore, in the next chapter, the **variability** of these influencing parameters are **characterized** in order to manage the **uncertainties** linked to the EI. After investigating how the EI varies due to the input random variables, a **sensitivity analysis** can thus be carried out for the purpose of simplifying the EI metric.

4

Variability and sensitivity analysis of global population exposure to EMF

Contents

4.1 Context

To respond to public risk perception about possible health effects of RF EMFs, it has become necessary to characterize the real human exposure to such fields. In most studies [De Marco and Maggi, 2006, Schmid et al., 2007] dedicated to the **risk assessment of EMF exposure**, a worst-case approach is often adopted. Furthermore, EMF exposure levels are quantified in terms of SAR expressed in W/kg and of incident field (e.g., electric field expressed in V/m), respectively, induced by maximum EMF radiations originating from personal wireless devices and from BTS (downlink). However none of these approaches alone allows assessing the **real global population exposure to RF EMFs**.

Therefore, the aim of the study detailed in this chapter was to develop **a simplified exposure index** that would characterize the average exposure of a population taking into account both the exposure induced by EM radiation emitted by wireless devices and received from BTS or access points. This simplified exposure index was developed based on the new exposure metric named EI implemented in the LEXNET project. In its raw definition, **EI is a complex index** to evaluate and calculate as presented in Section 3. **It was thus important to analyze the influence of each input parameter on the EI for the purpose of simplification**.

To achieve this goal, an approach evaluating the variability and uncertainties linked to the response of a physical system with multiple random inputs was used. **Uncertainty propagation methods** well suited to solve a Finite Element system were used. As a matter of fact, the issue of uncertainty analysis has attracted increasing attention in the last decades [Sudret, 2007, Silly-Carette, 2008, Blatman, 2009]. The simplest method is a **purely statistical sampling based method named Monte Carlo**. This, however, can require more than ten-thousands sample data in order to give a good estimation of the statistical distribution of the output, sometimes resulting in a great amount of computational processing time. In this case, the approach of **meta-modeling**, e.g., Kriging and Polynomial Chaos (PC) expansion , etc. is considered. In general, the Kriging method is accurate for non-liner issues, while difficult to build and use due to a global optimization process applied to identify the maximum likelihood estimators [Matheron, 1969]. However, PC is used to approximate statistically the system's output through a simple and fast-to-evaluate meta-model. This meta-model is less time consuming after evaluating a limited number of simulations provided by the computational model. When a substituted model is established, various stochastic quantities of output (e.g., mean, variance, PDF etc.) can be assessed through the approach of Monte Carlo. Furthermore, another advantage of using the expansion of PC is that a sensitivity analysis can be directly performed.

Furthermore, complex systems usually depend on a large number of input parameters which unfortunately increase the difficulty in probabilistic model construction. In fact, only a limited number of inputs influence the randomness of system's response [Sudret, 2007]. In this case, **the sensitivity analysis describes how much model's output is impacted by changes of input values, by providing a set of sensitivity indices**. To date, various sensitivity analysis techniques are available in the literature [Saltelli et al., 2000, Xu and Gertner, 2008]. Among them **variance-based sensitivity measures** (a form of global sensitivity

analysis also named as Analysis of Variance (ANOVA) techniques) are attractive since they decompose the variance of the model's output as a sum of contributions of single input variables or sets of input variables. As a result, they can deal with the nonlinear response and measure the effect of input interactions.

This chapter is organized as follows. **Statistical methods dedicated to the uncertainty propagation and global sensitivity analysis** are introduced in the first section. These methods are further used in Section 4.3 to assess the global population exposure through EI approach taking into account the **variability and uncertainties linked to input variables**. Section 4.4 details the simplified exposure metric which is obtained by **a sensitivity analysis of EI to input parameters**. We conclude in the last section.

4.2 Uncertainty propagation and sensitivity analysis

4.2.1 Probabilistic model building

4.2.1.1 Classical Monte Carlo method

Numerous techniques can be employed to estimate the variability and uncertainties linked to the output. A traditional approach for estimating the statistical properties of a system's output while considering inputs' uncertainties is the Monte Carlo method. Theoretically, Monte Carlo is a purely stochastic based computational method. As shown in Equation 4.1, an empirical average $\overline{h}_N$ can be obtained through a finite number (N) of data sample set $(x_1, ..., x_N)$ generated from the density function f_X.

$$\overline{h}_N = \frac{1}{N} \sum_{i=1}^{N} h(x_i) \tag{4.1}$$

According to the strong law of large number, with sufficiently large N, $\overline{h}_N$ converges surely to the expected value of function $h(X)$ (noted as $\mathbb{E}[h(X)] = \int_{\mathcal{X}} h(x) f_X(x) dx$).

Briefly, Monte Carlo approach gives good statistical estimation of the output parameter under the condition of a **sufficiently large N** (typically the sample number is 10^{3-4}). Since the evaluation of EI is not time consuming, **the variability of EI can thus be assessed using the Monte Carlo method.**

However, **this approach is not suitable when only a small number of simulations is affordable or available**. E.g., as shown in Section 3.3.2.4, enormous time were needed by one 3G radio network traffic simulation in order to obtain the network data . In this case, the purely computational model may be replaced by the approach of **meta-modeling** using a simple and fast-to-evaluate meta-model. This meta-model can be developed using a limited number of points in the input space. Detailed information about this method is presented below.

4.2.1.2 Polynomial Chaos Expansions

General principle The advanced statistical method of PC is well known and frequently used to model the random system response Y according to the random input parameters $\mathbf{X}$. Specially as described in [Blatman and Sudret, 2010], if the M input random variables in vector $\mathbf{X} = \{X_1, \ldots, X_M\}$ are independent, **the random model response Y may be expanded onto the finite-dimensional PC basis** $\Psi(\mathbf{X})$. In practice, PC basis is truncated after P terms to facilitate the computation of coefficients:

$$\mathbf{Y} = \mathcal{M}(\mathbf{X}) \approx \sum_{j=0}^{P-1} a_j \psi_j(\mathbf{X}) \tag{4.2}$$

In this equation (4.2), a_j are **unknown deterministic coefficients** for multi-indices $\boldsymbol{\alpha} = \{\alpha_1, \ldots, \alpha_M\}$. ψ_j (noted as the **predictor**) are multivariate polynomials of the basis $\Psi(\mathbf{X})$ which are orthogonal with respect to the joint PDF of the input random vector $\mathbf{X}$. For instance, if the input random vector $\mathbf{X}$ follows a uniform distribution over (-1, 1), the orthogonal polynomials constituting the basis of the probabilistic space are of Legendre polynomials [Xiu and Karniadakis, 2002]. Table 4.1 shows the suitable orthogonal polynomials for different kinds of input random variables. P corresponds to the **size of the polynomial basis**. Generally, the PC basis is commonly truncated by limiting the total degree of polynomials ($|\boldsymbol{\alpha}| = \sum_{i=1}^{M} \alpha_i$) with an upper bound i.e., $|\boldsymbol{\alpha}| \leq p$. Only the suited combinations of the α_i are used to build the Ψ_α. As a consequence, the size P of the polynomial basis of M variables with maximum accepted degree p equals to $\frac{(M+p)!}{M!p!}$.

Table 4.1: Classical orthogonal polynomials and corresponding random variables

Distribution	Orthogonal polynomial π
Uniform $\mathcal{U}(-1, 1)$	Legendre
Gaussian $\mathcal{N}(0, 1)$	Hermite
Gamma $\mathcal{E}(1)$	Laguerre

Estimation of the coefficients by regression Unknown deterministic coefficients of the truncated expansion need to be assessed (Equation 4.2). Let us consider a set of N executions $\mathcal{X} = \{\boldsymbol{x}^{(i)}, i = 1, \ldots, N\}$ of the input random vector $\mathbf{X}$ (so-called experimental design). The corresponding observations of the system response are $\mathbf{y} = \{\mathcal{M}(\boldsymbol{x}^{(1)}), \ldots, \mathcal{M}(\boldsymbol{x}^{(N)})\}$. The coefficients can thus be estimated by **least-square regression** to optimize the approximation of Y with respect to a set of observations:

$$\widehat{\boldsymbol{a}} = (\boldsymbol{\Psi}^T \boldsymbol{\Psi})^{-1} \boldsymbol{\Psi}^T \mathbf{y} \tag{4.3}$$

where $\boldsymbol{\Psi}$ is the data matrix defined by $\boldsymbol{\Psi}_{ij} = \psi_{\alpha_j}(\boldsymbol{x}^{(i)})$ with i=1,...N and j=0,...,P-1. Nonetheless, P can still grow rapidly with the size M and the accepted degree p, which leads to a large number of observations (N) that have to be defined in the experimental design. In this case, **a sparse PC expansion named Least**

Angle Regression Selection (LARS) [Blatman and Sudret, 2011] **seems particularly appropriate since it is well suited to the case in which the number of PC coefficients is significantly larger than the number of observations**. Briefly, only the polynomials among possible candidates $\Psi(\boldsymbol{X})$ that have the greatest impact on the model response Y will be selected. **LARS provides a collection of PC representations** in a way that the first meta-model includes a single predictor, the second one includes two predictors and so on. **The best one among these meta-models needs to be evaluated through a meta-model validation**.

Meta-model validation First of all, it is important to stress out that the model prediction accuracy is a concept differing from the model fitness one. The latter estimates the response for objects that do not participate to the calculated model. The model fitness capability can be evaluated, for instance, by the coefficient determination (noted as R^2). The assessment of the model prediction accuracy can be performed with the **Leave-One-Out Cross Validation (LOOCV)** [Blatman and Sudret, 2011, Kersaudy et al., 2014]. LOOCV demands to take one point out (e.g., removing the i-th observation) from the experimental design $\mathcal{X}$. According to the left points one meta-model $\widehat{\mathcal{M}}^{(-i)}$ is built. As indicated in Equation 4.4, the predicted residual (noted as $\Delta^{(i)}$) is the difference between the model's output value at $x^{(i)}$ and its model prediction according to $\widehat{\mathcal{M}}^{(-i)}$:

$$\Delta^{(i)} = \mathcal{M}(\boldsymbol{x}^{(i)}) - \widehat{\mathcal{M}}^{(-i)}(\boldsymbol{x}^{(i)}) \tag{4.4}$$

The leave-one-out error (Err_{Loo}) is evaluated by repeating moving each point out of the experimental design (Equation 4.5), from which one determination indicator Q^2 can be derived (Equation 4.6). Thus among the collection of PC expansions provided by LARS, **one selects the best model with the highest Q^2**.

$$Err_{Loo} = \frac{1}{N}\sum_{i=1}^{N}\Delta^{(i)^2} \tag{4.5}$$

$$Q^2 = 1 - \frac{Err_{Loo}}{Var(\mathbf{y})} \tag{4.6}$$

4.2.1.3 Experimental design

Sampling method **The sampling of input random variables in an experimental design is crucial for an accurate representation of one computational model**. Various sampling methods exist, e.g., Monte Carlo sampling, Quasi random sequences, etc. Latin Hypercube Sampling (LHS) [Park, 1994] was implemented in many studies for spreading the sample points evenly across all possible values for all input variables. It partitions every axis in the M-dimensional sample space into N intervals of equal probability, and selects one sample from each interval. An illustration of a 3-dimensional sample space for a design of 10 samples in each dimension is given in Figure 4.1. As shown in Figure 4.1, each colored line crosses the sample space once, leaving a sampling value for each dimension (presented by colored points). It was observed that samples from each dimension are uniformly distributed between 0 and 1.

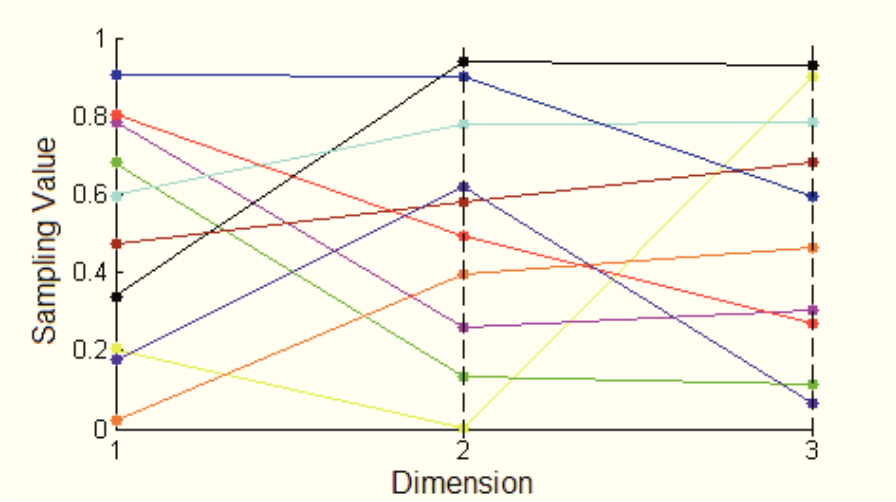

Figure 4.1: Latin Hypercube sampling of 10 samples in the 3-dimensional space

Observation set Sample values provided by LHS are uniformly distributed probabilities between 0 and 1 (Figure 4.1). Thus, for an input variable, it necessitates to associate each probability value (U) with one realization (x_i) by using its inverse Cumulative Density Function (CDF) ($F_{x_i}^{-1}(\cdot)$) (Equation 4.7). Finally, obtained variables will be used as inputs to a computational model.

$$x_i = F_{x_i}^{-1}(U) \tag{4.7}$$

One should note that a linear transformation has to be applied in the process of meta-modeling to transform $\boldsymbol{U}(0,1)$ into a standard uniform variable $\mathcal{U}(-1,1)$, which is adapted to the Legendre polynomial basis as shown in Table 4.1. An illustration sketch is given in Figure 4.2

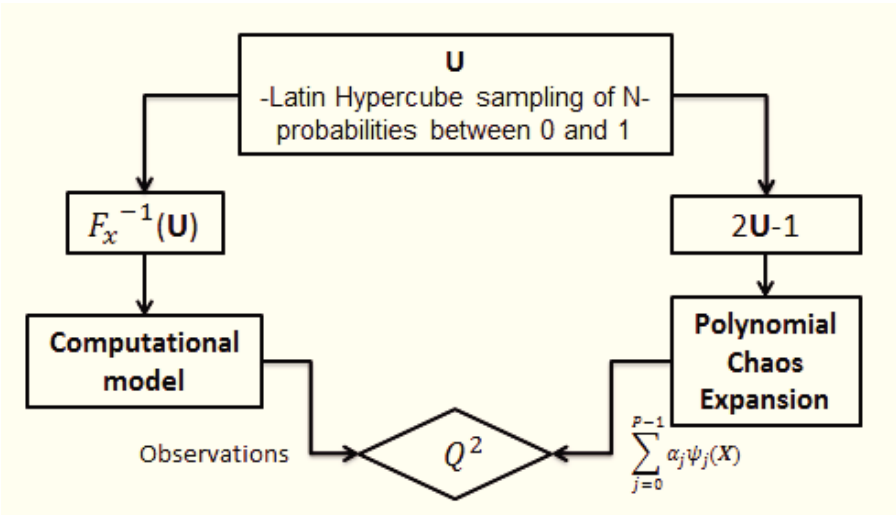

Figure 4.2: Illustration sketch of experimental design

Dependence Modeling using copulas In fact, the input random variables may be statistically dependent. Under the condition that two variables are highly correlated, one should take into account the **dependent structure** of these variables to construct the joint distribution. In this case, **copula** is introduced to decouple the marginal properties of the random variables and the dependence structures. A M-dimensional copula is defined by a multivariate distribution C, with uniformly distributed marginal U(0,1) on [0,1] (e.g., $C(u_1, ..., u_M)$). For the sake of simplicity, we let M=2 in the following content. Copulas are important because of Sklar's theorem, which [Sklar, 1959] proves that a joint distribution (e.g., $F(x_1, x_2)$) can be expressed according to a copula function (e.g., $C(\cdot)$) and the marginal distributions (e.g., $F_i(x) = P(X_i \leq x), i = 1, 2$) for x_1, x_2 over $[-\infty, +\infty]^2$ as follows:

$$F(x_1, x_2) = C(F_1(x_1), F_2(x_2)) \tag{4.8}$$

In other words, Sklar's Theorem allows separating the marginal distributions from the dependent structure, which is expressed by C. In addition, C is unique only if marginal distributions are continuous. Conversely, C can thus be read as:

$$C(u_1, u_2) = F(F_1^{-1}(u_1), F_2^{-1}(u_2)) \tag{4.9}$$

In addition, the dependent structure can be measure by Spearman's rank correlation coefficient (denoted as ρ_S). The advantage of using ρ_S to measure the dependence between two variables is, on one hand, that it suits to the case of non-linear dependence, and on the other hand, that it is independent from the marginal distribution. The closer ρ_S is to 1 or -1, the stronger two variables being compared are monotonically related[1]. Furthermore, Spearman's ρ_S can be expressed in terms of the copulas according to the proofs in [Nelsen, 1999]. Spearman's ρ_S of two variables X_1 and X_2 is given by:

$$\rho_S(X_1, X_2) = 12 \int \int_{[0,1]^2} C(u, v) du dv - 3 \tag{4.10}$$

In fact, several families of copulas adapted to different cases exist. E.g., using Sklar's theorem, Normal copula (or Gaussian copula), which is also called Nataf model [Nataf, 1962], C can be obtained as:

$$\begin{aligned} C(u_1, u_2; \Sigma) &= \Phi_\Sigma(N^{-1}(u_1), N^{-1}(u_2)) \\ &= \frac{1}{2\pi det(\sum)} exp\left[\frac{[N^{-1}(u_1)\ N^{-1}(u_2)]\, \Sigma^{-1}\, [N^{-1}(u_1)\ N^{-1}(u_2)]^T}{-2}\right] \end{aligned} \tag{4.11}$$

$$\Sigma = \begin{bmatrix} 1 & 2sin(\frac{\pi}{6}\rho_S) \\ 2sin(\frac{\pi}{6}\rho_S) & 1 \end{bmatrix} \tag{4.12}$$

where N is the univariate standard normal distribution, Φ_Σ is the standard multivariate (bivariate in this case) normal distribution with correlation matrix Σ (expressed in terms of Spearman coefficient by solving Equation 4.10) and $det(\Sigma)$ denotes the determination of matrix Σ.

[1] Monotonically related: A monotonically related function is the one that either never increases or decreases when its variable increases.

According to Equation 4.11, a sample of the joint cumulative function with a Normal copula from uniform variables can be generated as follows:
a) generate uniform sample of two uniform iid variables u_1 and u_2;
b) transform every element of obtained uniform sample into a standard normal vector with zero mean and unit variance by $N = (\Phi^{-1}(u_1), \Phi^{-1}(u_2))^T$;
c) find Cholesky decomposition of correlation matrix Σ: $AA^T = \Sigma$;
d) get vector $\boldsymbol{X}$ which follows 2-dimension normal distribution : $\boldsymbol{X} = A \times \boldsymbol{N}$
e) an additional step is required in order to get an uniformly distributed random vector: $\boldsymbol{U} = \Phi(\boldsymbol{X})$
In our study, the copula of Gaussian type was used to model the dependence between input variables through the above procedures.

4.2.2 Global sensitivity analysis

To achieve the goal of simplifying the EI, it is necessary to determine the impact of each input parameters on EI through a variance-based sensitivity analysis. Different methods exist according to the dependence of input variables.

4.2.2.1 Sobol' indices for models with independent input variables

In the framework of ANOVA, if the input variables $X_1, ..., X_M$ are independent, the variance of a deterministic model's output can be decomposed as follows [Efron and Stein, 1981]:

$$Var(Y) = \sum_{i=1}^{M} D_i(Y) + \sum_{i<j}^{M} D_{ij}(Y) + \cdots + D_{12...M}(Y) \tag{4.13}$$

with $D_i(Y) = Var[E(Y \mid X_i)]$, $D_{ij}(Y) = Var[E(Y \mid X_i, X_j)] - D_i(Y) - D_j(Y)$ and so on. $E(Y \mid X_i)$ is the expectation of Y conditionally to a fixed variable of X_i. Based on that, sensitivity indices introduced by Sobol [Sobol, 2001], for the purpose of evaluating the relative influence of individual variables or sets of variables on the model output are defined as:

$$S_i = \frac{D_i(Y)}{Var(Y)}, \; S_{ij} = \frac{D_{ij}(Y)}{Var(Y)}, \ldots \tag{4.14}$$

S_i is the first order index of Sobol defined to express the contribution of main effect of X_i to the output variance, while the second order index takes into account the effect of varying X_i and X_j simultaneously, additional to the effect of their individual variations. Total index was introduced latter by Homma and Saltelli [Homma and Saltelli, 1996] as follows:

$$S_{T_i} = S_i + \sum_{i<j} S_{ij} + \sum_{j \neq i, k \neq i, j<k} S_{ijk} + \cdots \tag{4.15}$$

In practice, Sobol' first order and total indices are usually adopted in the sensitivity analysis. To estimate them, Monte Carlo simulation based methods as described in [Sobol, 2001, Saltelli, 2002] have been developed. Furthermore,

analytic expressions for Sobol' indices based on a PC expansion have been derived from [Sudret, 2008]:

$$S_i = \frac{\sum_{j=1}^{P-1} \gamma_{(0,1)} a_j^2 E(\psi_j^2)}{D_{PC}} \tag{4.16}$$

where S_i is the first index for variable X_i, D_{PC} is the total variance of the meta-model, $\gamma_{(0,1)}$ equals to 1 when $\psi_j(\cdot)$ encompass the attribute of X_i and only X_i (if not $\gamma_{(0,1)}$=0). As for the total Sobol' index for variable X_i (noted as S_{T_i}), it can be calculated in the same way as illustrated in Equation 4.16, with $\gamma_{(0,1)}$ equals to 1 when $\psi_j(\cdot)$ encompass not only the attribute of X_i but also the combinations of X_i with other input variables.

Sensitivity analysis of Sobol' indices assume the independence between model's inputs, keeping in mind that the ANOVA decomposition (Equation 4.13) is unique only if the inputs are independent. However, in many fields, model's inputs can be strongly correlated. As a consequence, the dependence can restrict the space of inputs and thus modify the decomposition formula 4.13. Therefore, a generalization of the variance-based sensitivity analysis for the dependent case is introduced below.

4.2.2.2 Kucherenko indices for models with dependent input variables

An approach of variance-based sensitivity analysis for models with dependent variables was introduced by Kucherenko [Kucherenko et al., 2012]. Both the first order and total indices were derived as generations of Sobol' indices based on the classical decomposition of total variance. Theoretical formulas as well as their estimations by Monte Carlo method can be found in Kucherenko et al. [Kucherenko et al., 2012].

As presented in the study of Kucherenko, a M dimensional multivariate set $\boldsymbol{x} = \{x_1, ...x_M\}$ was divided into a subset $\boldsymbol{v} = \{x_{i_1}, ..., x_{i_s}\}$ and a complementary one $\boldsymbol{w} = \{x_{i_{M-s}}, ..., x_{i_M}\}$. The total variance of the model $f(\boldsymbol{x})$ (noted as D) can be decomposed according to:

$$D = V_v[E_w(f(\boldsymbol{v}, \overline{\boldsymbol{w}}))] + E_v[V_w(f(\boldsymbol{v}, \overline{\boldsymbol{w}}))] \tag{4.17}$$

where,

$$E_w(f(\boldsymbol{v}, \overline{\boldsymbol{w}})) = \int_{\mathcal{R}^{M-s}} f(\boldsymbol{v}, \overline{\boldsymbol{w}}) p(\boldsymbol{v}, \overline{\boldsymbol{w}} \mid \boldsymbol{v}) d\overline{\boldsymbol{w}} \tag{4.18}$$

$$V_v[E_w(f(\boldsymbol{v}, \overline{\boldsymbol{w}}))] = \int_{\mathcal{R}^{s}} [E_w(f(\boldsymbol{v}, \overline{\boldsymbol{w}}))]^2 p(\boldsymbol{v}) d\boldsymbol{v} - f_0^2 \tag{4.19}$$

$$V_w(f(\boldsymbol{v}, \overline{\boldsymbol{w}})) = \int_{\mathcal{R}^{M-s}} [f(\boldsymbol{v}, \overline{\boldsymbol{w}})]^2 p(\boldsymbol{v}, \overline{\boldsymbol{w}} \mid \boldsymbol{v}) d\overline{\boldsymbol{w}} - f_0^2 \tag{4.20}$$

$$E_v[V_w(f(\boldsymbol{v}, \overline{\boldsymbol{w}}))] = \int_{\mathcal{R}^{s}} [V_w(f(\boldsymbol{v}, \overline{\boldsymbol{w}}))]^2 p(\boldsymbol{v}) d\boldsymbol{v} \tag{4.21}$$

Kucherenko normalized the Equation 4.17 by the total variance D. Hence, this equation becomes the sum of the first order index of the subset $\boldsymbol{v}$ (noted as S_v) and the total index of the subset $\boldsymbol{w}$ (noted as S_{T_w}) expressed as:

$$1 = \underbrace{\frac{V_v[E_w(f(\boldsymbol{v}, \overline{\boldsymbol{w}}))]}{D}}_{S_v} + \underbrace{\frac{E_v[V_w(f(\boldsymbol{v}, \overline{\boldsymbol{w}}))]}{D}}_{S_{T_w}} \tag{4.22}$$

Consistently, the total index of the subset $\boldsymbol{v}$ (noted as S_{T_v}) can be obtained through:

$$S_{T_v} = \frac{E_w[V_v(f(\overline{\boldsymbol{v}}, \boldsymbol{w}))]}{D} \tag{4.23}$$

In addition, the estimations of S_v and S_{T_v} can be assessed through the following crude Monte Carlo formula [Kucherenko et al., 2012]:

$$S_v = \frac{\frac{1}{N}\sum_{i=1}^{N}[f(\boldsymbol{v}^{(i)}, \boldsymbol{w}^{(i)}) f(\boldsymbol{v}^{(i)}, \overline{\boldsymbol{w}}^{(i)})] - (\frac{1}{N}\sum_{i=1}^{N} f(\boldsymbol{v}^{(i)}, \boldsymbol{w}^{(i)}))^2}{D} \tag{4.24}$$

$$S_{T_v} = \frac{\frac{1}{N}\sum_{i=1}^{N}(f(\boldsymbol{v}^{(i)}, \boldsymbol{w}^{(i)}) - f(\overline{\boldsymbol{v}}^{(i)}, \boldsymbol{w}^{(i)}))^2}{2D} \tag{4.25}$$

where

$$D = \frac{1}{N}\sum_{i=1}^{N} f(\boldsymbol{v}^{(i)}, \boldsymbol{w}^{(i)})^2 - f_0^2 \tag{4.26}$$

In order to generate the sample sets presented in Equation 4.24 and 4.25, authors of the study [Kucherenko et al., 2012] propose to use a Gaussian copula which allows reducing the problem of evaluation of first order and total indices to the case of the correlated normal distribution. In this case, sample vectors, such as $\{\boldsymbol{v}, \boldsymbol{w}\}$ can be generalized from the joint PDF $p(\boldsymbol{v}, \boldsymbol{w})$ by using the Nataf transformation as shown previously (see Section 4.2.1.3). To obtain the conditional sample vector, e.g., $\overline{\boldsymbol{w}}$, let us first consider a M dimensional multivariate Gaussian distribution with mean $\boldsymbol{\mu}$ and covariance matrix Σ:

$$\Phi_M(\boldsymbol{x}) = \frac{1}{(2\pi)^{\frac{M}{2}} det(\Sigma)} exp\left[\frac{(\boldsymbol{x}-\boldsymbol{\mu})^T \boldsymbol{\Sigma}^{-1}(\boldsymbol{x}-\boldsymbol{\mu})}{-2}\right] \tag{4.27}$$

Furthermore, it should be note that the components $\boldsymbol{v}$ and $\boldsymbol{w}$, such that $\boldsymbol{x} = \{\boldsymbol{v}, \boldsymbol{w}\}$, are also normally distributed. The mean vector $\boldsymbol{\mu}$ and covariance matrix Σ can be partitioned as shown in Equation 4.28.

$$\boldsymbol{\mu} = \begin{bmatrix} \boldsymbol{\mu_v} \\ \boldsymbol{\mu_w} \end{bmatrix} \quad \boldsymbol{\Sigma} = \begin{bmatrix} \boldsymbol{\Sigma_v} & \boldsymbol{\Sigma_{vw}} \\ \boldsymbol{\Sigma_{wv}} & \boldsymbol{\Sigma_w} \end{bmatrix} \tag{4.28}$$

Consistently, the conditional distribution of $\Phi_{M-s}(\boldsymbol{v}, \overline{\boldsymbol{w}} \mid \boldsymbol{v})$ is also a normal distribution with mean $\boldsymbol{\mu_{wc}}$ and covariance matrix $\boldsymbol{\Sigma_{wc}}$, which can be cast as:

$$\Phi_{M-s}(\boldsymbol{v}, \overline{\boldsymbol{w}} \mid \boldsymbol{v}) = \frac{1}{(2\pi)^{\frac{M-s}{2}} det(\boldsymbol{\Sigma_{wc}})} exp\left[\frac{(\overline{\boldsymbol{w}}-\boldsymbol{\mu_{wc}})^T \boldsymbol{\Sigma_{wc}^{-1}}(\overline{\boldsymbol{w}}-\boldsymbol{\mu_{wc}})}{-2}\right] \tag{4.29}$$

where

$$\boldsymbol{\mu_{wc}} = \boldsymbol{\mu_w} + \boldsymbol{\Sigma_{vw}}\boldsymbol{\Sigma_v^{-1}}(\boldsymbol{v} - \boldsymbol{\mu_v}) \tag{4.30}$$

$$\boldsymbol{\Sigma_{wc}} = \boldsymbol{\Sigma_w} - \boldsymbol{\Sigma_{wv}}\boldsymbol{\Sigma_v^{-1}}\boldsymbol{\Sigma_{vw}} \tag{4.31}$$

Thus the conditional sample vector $\overline{\boldsymbol{w}}$ which follows the (M-s)-dimensional condition distribution (Equation 4.29) can be computed through the Nataf transformation. Furthermore, the conditional sample vector of $\overline{\boldsymbol{v}}$ can be constructed following the same manner. Briefly, the procedures of generating the sets of ($\boldsymbol{v}$,$\overline{\boldsymbol{w}}$) and ($\overline{\boldsymbol{v}}$,$\boldsymbol{w}$) of normal random variables required respectively in Equation 4.24 and 4.25 are explained step by step in the study of Kucherenko et al. [Kucherenko et al., 2012]. Finally, the first as well as the total indices of the subset $\boldsymbol{v}$ can be assessed.

4.3 EI variability and uncertainty

In Section 3, we analyzed the level of human EMF exposure in view of existing 3G networks using the LEXNET EI. However, in its raw definition, EI is a complex index to evaluate. To achieve evaluating the average exposure and integrating the EI in different scenarios, many parameters influencing the exposure are taken into account, i.e., life segmentation data, reference SAR data, ICT usage data and network data.

In fact, studies analyzing the day-to-day exposure to EMF are facing the characterization and quantification of ICT usage data. Such information is fundamental to analyze the differences among mobile device usages. In addition, traffic load has a strong influence on emitted and received powers and network performances (e.g., mobile' throughput), all of them directly impacting the EI. Making things more complicated these influencing parameters (ICT usage data, emitted and received powers, mobile' throughput) should not be regarded as constant values but highly variable. As a consequence, how to manage uncertainties linked to these influencing parameters and how the EI varies due to these random parameters are the main issues. And finally, in order to simplify the EI, it is necessary to determine the impact of each input parameter on EI through a sensitivity analysis.

As presented in Section 3.3.2.4, emitted and received powers and mobile's throughputs have been simulated through a 3G radio network planning tool. This tool is based on a vast amount of data extracted from geographical area, building locations, network deployments, etc. It offers an accurate estimation of the network quality, the throughput, etc., while at the same time it requires a large amount of preparing and computing time. Hence, the approach of meta-modeling was used to model the emitted and received powers as well as mobile's throughput. The variability and uncertainties linked to these variables can thus be characterized and further used as inputs to evaluate the EI.

4.3.1 Meta-modeling of network data varying ICT usage data

4.3.1.1 Definition of input random variables and system outputs

The method of PC expansion has been applied in this part to predict outputs of a 3G radio network planning tool taking into account the variability of ICT usage data (information about this tool can be found in 3.3.2.4). These ICT usage data were obtained in one urban area through measurement probes installed in 3G Orange network as explained in 3.2.1. Usage data have been identified by 9 independent variables so as to represent differences among mobile phone usages in a comprehensive way. The input random vector involves:

– 3 variables for voice call durations, respectively for heavy, moderate and light users.
– 3 variables for data volumes per downlink session, respectively for heavy, moderate and light users.
– 3 variables for data volumes per uplink session, respectively for heavy, moderate and light users.

The classification of different user profiles, respectively heavy, moderate and light,

has been presented in section 3.2.3. Considering the effect of traffic variations over time, one day was segmented into 2 periods: day from 8 a.m. to 6 p.m. and night from 6 p.m. to 8 a.m. Usage statistics were gathered from live urban 3G networks in France for these 9 parameters in terms of day and night periods.

The outputs consist of the emitted power by mobiles (for both voice and data services), the received power from BTS and the mobiles' throughput in different environments (i.e., indoor and outdoor) during different periods (i.e., day and night).

4.3.1.2 Statistical characterization of input random variables

A first step before establishing an experimental design is to **characterize every input random variable through a probabilistic distribution**. Akaike Information Criterion (AIC) was implemented to characterize one variable by a distribution for its ability in encouraging the goodness of fit (by maximizing the likelihood value) while avoiding overfitting (by minimizing the number of estimated parameters). As shown in Figure 4.3a-1, the best fitted distribution for heavy users' voice call durations in daytime was found to be the Generalized Extreme Value (GEV) among some given statistical models (e.g., Normal, Lognormal, Weibull, Gamma, etc.). Finally, to judge the fitting quality, several statistical tests are available, e.g., Kolmogorov–Smirnov test, Quantile-Quantile (QQ) plot, etc. However, apart from that, the visual judgment (checking the fitting quality by the visual representation of law) is also valid. E.g., QQ plot offers a comparison between two probability distributions by establishing a graph of variable values of these two distributions with respect to different quantiles. As Figure 4.3a-2 depicts, the distribution of voice call duration during day time for heavy users and the GEV distribution provided by AIC are similar since the graph approximately lies on the line of y=x except at the end of graph. Nonetheless, this heterogeneity should be ignored when taking into account the probability of voice call durations close to 1000 s. In the same way, distributions followed by 9 variables in terms of day and night periods were characterized (Table 4.2).

4.3.1.3 Meta-modeling of system outputs

3G urban network scenarios as introduced in section 3.3.1 were implemented in the simulations. In view of enormous time consumed by one simulation run and output data processing, 50 simulations were executed respectively in case of day and night through LHS method (100 simulations in total). The system outputs for day time case (respectively night time case) is shown in Figure 4.4(a) (respectively in Figure 4.4(b)). Simulation results have shown a 20 dB difference between received power in the environment of indoor and outdoor. While for mobiles' emitted power, a maximal 15 dB difference was found between indoor and outdoor locations. It was also observed a difference of 4-7 dB between emitted powers by mobiles in data and voice services.

Consequently, these network data are more or less dependent on each other. The correlation among them can be expressed by Spearman correlation coefficient as introduced before. An example of Spearman correlation matrix of all output variables for day time case is given in Appendix A.1 (Figure A.1). It was observed that some variables are strongly correlated. Emitted and received powers

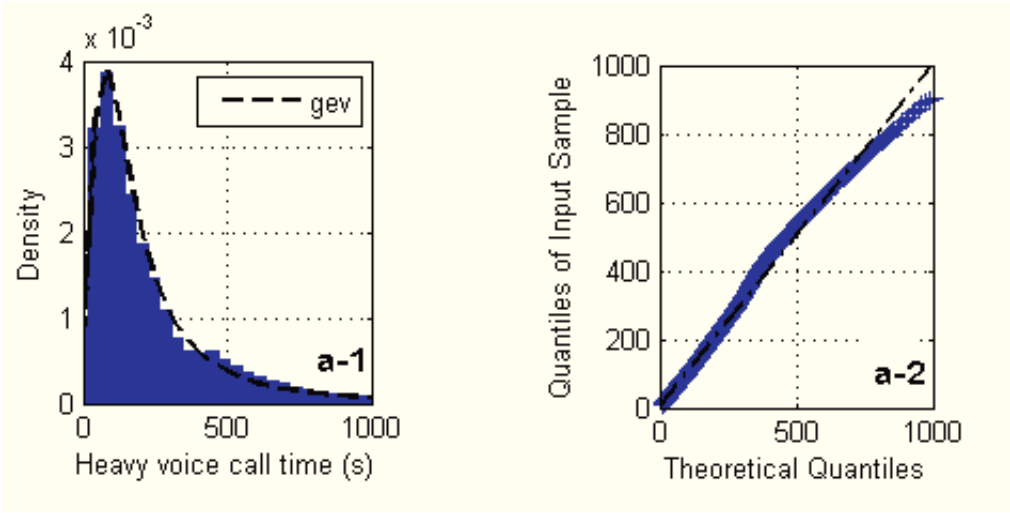

Figure 4.3: Probability Density Function and best fitted statistical model for the data set of heavy users' voice call durations during day time (a-1) and corresponding Quantile-Quantile plot test for its statistical model (a-2)

Table 4.2: Distributions of 9 input variables in terms of day and night periods

User profiles	Day[a] Voice (s)[c]	Data (kB)[d] UL[e]	DL[f]	Criterion
Heavy	gev[g](116, 106, 0.5) on [1, 3×10^4]	ln$\mathcal{N}$[j](5.02, 1.52^2) on [2, 2×10^5]	ln$\mathcal{N}$(6.79,1.57^2) on [13, 5×10^5]	QQ plot
Moderate	gam[h](1.75, 63) on [1, 499]	ln$\mathcal{N}(4.25, 1.25^2)$ on [2, 10^4]	ln$\mathcal{N}(6, 1.3^2)$ on [10, 1.7×10^4]	QQ plot
Light	wbl[i](32, 1.17) on [1, 118]	gev(8.66, 7.67, 0.86) on [1, 3×10^3]	gev(48, 39, 0.84) on [10, 2×10^3]	QQ plot
User profiles	Night[b] Voice (s)	Data (kB) UL	DL	Criterion
Heavy	wbl(343, 0.88) on [1, 4×10^4]	ln$\mathcal{N}(5.08, 1.56^2)$ on [2, 2.4×10^5]	ln$\mathcal{N}(6.87, 1.6^2)$ on [12, 3×10^5]	QQ plot
Moderate	wbl(120, 1.21) on [1, 498]	ln$\mathcal{N}(4.17, 1.32^2)$ on [2, 10^4]	ln$\mathcal{N}(5.91, 1.38^2)$ on [11, 2×10^4]	QQ plot
Light	wbl(31, 1.13) on [1, 118]	gev(8.71, 7.78, 0.87) on [2, 3×10^3]	gev(48, 39, 0.85) on [10, 2×10^3]	QQ plot

[a]Day, during day time from 8 a.m. to 6 p.m.
[b]Night, during night time from 6 p.m. to 8 a.m.
[c]Voice (s), voice call durations in seconds.
[d]Data (kB), data volumes per session in kilobyte.
[e]UL, uplink; [f]DL, downlink.
[g]gev(μ, σ, ξ), Generalized Extreme Value; [h]gam(k, θ), Gamma; [i]wbl(λ,k), Weibull; [j]ln$\mathcal{N}(\mu, \sigma^2)$, Lognormal.

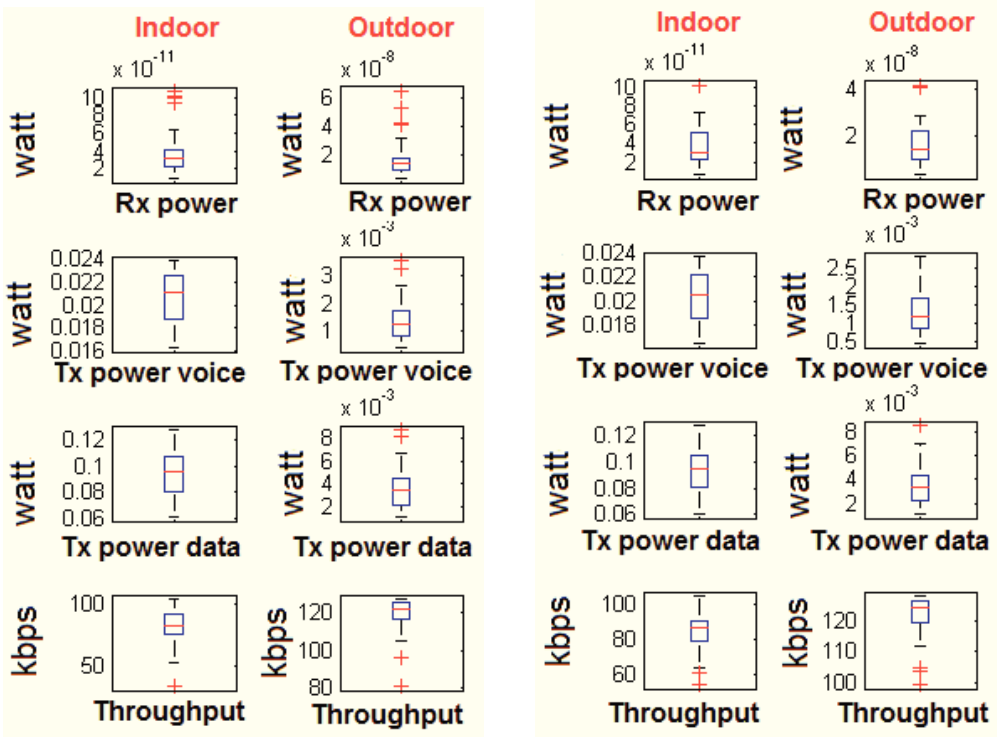

(a) Observations from 50 simulations in day time case

(b) Observations from 50 simulations in night time case

Figure 4.4: Received power from base stations, emitted power by mobiles in voice and data services and mobiles' throughput (uplink) in indoor and outdoor areas during day time (a) and night time (b)

and uplink throughput indoor were highly correlated to the ones outdoor (Spearman correlation coefficient was found to be more than 0.8). A strong correlation between emitted powers resulting from voice and data traffic, approximately equal to 0.99, was also measured. Similar results can be drawn for output variables for night time case.

Based on these observations, the meta-model was built for each one of the outputs with a maximum accepted degree of Legendre polynomials ($p \leq 15$). The choice of p is arbitrary depending on the desired accuracy of the PC expansion indicated by factor Q^2. A comparison between the empirical distribution obtained from network traffic simulations and the approximate one by the meta-model is illustrated in Figure 4.5. It was observed that the approximate distribution provided by the meta-model appears consistent with the one provided by simulations. One should also notice that the determination indicator Q^2 was estimated around 90%. Given the fact of the large number of input variables and the considered simulation runs, the quality of the meta-model is acceptable.

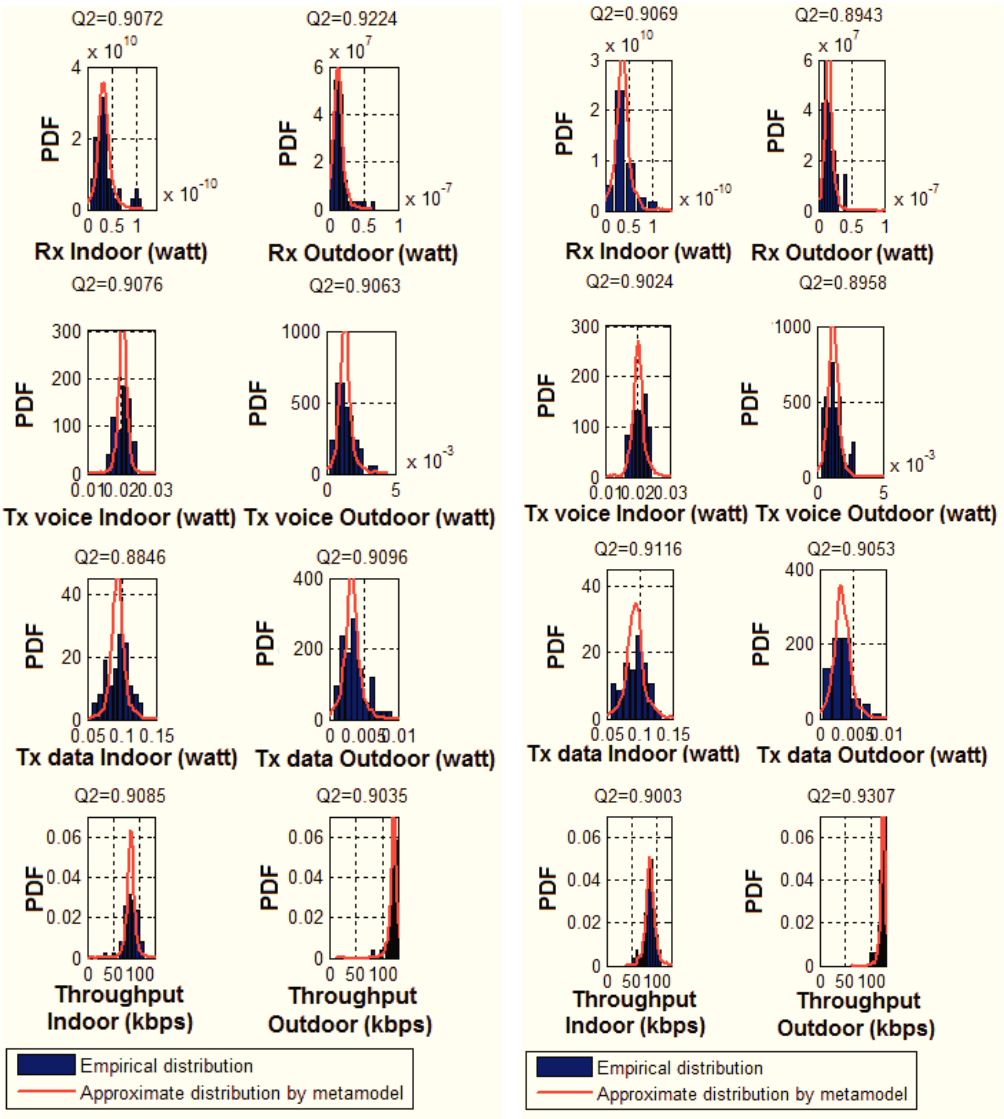

(a) Day time case (b) Night time case

Figure 4.5: Comparison between the empirical distribution obtained from simulations and approximate distribution obtained from meta-model

4.3.1.4 Usage of Meta-models

The network output data obtained by varying ICT usage data have been modeled through the approach of meta-modeling. **We were interested in distributions of different output variables representing network performances and further used in analyzing the variability of EI.**

10^4 executions were selected randomly for each output variable based on its corresponding meta-model. A comparison of statistical characteristics between observations from simulations and executions generated by meta-modeling for each variable was performed. Results have shown that diversities of traffic consumptions can impact the network performance. Coefficients of variation (CV) of received power were up to 50%. CV of emitted power by mobiles located outdoor were found to be

about 4 times higher than those evaluated indoor. Mobiles' throughput was found to be quite stable. Detailed information can be found in Appendix A.2 (Table A.1).

In addition, a statistical model was selected for each variable based on the 10^4 executions. As shown in Table 4.3, e.g., the power emitted by mobile devices located indoor in voice usage during day time can be characterized by the normal distribution with R^2 equals to 0.95. R^2, ranging from 0 to 1, is used to determine the degree of correlation between the empirical data distribution and a law of statistics. The higher is the value, the better is the fit. All statistical distributions are presented in Appendix A.2 (Table A.1).

4.3.2 EI Variability

To assess the variability of EI with respect to ICT usage data and network data, the Monte Carlo method was adopted. It is important to note that the dependence exists between some network data (Figure A.1). Therefore, the dependence among these variables was modeled using Normal copulas as presented in Section 4.2.1.3. ICT usage data considered in the EI evaluation include only the total uplink traffic usage (for both voice and data) during day and night periods. The results of adjustments of different statistical laws for ICT usage variables are presented in Table 4.4.

Table 4.3: Statistical characteristics of power emitted by devices located indoor in voice usage during day time

During day time from 8 a.m. to 6 p.m.			
	50 observations	10^4 executions	Statistical model selection
	Tx[a] power voice Indoor		$\mathcal{N}(\mu, \sigma)$
Mean (W)	0.0206	0.0207	$\mu(10^{-2})$ $\sigma(10^{-3})$
Standard deviation	0.0021	0.0015	2.07 1.45
CV[a]	10%	7%	$R^2 = 95\%$

[a]Tx, emitted
[b]CV, Coefficients of variation

Table 4.4: Distributions of ICT usage variables considered in EI evaluation

	Day[a]		
	Voice (s)[c]	Data (kB)[d]	
User profiles		UL[e]	Criterion
Heavy	gev[f](512, 453, 0.36) on $[1, 4 \times 10^4]$	wbl[g]$(3.79 \times 10^3, 0.64)$ on $[2, 2 \times 10^6]$	QQ plot
Moderate	gev(157,89, -1.56) on [1, 499]	wbl(590, 0.97) on $[2, 2 \times 10^4]$	QQ plot
Light	wbl(41, 1.21) on [1, 118]	ln$\mathcal{N}$[h]$(3.13, 1.3^2)$ on $[1, 3 \times 10^3]$	QQ plot
	Night[b]		
	Voice (s)	Data (KB)	
User profiles		UL	Criterion
Heavy	wbl(904, 0.88) on $[1, 4 \times 10^4]$	wbl$(4.5 \times 10^3, 0.63)$ on $[2, 2 \times 10^6]$	QQ plot
Moderate	wbl(192, 1.55) on [1, 498]	wbl(541, 0.92) on $[2, 2 \times 10^4]$	QQ plot
Light	wbl(38, 1.16) on [1, 118]	ln$\mathcal{N}(3.13,1.31^2)$ on $[2, 3 \times 10^3]$	QQ plot

[a]Day, during day time from 8 a.m. to 6 p.m.
[b]Night, during night time from 6 p.m. to 8 a.m.
[c]Voice (s), voice call durations in seconds.
[d]Data (kB), data volumes per session in kilobyte.
[e]UL, uplink.
[f]gev(μ, σ, ξ), Generalized Extreme Value; [g]wbl(λ,k), Weibull; [h]ln$\mathcal{N}(\mu, \sigma^2)$, Lognormal.

10^6 sample sets were taken into account to guaranty the large amount of simulations required by Monte Carlo method. To this end, a Quasi-random sampling of Sobol sequence was carried out for all input variables (28 variables in total). Executions of input variables were thus obtained based on their inverse CDF by using the sampling data (probability distributions can be found in Tables A.1 and 4.4). Finally, aggregating all executions of input variables by using the EI equation, we were able to evaluate the global exposure of a population in an urban area considering a macro 3G network.

The mean estimated central tendency and 95% confidence interval as a function of simulation iterations is given in Figure 4.6. It was observed that the results were convergent after 4×10^5 simulations. The average global exposure was finally convergent to 2.42×10^{-7} W/kg. The median value of global exposure was about 1.92×10^{-7} W/kg, while the 0.9 quantile was found to be 4.48×10^{-7} W/kg. One can notice that all these values are far below international standard limits for human exposure. The PDF and CDF of global exposure obtained from 10^6 runs are shown in Figure 4.7. The distribution of global exposure follows the statistical law of GEV. Moreover, the CV, equal to 73%, was calculated by dividing the standard deviation by the corresponding average value. The important variation shows that the global exposure is very sensitive to the variability of ICT usage and network data.

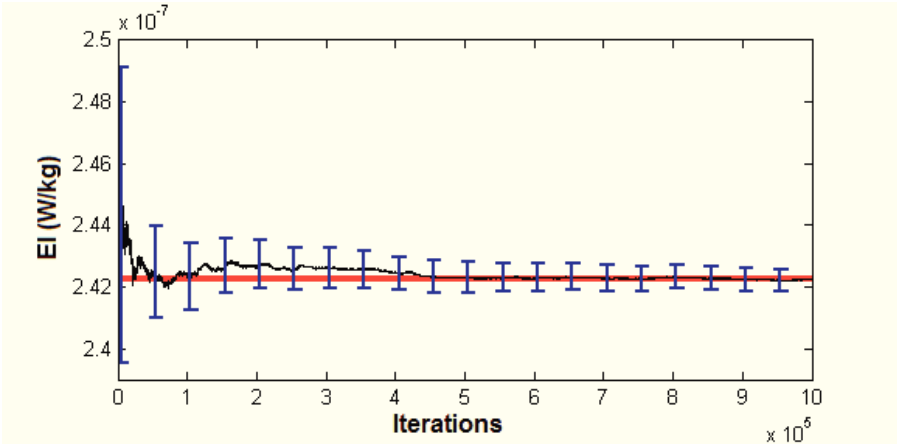

Figure 4.6: Mean estimated central trend of EI ($2.42 \times 10^{-7}\ W/kg$) and 95% confidence interval as a function of simulation iterations

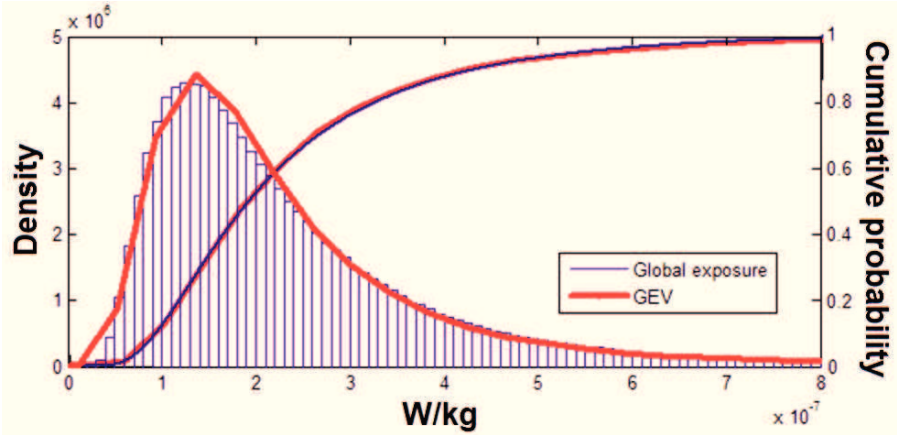

Figure 4.7: Distribution and Cumulative Density Function of EI values provided by 10^6 simulations. The distribution of EI follows the statistical law of GEV

4.4 Global sensitivity analysis

A sensitivity analysis was carried out to assess the influence of input parameters on EI considering the dependence among network data. Variance based sensitivity indices of Kucherenko (see Section 4.2.2.2) were used. Indices of Kucherenko were evaluated based on 10^6 Monte Carlo simulations.

Figure 4.8 shows sensitivity indices of first order for all inputs for both day and night periods. It was clearly observed that the **uplink data traffic generated by heavy users influences significantly the 3G global exposure** (Figure 4.8a). The corresponding first order index of heavy uplink data traffic equals to 35% for the day period, and 49% for the night period. The influence of uplink data traffic on the global exposure is due to the **limited uplink throughput provided by 3G network**. The great amount of data traffic generated by heavy users with the slow uplink throughput leads to long durations of emissions, which are important in the evaluation of global exposure. In addition, it was found that the global exposure is also affected by **heavy users' voice usage durations**. As shown in

Figure 4.8a, the first order index of voice usage durations for heavy users during day time was found to be 6% while 4% during night time, which make them respectively third and fourth. Indeed, the first index for heavy uplink data traffic is almost 10 times the index calculated for heavy voice traffic.

Furthermore, mobile usage traffic (for both voice and data modes) generated by moderate and light users influence slightly the global exposure compared to traffic generated by heavy users. **As a consequence, it is not essential to classify mobile users into three profiles, which adds complexity to EI metric**. We were also aware from these results that **downlink EM radiations from BTS less influence the global exposure than uplink EM radiations from mobile devices** (Figure 4.8b). The powers emitted by mobiles respectively in voice and data usages have almost the same influence on overall exposure. Figure 4.8b illustrates that indices of first order for network data were around 1%, which is far below the ones for ICT usage data for heavy users.

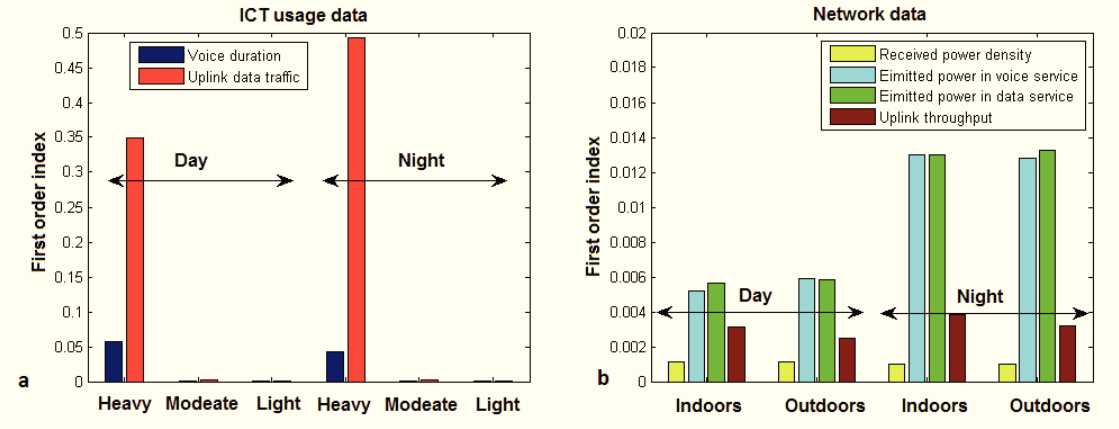

Figure 4.8: Kucherenko first order indices of input parameters (a: 12 ICT usage parameters and b: 16 network parameters) to quantify uncertainties linked to EI obtained from 1000000 simulations

To quantify the contribution of interactions among input parameters on the variance of global exposure, total indices of Kucherenko were evaluated (Figure 4.9). As depicted in Figure 4.9a, it was clearly shown that total indices of uplink data traffic for heavy users (for both day and night periods) were higher than total indices of other parameters. In addition, compared to Figure 4.8a, only a small difference exists between first and total indices of uplink data traffic for heavy users. Hence a small interaction exits between heavy uplink data traffic and other parameters. As for total indices of network data, it was observed that their total indices (Figure 4.9b) were very small. This can be explained by the effect of correlation between input variables. As proven by Kucherenko [Kucherenko et al., 2012], the relationship between the first order and total indices changes with the correlation coefficient. Total indices get close to zero as correlation coefficient gets close to 1 (or -1).

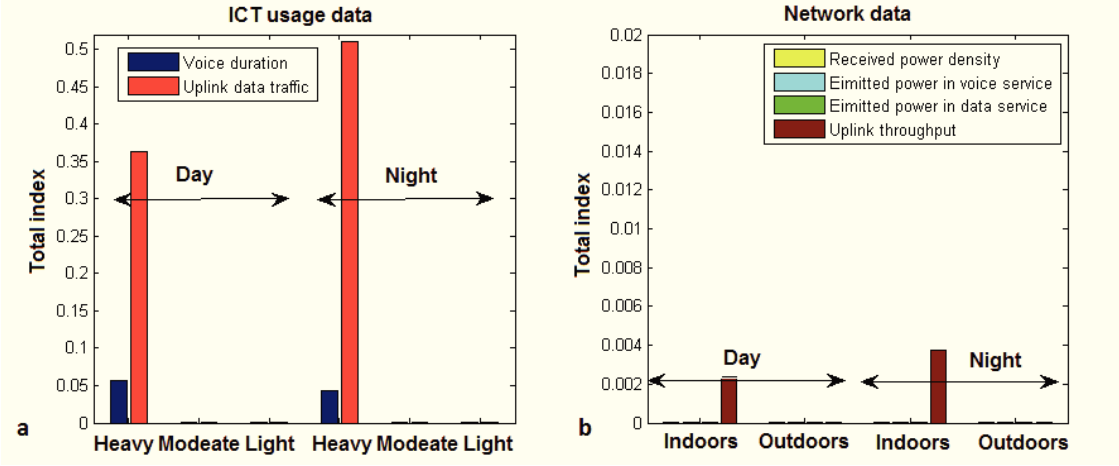

Figure 4.9: Kucherenko total indices of input parameters (a: 12 ICT usage parameters and b: 16 network parameters) to quantify uncertainties linked to EI obtained from 1000000 simulations

4.5 Discussion and conclusion

This chapter presents an assessment of global population exposure to RF-EMF from dense 3G networks through the EI approach and taking into account the variability linked to ICT usage data, emitted and received powers respectively by mobiles devices and from BTS, and uplink throughput. To do so, statistical methods dedicated to the uncertainty propagation were used.

First, surrogate models were built in order to predict exposure parameters dedicated to EMFs and network performances, such as emitted and received powers and uplink throughput, using the method of PC expansion. Then, by varying these exposure parameters as well as the ICT usage data, the uncertainties of global EMF exposure of a population in urban area have been characterized through the approach of Monte Carlo. Results have shown that the global EMF exposure distribution follows the GEV distribution. The global EMF average exposure was finally convergent to $2.42 \times 10^{-7} W/kg$. Its 0.9 quantile value was estimated to $4.48 \times 10^{-7} W/kg$. It is important to note that these values are far below the international standard limits. In addition, the global EMF exposure was found very sensitive with a CV of 73%.

A sensitivity analysis was carried out to determine the effect of input parameters to the issue of global EMF exposure of a population induced by a macro 3G network. It was found that the heavy usage traffic, especially, the uplink data traffic has a dominant impact on the global EMF exposure. Uplink data traffic's first order indices for respectively day and night periods were evaluated to 35% and 49%. And these values were found to be almost 10 times the first order indices calculated for heavy voice traffic. This can be explained by the effect of the limited upload speed provided by 3G network. As a result, the LEXNET EI can be simplified by considering only two different ICT user profiles: heavy and non-heavy. Moreover, results have also shown that downlink EM radiations from BTS less influence the global exposure than uplink EM radiations from mobile devices in the context of 3G network.

However, as presented in this chapter, emitted and received powers as well as uplink throughput have been assessed only taking into account the variability of ICT usage data. As a matter of fact, propagation environment also plays a significant role in assessing these data. The impact of propagation environment, in other words, **the impact of building and field data in RF waves propagation should also be considered in charactering the variability of network data**. Moreover, we have seen that, due to limited 3G upload speeds, heavy uplink data traffic have a major influence on the global exposure to a 3G network. Nowadays, to meet high QoS and high traffic capacity, LTE networks have been deployed worldwide. As a result, **uplink peak rates provided by LTE** can reach up to 75 $Mbit/s$. We therefore propose in the next chapter to apply the advanced statistical methods to a simplified assessment of population exposure induced by a LTE Network.

5

Surrogate EMF exposure model

Contents

5.1 Context

So far the EI had been evaluated using a deterministic approach, whether for a scenario involving an LTE network [Varsier et al., 2015b], or to explore the level of human EMF exposure in view of existing 3G networks (Section 3) In these studies, for specific geographical areas (e.g., Paris seventh district, Lyon city) precise attenuation maps were considered using a complex deterministic propagation model (e.g., Siradel Volcano model, MYRIAD model). Such deterministic model can be time consuming in terms of calculation and strongly dependent on detailed building and field data. As a matter of fact, RF wave propagation in a geographical area plays a very important role in assessing received and emitted powers, respectively, from BTS (or E-UTRAN Node B, also known as Evolved Node B (eNB)) and by wireless devices. Meanwhile, geographical data differ from one city to another. **Thus, one of the main issues of assessing an EM attenuation map lies in the integration of the variability of a geographical area topology into the propagation model.**

In addition, **received and emitted powers and network performances also depend on the traffic load** [Huang et al., 2014]. As shown in the previous chapter, ICT usage data are fundamental in the evaluation of a global EMF exposure to a wireless network.

As reported by Cisco [Cisco, 2016], in 2015, the **4G traffic** exceeded for the first time the 3G traffic. Although 4G connections represented only 14% of mobile connections in 2015, whereas, they accounted for 47% of mobile data traffic. A 4G connection generates more than 6 times the traffic generated by a non 4G connection. It was therefore important to analyze the EMF exposure induced by such a network and to do so to collect and characterize ICT usage data generated by a 4G network.

Hence, **this chapter aimed at introducing a simplified way via a surrogate modeling to evaluate the EI generated by a 4G network in order to characterize the day-to-day EMF exposure of a population taking into account the variability and uncertainties linked to geographical environment specificities, ICT usage data and EMF radiations originating from personal wireless devices and eNB**. To this end, advanced statistical methods were applied to a simplified assessment of a population EMF exposure induced by LTE networks.

The EI for LTE macro scenarios is described at the beginning of Section 5.2. Then Section 5.3 focuses on a statistical approach to explore the distribution of the Path Loss Exponent (PLE) due to the influence of propagation environment using stochastic city models. This distribution is further used as one of the inputs to a simplified LTE network traffic simulator. Based on this simulator, network data such as emitted and received powers and uplink throughput are obtained and statistically analyzed by varying PLE and ICT usage data. Then, in Section 5.5, the variability of EI is characterized in terms of ICT usage data and network data using Monte Carlo simulations. In addition, the importance of each input parameter on the EI is assessed by a variance-based sensitivity analysis. We conclude in the last section.

5.2 EI for an LTE macro scenario

An EI evaluated over 24 h for an entire population exposed to a LTE macro network in a dense urban area was considered. As illustrated in Figure 5.1, complex sets of data is aggregated in the chain of exposure and averaged over time period T (24 h). All categories of population and two user profiles (heavy and non-heavy) were taken into account considering a mobile phone usage in data service (Figure 5.1). The formalization of the EI metric passed through the characterization of variability and uncertainties linked to input parameters, which are life segmentation data, ICT usage data, network data and a set of EMF exposure values for typical postures and usages of mobile devices.

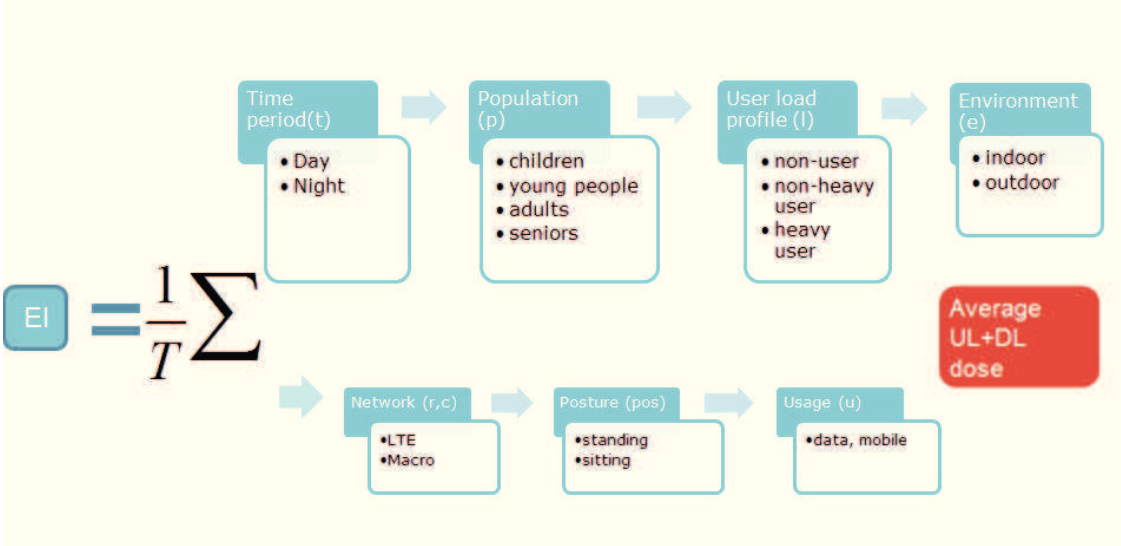

Figure 5.1: The LEXNET chain of exposure for a LTE macro scenario

Up-to-date life segmentation data collected from surveys performed in different European countries were used to identify the time spent in different environments and for different categories of population (Table 3.6).

An urban area in the North of Paris was monitored to collect the real-life mobile usage data in a LTE Orange network. Total data traffic volumes generated by all the users connected to the monitored eNB (258 eNB in total) were recorded during one busy hour of a day for the whole month of June in 2014. Since the traffic generated during one busy hour represent only a part of the daily traffic, in order to get the daily traffic, we multiplied this hourly traffic by a factor 3 (this factor was derived from the measurements presented in [Korowajcznk, 2014]). Based on these collected data, two user profiles, respectively, heavy and non-heavy were defined. Figure 5.2 corresponds to the classification of users. Heavy users are those consuming 80% of the total amount of data traffic. The rest of users, consuming 20% of the total data, are regarded as the non-heavy users. The results of adjustments of statistical laws for the heavy (Figure 5.3) and non-heavy (Figure 5.4) data traffic are shown in Table 5.1. Furthermore, a downlink/uplink traffic ratio of 90/10% was evaluated, and a day/night ratio of 43/57%. 14% of mobile users were reported using LTE network [Cisco, 2016].

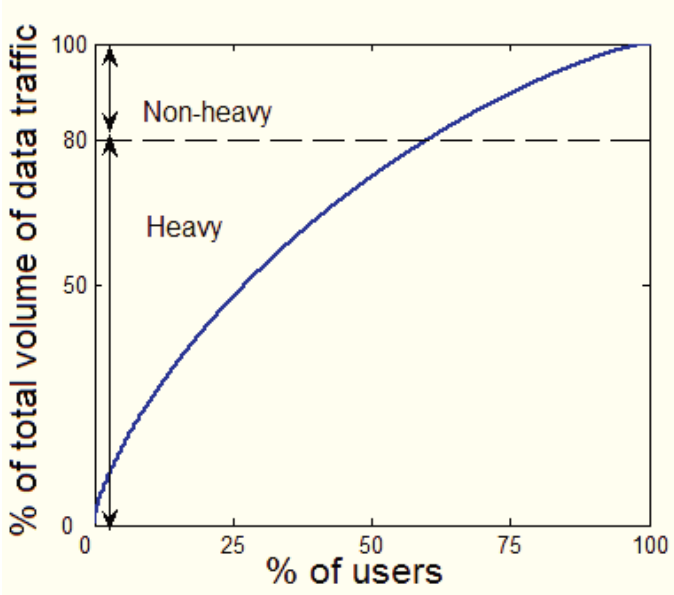

Figure 5.2: Percentages of total volume of data traffic versus percentages of users defining two user profiles based on the data collected from monitored LTE networks in the North of Paris

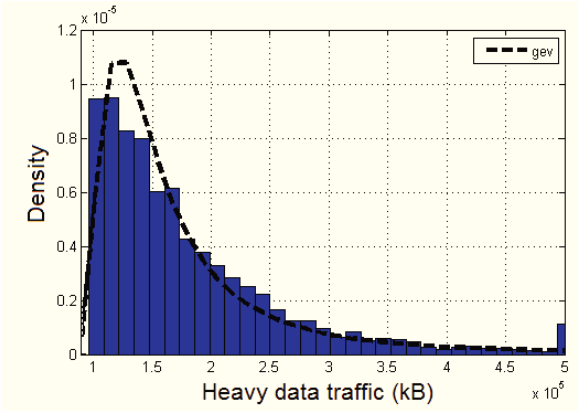

Figure 5.3: PDF of data traffic (kB) generated by heavy users during a busy hour following the distribution of Generalized Extreme Value (GEV)

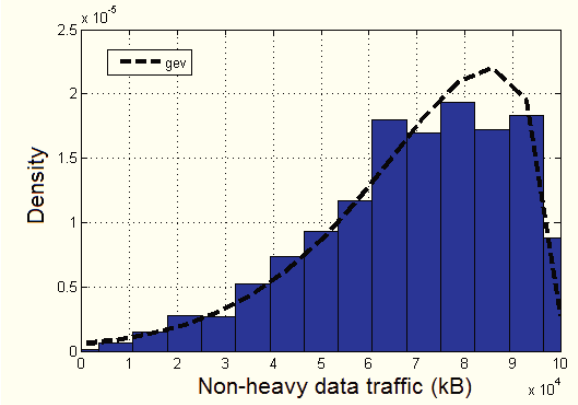

Figure 5.4: PDF of data traffic (kB) generated by non-heavy users during a busy hour following the distribution of Generalized Extreme Value (GEV)

Table 5.1: Distributions of ICT usage variables for an LTE macro scenario

User profiles	Data (kB)[a]	Criterion
Heavy	gev[b](1.35×10^5, 3.72×10^4, 0.53)	QQ plot
Non-heavy	gev(6.66×10^4, 2.32×10^4, -0.69)	QQ plot

[a]Data (kB), total data volumes during busy hour in kilobyte.
[b]gev(μ, σ, ξ), Generalized Extreme Value.

Table 5.2 presents the proportions of users (respectively heavy and non-heavy users) and non-users of mobile phones in data service per population category [Bigot et al., 2013]. The repartition of the population is given in Table 5.3 [Website Cartesfrance.fr,

Table 5.2: Proportions of users of mobile phones in data service per population category

Mobile phone user	Children	Young	Adults	Seniros
Non-user	45%	33%	59%	90%
Heavy user	27.5%	33.5%	4%	0.5%
Non-heavy user	27.5%	33.5%	37%	9.5%

Table 5.3: Repartition of the population

Population category	Percentage
Children	15.4%
Young	34.7%
Adults	36.3%
Seniors	13.6%

In addition, whole-body SAR values induced by LTE mobiles and eNB for adult and child for a data usage were extracted from values calculated in the framework of LEXNET [Varsier et al., 2015a]. Network data were simulated through a LTE network traffic simulator varying path loss exponent and ICT usage data.

It is important to note that the parameters e.g., **ICT usage data, network data have a strong variability**, which is why we proposed to go through a sensitivity analysis assessing the impact of these parameters on EI. In order to characterize the variability of network data, the uncertainties linked to the PLE had to be first assessed. **In the next section, we focus on a statistical approach to explore the distribution of PLE in urban environments**.

5.3 Statistical analysis of path loss exponent in urban environments

Propagation model is one of the significant issues in assessing received and emitted powers. One of the major challenges in propagation modeling is the

integration of influences of building and field data into RF waves propagation. Theoretically, the propagation modeling can be approximated by signal attenuation as a function of the geographical distance between the transmitter and the receiver. In practice, the signal strength can be modeled as a function of $\frac{1}{d^{\alpha}}$, where d is the geographical distance between two nodes and α is the PLE. Based on that, the path loss model can be characterized as follows:

$$P(d) = \beta - 10\alpha log_{10}(d) + \chi \tag{5.1}$$

where P is the received power in dB, χ is assumed to be a Normal random variable with zero mean and σ^2 variance. According to the Equation 5.1, let $\mathbf{P}$ denotes a vector of received powers based on the corresponding vector $\mathbf{d}$ of distances. With the help of the least square solution of the linear system, the two parameters α and β verify:

$$[\alpha\ \beta]^T = (\mathbf{A}^T\mathbf{A})^{-1}\mathbf{A}^T\mathbf{P} \tag{5.2}$$

with $\mathbf{A} = [-10log_{10}(\mathbf{d})\ \mathbb{1}_\ell]$, $\mathbb{1}_\ell \in \mathbb{R}$ the first column vector.

The PLE value is an indicator of how fast the energy is attenuated between the transmitter and the receiver (e.g., α equals to 2 in free space). A summary of PLE values for diffrent propagation environments derived from [Gibson, 2012] is given in Table 5.4. As can be seen from the table, **the PLE value varies widely across propagation environments**. Therefore, the variability linked to the propagation environment should be characterized.

Table 5.4: Path loss exponent (PLE) values for different propagation environments

Propagation environments	PLE values
Urban area cellular network	2.7 - 4
Shadowed urban area cellular network	5 - 6
Line-of-sight propagation in building	1.6 - 1.8
Obstructed in building	4 - 6
Obstructed in factories	2 - 3

5.3.1 Stochastic city models

To cover the variability of topologies that would be observed among urban cities, stochastic geometry was used in modeling field topology and building distribution. As presented in the study of Courtat [Courtat et al., 2016], the building deployments in cities can be modeled by using crack STIT tessellations parameters. Three dimensional (3D) models were built randomly based on main features of a typical urban city. Parameters used to build stochastic city models, e.g., anisotropy ratio, mean building block area, mean street width, mean building height and other parameters can be found in Table 5.5. Figure 5.5 illustrates an example selected from 3D urban-based city samples.

Thus, in the next section, **instead of determining the precise EM propagation attenuation for a particular city, a statistical approach was proposed to explore the PLE due to the influence of propagation environment using stochastic city models**. EM attenuation map related to each urban-based city sample was obtained through a 3D ray tracing simulator.

Table 5.5: Mean values for morphological features of a typical urban city

Parameters	Mean values	Reference
Street width	14 m	values of 2 way roads with sidewalks derived from [Long et al., 2003] and [Website Accomplir.asso.fr, 2011]
Building height	15 m	[Website Wikipedia.org, 2016]
Building facade	50 m	
Anisotropy	0.7	manathan=1

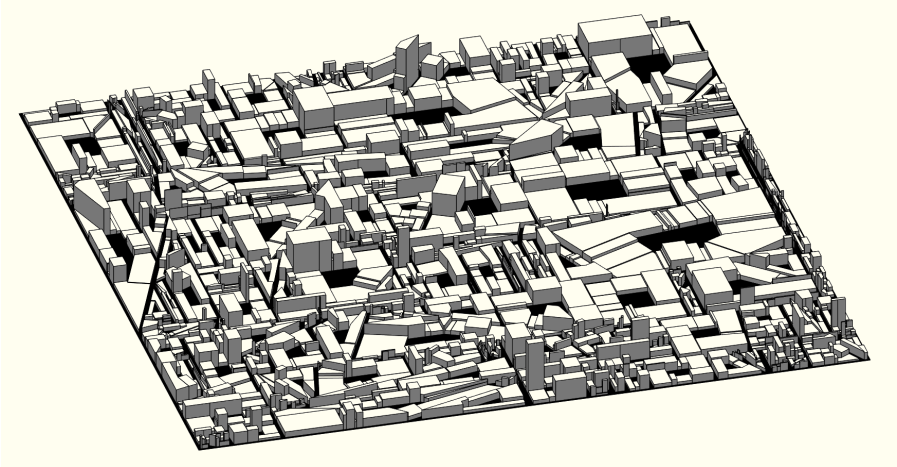

Figure 5.5: Example of a 3D stochastic city model

5.3.2 3D ray tracing simulator

A ray tracing technique was used to obtain the signal attenuation map for each stochastic city model. Ray tracing is often used to propagate EMF in urban area [Wiart, 1996, Courtat et al., 2016]. A new approach has been developed using stochastic city model [Frederic et al., 2016]. In a given stochastic city model, an antenna of total incident power P_0 has been placed in the center of the city, i.e., on top of the nearest roof to the central coordinate (0,0). N rays were launched from the source in the sphere portion Ω parametrized by $[\theta_0 - d\theta, \theta_0 + d\theta] \times [\varphi_0 - d\varphi, \varphi_0 + d\varphi]$ (Figure 5.6). The directions of rays were sampled by LHS. An illustration is shown in Figure 5.7 for launching 10 rays.

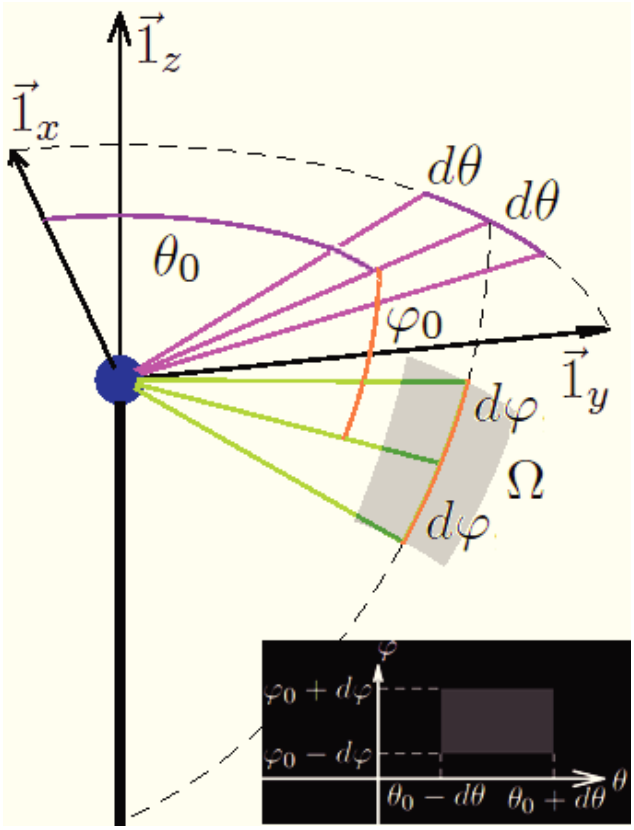

Figure 5.6: Illustration of angular parameters of the source. The grey surface Ω represents a portion of the source as a unit sphere captured by the spherical coordinates $(\theta_0 \pm d\theta, \varphi_0 \pm d\varphi)$

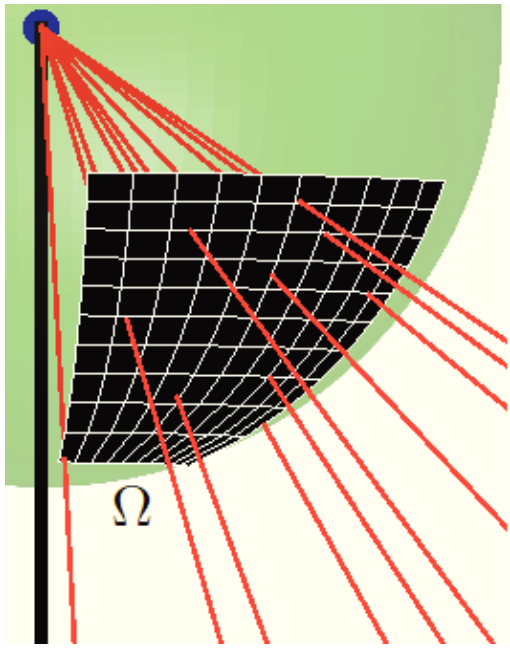

Figure 5.7: LHS sampling of 10 rays (red lines) crossing the sphere portion Ω defined by the angular parameters of the source

When hitting a surface, rays produce reflection and diffraction, and a portion of their power is absorbed by the surface. By summing up all the rays that hit the measurement plane (1.5 m above the ground), the signal attenuation map can thus be obtained.

Briefly, with the help of the ray tracing simulator presented above, instead of determining the precise EM propagation attenuation for a particular city, a statistical approach was proposed to explore the PLE due to the influence of the propagation environment using stochastic city models. According to the morphological features of a typical urban city defined in Table 5.5, 500 city models were built randomly. An EM power map related to each urban-based city sample was thus obtained through the algorithm developed in the ray tracing simulator. Finally, via Equation 5.2, the typical urban PLE was obtained using the EM power map. Antenna and simulation parameters used in the simulations can be found in Table 5.6.

Table 5.6: Summary of antenna and simultion parameters used in the simulations

Parameters	values
Simulation window	1000 m
Total incident power of the antenna P_0	40 W
Horizontal aperture	120°
Vertical aperture	30°
Frequency (LTE)	2600 MHz
Number of rays used in a simulation	2×10^6
Number of maximal reflections per ray	100
Power gain after a refection	-3 dB

Results from 500 simulations show that the average value of urban-based PLE was found to be equal to 4.2. Figure 5.8 corresponds to its distribution. It was observed that PLE of a typical urban city follows the Gamma distribution($k = 12.5$, $\theta = 0.34$) with R^2 equals to 0.99. This distribution was further used as input to a simplified LTE network traffic simulator.

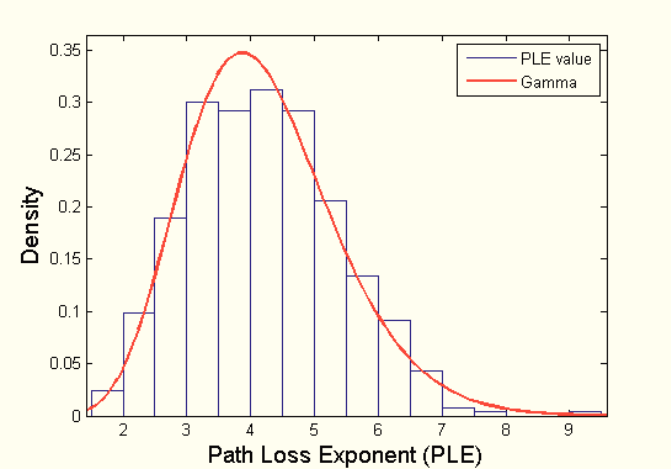

Figure 5.8: Distribution of urban-based path loss exponents

5.4 Influence of path loss exponent and ICT usage on network data

5.4.1 Simplified LTE network traffic simulator

To assess the network data taking into account the influence of PLE and ICT usage, a simplified LTE network traffic simulator was developed in Matlab based on the study of Sidi et al. [Sidi et al., 2014]. In this simplified network traffic planning tool, the general Log-distance propagation model with correlated shadowing was implemented:

$$PL = \frac{K\chi}{d^{\alpha}} \tag{5.3}$$

where K is a correction parameter to further adapt the pathloss model, α denotes the PLE, d is the distance between the emitter and receiver, χ is due to the slow fading effects following the log-normal distribution (standard deviation = 4 dB).

The actual emitted power over a time interval by an eNB was configured by taking a load factor [Saker et al., 2012]:

$$P_{eNB}(\Delta T) = L(\Delta T) \cdot P_{eNB}^{max} \tag{5.4}$$

where $L(\Delta T)$ is the downlink load in the considered cellular averaged over ΔT and P_{eNB}^{max} is the maximum emitted power by a eNB equal to 46 dBm.

When considering uplink transmissions, a power control loop was used to set the transmitted power by the User Equipment (UE) (Equation 5.5). In general, the uplink power control loop consists of an open-loop correction term [Castellanos et al., 2008] based on the signal strength received by the UE as well as a closed-loop term based on the measurements done by eNB [Simonsson and Furuskar, 2008].

$$P_{UE} = min\{P_{UE}^{max}, \overbrace{P_0 + 10log_{10}(M) + a \cdot 10log_{10}(PL)}^{open-loop\ correction\ factors} + \underbrace{\Delta_{mcs} + f(\Delta_r)}_{closed-loop\ correction\ factors} \} \tag{5.5}$$

However, as explained in [Sidi et al., 2014], only the open-loop factors were considered since they have the dominant effect to the emitted power. In the Equation 5.5, P_{UE}^{max} is maximum emitted power by mobiles (24 dBm), M is the number of assigned Physical Resource Blocks to a certain users, PL denotes the estimated pathloss, P_0 is a cell specific parameter related to target received power at eNB and a is the cell specific pathloss compensation factor. (P_0, a) will significantly impact the inter-cell interference [Góra et al., 2010]. The choice of (-80 dBm, 0.8) was derived from the study of Góra [Góra et al., 2010] according to the performance of the network.

5.4.2 Simulation scenario description

The main inputs of this network traffic simulator are the PLE value and the traffic configuration. Outputs consist of uplink transmitted power and throughput by mobiles in data usage as well as downlink received power over all the covered geographical area. Two different user profiles, respectively heavy and non-heavy, were considered in the traffic configuration with different repartitions. For each user profile, the data volumes were obtained through statistical analyses of mobile usage data. The traffic was uniformly distributed within the simulation area without considering users' mobility. Macro eNB (each with 3 sectors) are deployed hexagonally with an inter-site distance of 500 m. 57 sectors were simulated in the simulation, while statistics were derived only from the three sectors of the central macro-site (Figure 5.10).

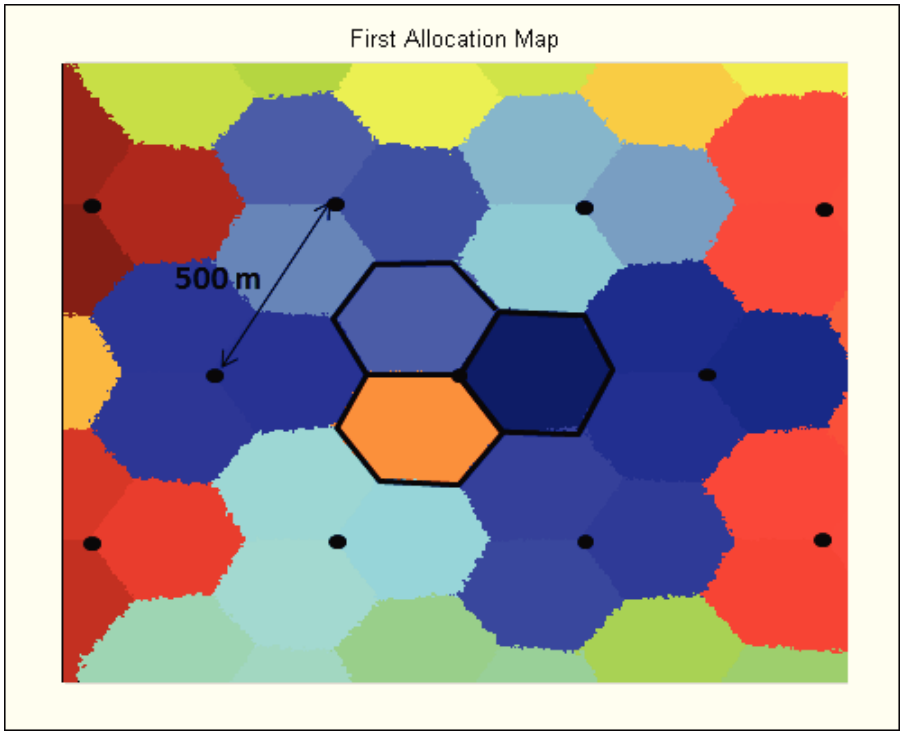

Figure 5.9: Allocation map of the deployment of macro LTE network with 500 m inter-site distance (path loss exponent equals to 4.2 was considered)

Results such as downlink received and uplink emitted powers and uplink throughput were obtained by varying PLE values and data traffic consumed for each user profile (respectively, heavy and on-heavy). The Aeff equals to $A_{eff} = \frac{G \times (c/f)^2}{4\pi}$, where $G = 1$, $c = 3 \times 10^8\ m/s$, $f = 2600\ MHz$ is considered. The A_{eff} value leads to quantify the corresponding received power density. 1000 runs were simulated based on an experimental design of the input random variables generated through a LHS.

Figure 5.10 shows the results. For the sake of clarity, the emitted and received powers have been expressed in dBm. Simulation results show a 10 dB difference between received power in indoor (5.10a) and outdoor (5.10b) environments while for mobiles' emitted power, a maximum of 9 dB difference (3 dB in average) is observed

between indoor (5.10c) and outdoor (5.10d) locations. It was clearly observed from Figure (5.10c-d) that the emitted power by devices in data service is important. The average emitted power was approximated to its maximum power. However, from the results, it was found that a strong relationship exists between some output parameters. E.g., emitted and received powers and uplink throughputs indoor were highly related to the ones outdoor (Spearman correlation coefficient was found to be more than 0.98). Furthermore, a strong correlation was observed between the emitted power and received power (Spearman correlation coefficient was around 0.97).

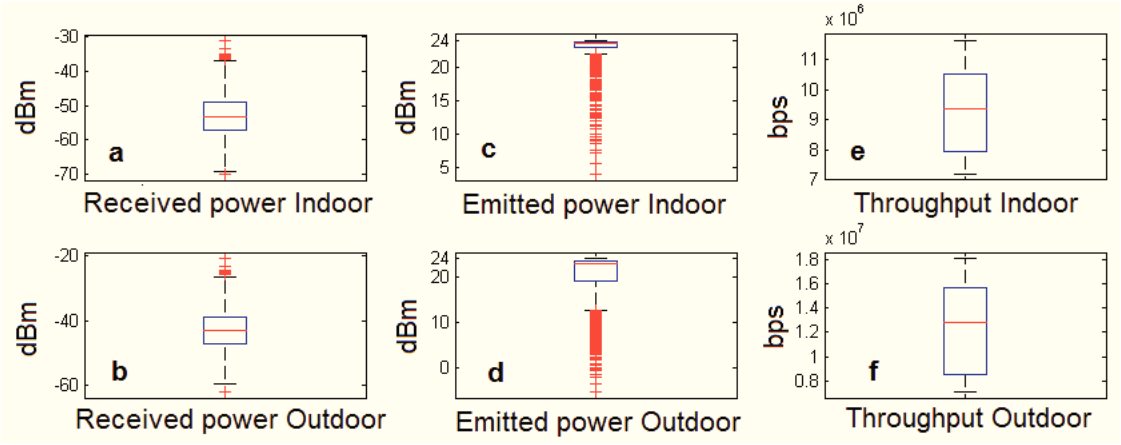

Figure 5.10: Received power from eNB, emitted power by mobiles in data service and mobiles' uplink throughput in indoor and outdoor environments

5.4.3 Statistical prediction of network data using Polynomial Chaos expansion

In addition, we were interested in the distributions of network data that are further used in analyzing the variability of EI. To achieve this objective, an advanced statistical method of PC expansion based on LARS, as introduced in Section 4.2.1.2, was used to predict the random system response (network data), according to the random input variables, such as PLE and ICT usage data. 1000 simulation results were used to build the meta-models for network data. A comparison between the empirical distribution of network data from traffic simulations and the approximated distribution obtained by meta-model is illustrated in Figure 5.11. It was observed that the approximate distribution by meta-model appears consistent with the one provided by simulations. The determination indicator Q^2 was estimated around 0.99. 10^4 executions were thus randomly generated for each output according to the corresponding meta-model. The results of adjustments of statistical laws for network data are shown in Figure 5.11. One should note that, according to the statistical test, the distribution for the uplink throughput may be approximated by a combination of three Gaussians (Figure 5.11). Table 5.7 corresponds to the detailed information about the statistical laws followed by network data.

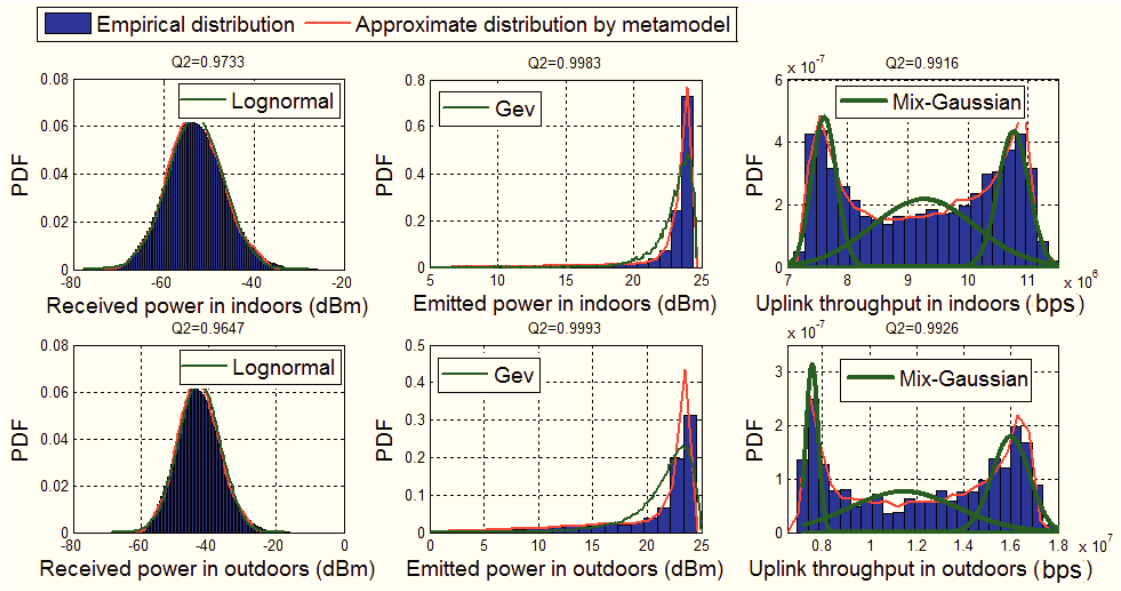

Figure 5.11: Comparison between the empirical distributions obtained from simulations and distributions obtained from meta-models and corresponding statistical distributions

Table 5.7: Distributions of ICT usage variables considered in EI evaluation

Network Data	Distribution	Criterion
Rx[a] Indoor (mW)	$\ln\mathcal{N}$[c](-12.2, 1.4^2)	$R^2 = 90\%$
Rx Outdoor (mW)	$\ln\mathcal{N}$(-9.9, 1.4^2)	$R^2 = 91\%$
Tx[b] Indoor (mW)	gev[d](198,57.7, -6.2)	$R^2 = 88\%$
Tx Outdoor (mW)	gev(137,88.5, -4.9)	$R^2 = 90\%$
Uplink throughput Indoor (bps)	$\ln\mathcal{N}_1(7.6\times10^6, 2.2\times10^5)$ with weight 25.86% $\ln\mathcal{N}_2(9.3\times10^6, 8.6\times10^5)$ with weight 47.65% $\ln\mathcal{N}_3(10.8\times10^6, 2.4\times10^5)$ with weight 26.49%	$R^2 = 60\%$
Uplink throughput Outdoor (bps)	$\ln\mathcal{N}_1(7.6\times10^6, 3.6\times10^5)$ with weight 22.77% $\ln\mathcal{N}_2(11.9\times10^6, 2.3\times10^6)$ with weight 45% $\ln\mathcal{N}_3(16.1\times10^6, 6.4\times10^5)$ with weight 32.23.49%	$R^2 = 60\%$

[a]Rx, received power.
[b]Tx, emitted power.
[c]$\ln\mathcal{N}(\mu, \sigma^2)$, Lognormal.
[d]gev(μ, σ, ξ), Generalized Extreme Value.

5.4.4 Sensitivity analysis

The advantage of using the PC method is that a sensitivity analysis can be performed directly as presented in Section 4.2.2.1. In this section, a sensitivity analysis was carried out to determine the most influencing input parameters on the output network data. As shown in Table 5.8, both the first order and total Sobol's sensitivity indices of input parameters (i.e., PLE, heavy data traffic, non-heavy data traffic) were calculated in order to quantify uncertainty linked to received power in

indoor environment. **It was clearly observed that the PLE has a dominate effect on the received indoor power**. The Sobol' first order index was found to be equal to 0.9763. Its corresponding total index was 0.9903. **Hence a small interaction exits between PLE and data traffic parameters**. In addition, similar results were obtained for other network parameters. Results indicated that the PLE is the most impacting parameter.

Table 5.8: First and total Sobol's indices of input parameters to quantify uncertainties linked to received power in indoor environments

Input parameters	Indices of first order	Total indices
Path Loss Exponent	0.9763	0.9903
Heavy data traffic	0.0039	0.0179
Non-heavy data traffic	0.0028	0.018

5.5 Variability of EI

In order to characterize the variability of EI with respect to ICT usage data and network data, Monte Carlo simulations were performed. 10^6 simulations were performed to guaranty a good quality of estimation. Executions of input variables were obtained based on their inverse CDF (probability distributions can be found in Table 5.1 and 5.7) by using the Quasi-random sampling data. It is important to note that the dependence exists between some input network variables as presented above. Therefore the copula of Gaussian type was used to model the dependence between input variables. Finally, aggregating the executions of input variables via the EI equation, the global exposure of a population in an urban area considering a macro LTE network could be assessed.

Based on the 10^6 simulation results, the mean estimated central tendency of EI for a whole population in an urban city considering a macro LTE network and 95% confidence interval as a function of simulation iterations are illustrated in Figure 5.12. We can observe that the Monte Carlo average is converging after 8×10^5 simulations. The average global EI was finally convergent to 1.19×10^{-7} W/kg, of which 25% was caused by uplink exposure coming from mobiles in data service. One should note that only 10% of the total data traffic was assigned to uplink, while 90% to downlink. Furthermore, the entire population is exposed to downlink EM radiation from eNB everywhere and all day long when mobile users received uplink EM radiation from their devices only during uplink data traffic emissions. Despite the fact that the emitted power by devices in data service is important, the duration of data traffic emissions is limited by the small amount of uplink data traffic and **high speed of uplink throughput provided by LTE network. As a consequence, on the contrary to what have been observed in the 3G-induced global exposure (uplink exposure accounts for more than 90% of global exposure), the uplink exposure is less important in the issue of LTE-induced global exposure**.

Furthermore, it was observed that the LTE-induced global exposure follows the statistical law of GEV (Figure 5.13). From Figure 5.13, we can also see that the

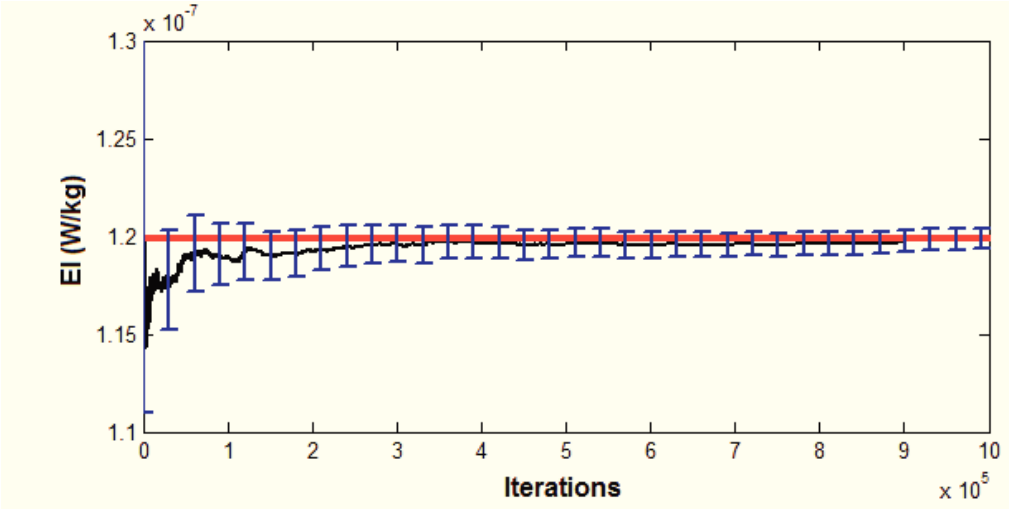

Figure 5.12: Mean estimated central trend of EI (1.19×10^{-7}) and 95% confidence interval as a function of simulation iterations

median value of LTE-induced exposure was found to be 5.19 $\times 10^{-8}$ W/kg, while the 0.9 quantile was about 2.56 $\times 10^{-7}$ W/kg. These values were less than the ones calculated in view of 3G networks, bearing in mind that the median (respectively, 0.9 quantile) value of 3G-induced global exposure was found to be 1.92 $\times 10^{-7}$ W/kg (respectively, 4.48 $\times 10^{-7}$ W/kg). The main reason of that is high speed of uplink throughput provided by LTE network leading to the short durations of uplink data traffic emissions. However, it should also be noted that only the mobile devices in data usage was considered in LTE scenarios.

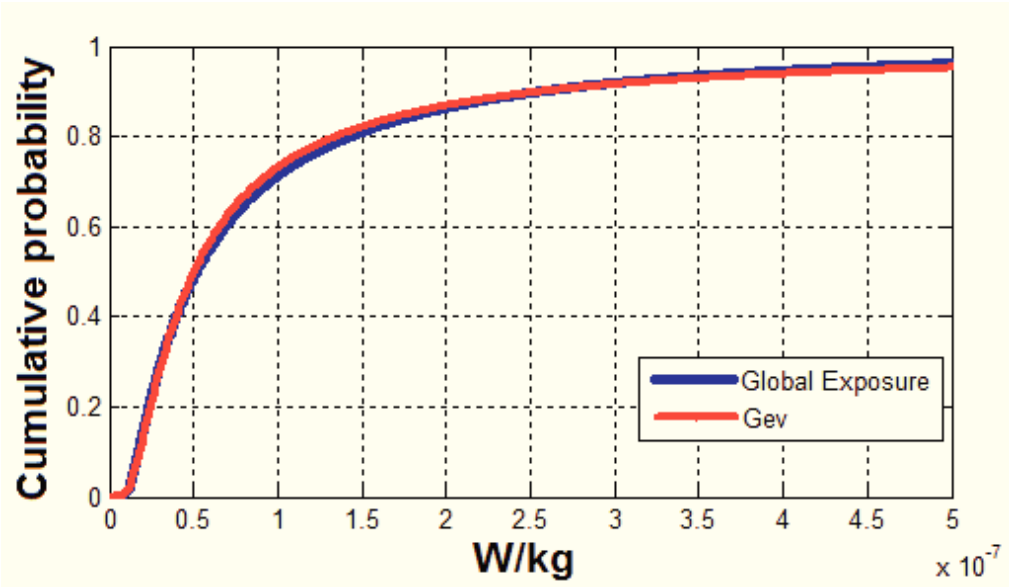

Figure 5.13: Cumulative Density Function of EI values provided by 10^6 simulations and its best fitted statistical law of Generalized Extreme Value

5.6 Global sensitivity analysis

In addition, a sensitivity analysis was carried out in this section. Variance based sensitivity indices suited to the case where input parameters are not independent as presented in Section 4.2.2.2 were implemented. Indices of Kucherenko [Kucherenko et al., 2012] were evaluated based on Monte Carlo simulations (10^6 runs in total) and dedicated to describe the influence of each input parameter on the variance of the output, which represents the EMF exposure in the issue of LTE scenarios.

Both first order and total Kucherenko sensitivity indices were evaluated to the quantify uncertainties of output. As shown in Figure 5.14, **it was clearly observed that the most influencing parameter in the issue of global exposure considering a macro LTE network is the received power density (both in indoor and outdoor environments) from eNB**. The corresponding first order index of received power density in indoor environment equals to 36.46%, and was evaluated to 39.54% for the received power density in outdoor environment. This can be explained by the considered macro LTE network: **mobile phones in data usage**. On one hand, **short durations of uplink data traffic emissions** are due to the high uplink throughputs. On the other hand, this study focused on the **whole-body exposure**. Exposure values for mobile devices in data usage used in front of the chest were considered. Therefore, results are not applicable for the local exposure (e.g., exposure values in specific organs/tissue) or for a mobile phone close to the head usage (e.g., voice over IP).

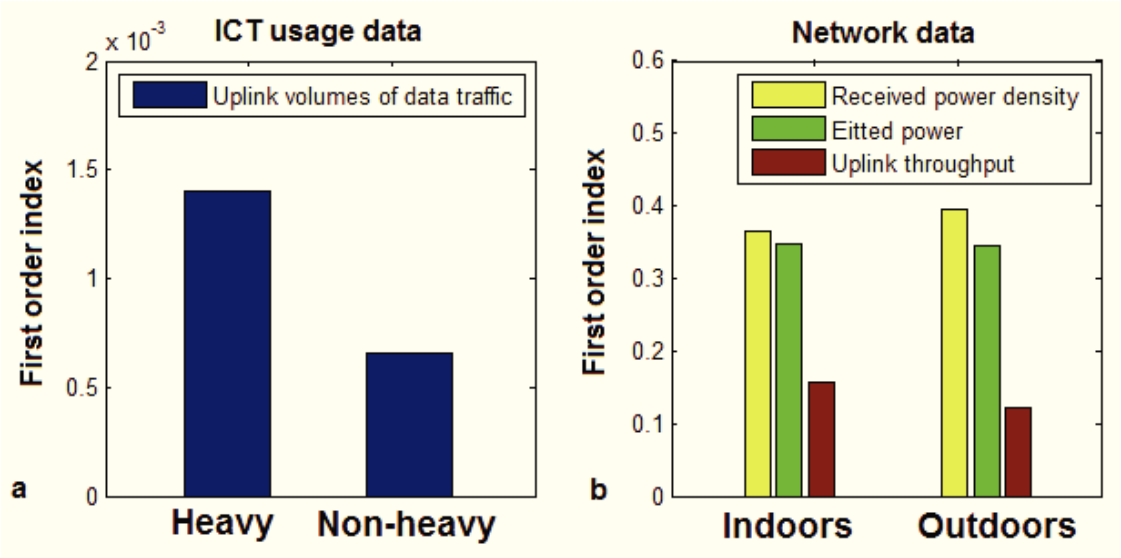

Figure 5.14: Kucherenko first order indices of input parameters (a: 2 ICT usage parameters and b: 6 network parameters) to quantify uncertainties linked to EI obtained from 1000000 simulations

Furthermore, as illustrated in Figure 5.15b, it was observed that a total index of received power density was found to be 50.65% indoor, while 61.69% outdoor. We noticed that a large difference exists between first and total indices of received

power density. **As a consequence, the interaction between received power density and other parameters is in fact very high**.

Concerning emitted power by mobiles, we were aware that the global exposure is also impacted by them. According to Figure 5.14b, the first order index of emitted powers by mobiles located outdoor and indoor was respectively 34.45% and 34.89%, which make them respectively at the third and fourth ranks. Furthermore, from the same figure, we observed that the **uplink throughputs indoor and outdoor less affected the EI compared to other parameters** (their first order indices were respectively 15.66 % indoor and 12.27% outdoor).

Compared to network data, the influence of ICT usage data (respectively, uplink volumes of data traffic for heavy and non-heavy users) on the global exposure can be ignored (Figure 5.14a). The first order index of heavy uplink data traffic was found to be 0.14% and 0.07% for non-heavy uplink data traffic.

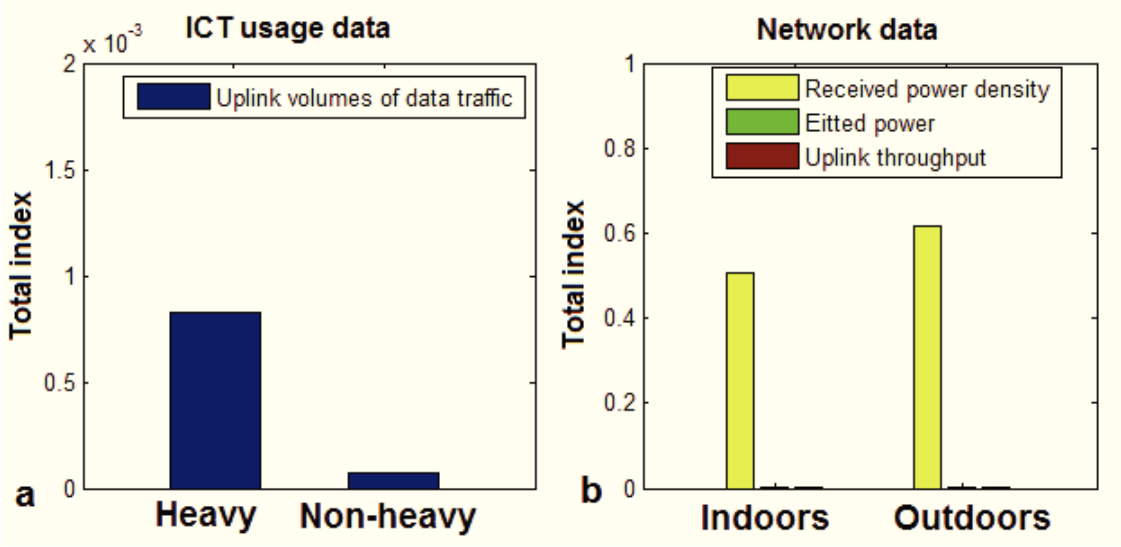

Figure 5.15: Kucherenko total indices of input parameters (a: 2 ICT usage parameters and b: 6 network parameters) to quantify uncertainties linked to EI obtained from 1000000 simulations

5.7 Conclusion

This chapter presented a surrogate model to assess the variability of global EMF exposure of a population induced by a macro LTE network in a dense urban area. The influence linked to propagation environment, ICT usage data, EMF radiations originating from mobiles and eNB, etc. was considered in the evaluation of EMF exposure. To this end, a statistical approach was proposed to explore the variability of PLE due to the geographical environment specificities. And ICT usage data generated by LTE networks were collected and characterized. Then, a simplified LTE network traffic simulator was used to simulate network data by varying PLE and ICT usage data. Results have shown that the PLE has a dominate effect on the network data(emitted and received powers and uplink throughput).

Furthermore, the variability of EI was characterized in terms of ICT usage data and network data using Monte Carlo simulations. Results have shown that the LTE-induced global exposure follows a GEV distribution with an average value of 1.19 $\times 10^{-7}$ W/kg. Its 0.9 quantile value was about 2.56 $\times 10^{-7}$ W/kg which is less than the one observed from the 3G-induced global exposure. This can be explained by the effect of the less important uplink exposure in the issue of LTE networks. The uplink exposure induced by LTE network accounts for only 25% of global exposure since the duration of data traffic emissions is limited by the high speed of uplink throughput. At last, it is important to note that all the values of global exposure are far below the exposure limits.

In addition, a variance-based sensitivity analysis was conducted in order to assess the influence of each parameter on EI. The results have highlighted the importance of received power density from eNB. However, since the whole-body exposure induced by EM radiation emitted by mobile phones in data usage was considered, results are not applicable for the local exposure or for a mobile phone used close to the head. Furthermore, it was also observed that the global exposure is also impacted by the emitted power followed by the uplink throughput, while the influence of ICT usage data on the global exposure can be ignored.

6

Conclusion and perspectives

Contents

6.1 Conclusion

This thesis work is dedicated to a new methodology developed to characterize the real day-to-day EMF exposure to a wireless network as a whole, exploring the people's daily life and including both downlink and uplink exposures. The principal objectives were the evaluation via dosimetric tools and statistical methods of the global exposure of a population to RF-EMF by taking into account different influencing parameters (technologies, usages, environments, etc.) and the analysis of the most influencing parameters that could serve as levers to optimize the population levels of EMF exposure.

Towards these objectives, the first part of the thesis has been devoted to the analysis of the average population exposure to 3G-induced EMFs using a deterministic approach, from both uplink and downlink radio emissions in different countries, geographical areas, and for different wireless device usages. For the first time we got insight of the real level of human exposure to EMF in view of existing 3G networks through the statistical analysis of mobile network operator data collected in France and Serbia and the use of the LEXNET approach and EI metric. It was observed that mobile usage is very variable over time and unbalanced among users. By aggregating the data collected from surveys, statistical measurements and simulations in the EI equation, the global EMF exposure could be assessed. Results, derived from device usage statistics collected in France and Serbia, have shown a strong heterogeneity of exposure, both in time (the traffic distribution over 24 h was found highly variable), and space (the exposure to 3G networks in France was found to be roughly two times higher than the one in Serbia). Among the results, we have also shown that, contrary to popular belief, exposure to 3G EMFs is dominated by uplink radio emissions, resulting from voice and data traffic. The average population EMF exposure was shown to differ from one geographical area to another, as well as from one country to another, due to the different cellular network architectures and variability of mobile usage. Finally, it should be noted that all the calculated EI values were found far below (10^5 less) the international standard limits.

One of the challenges in this thesis laid in identifying how the EI varies with the parameters characterizing the network performances, the usages, the population, etc. Therefore, in the second part of the thesis, the variability of EI input parameters were characterized in order to manage the uncertainties linked to the EI evaluation. However, some input variables, i.e., network data provided by a radio network planning tool were difficult to assess because of the great amount of computational processing time. Hence, there was a need to develop an analytical transfer function to predict the network data without executing large numbers of simulations. To do so, the approach of meta-modeling using polynomials was adopted to approximate statistically the output of a network planning tool from the inputs (i.e., ICT usage data). Thereafter, 3G-induced exposure was statistically assessed via Monte Carlo simulations by varying the ICT usage data and network data. Results have revealed that the global EMF exposure distribution follows the GEV law. In addition, the global EMF exposure was found very sensitive to the variability of ICT usage and network data. After investigating how the EI varies due to the input random variables, a variance-based sensitivity analysis was carried out for the purpose of simplifying the EI metric. It was found that the EMF exposure to a 3G network is significantly impacted by the heavy usage traffic, and especially, the uplink data

traffic due to the limited upload speed in 3G networks. As a consequence, the EI metric could be simplified by considering only two different ICT user profiles. Furthermore, results have also shown that downlink EM radiations from BTS less affect the EMF exposure than uplink EM radiations from mobiles in 3G networks.

One of the main findings was thus that uplink data traffic has a dominating impact on the 3G-induced EMF exposure due to the limited upload throughputs. However, nowadays, LTE networks can provide high quality services and high traffic capacity. Furthermore, signal attenuation map for a specific geographical area (e.g., Lyon city) was used through a deterministic propagation model in previous. As a matter of fact, propagation environments also play a important role in assessing signal attenuation, i.e., the impact of building and field data in RF waves propagation should also be taken into account. We therefore proposed a simplified methodology based on advanced statistical tools to evaluate the day-to-day global EMFs exposure of a population induced by such a network (LTE) taking into account the variability and uncertainties linked to propagation environment, usage, as well as EMFs from personal wireless devices and base stations. To this end, the uncertainties linked to PLE due to the influence of propagation environment were quantified and characterized using stochastic city models and a newly developed 3D ray tracing simulator. Furthermore, the distributions of PLE as well as ICT usage data were used as inputs of a simplified LTE network traffic simulator (developed in Matlab) in order to assess the network data. One of the main results was that the network data are mainly affected by the PLE (total Sobol's index was about 99%). Finally, the variability of EI was characterized in terms of ICT usage and network data using Monte Carlo simulations. A sensitivity analysis was carried out to assess the importance of each input parameters on the EI. In contrary to what we observed for 3G networks, results have highlighted the importance of received power density (both in indoor and outdoor environments) from eNB on the global average exposure induced by a macro LTE network. Moreover, emitted powers outdoor and indoor were ranked respectively third and fourth among all the influencing input parameters on the EI.

Finally we must stress out that the results achieved in the framework of this thesis have contributed to the European project LEXNET, aiming to develop a new RF-EMF exposure metric assessing the global exposure of a population to a network as a whole to be used as a KPI to test and optimize wireless telecommunication networks in terms of EMF exposure.

6.2 Perspectives

Taking advantage of progress in high performance calculation, simulators are nowadays becoming more able to handle complex problems and are used in the system design, KPI assessment (e.g., EMF exposure), etc. On the other hand, to explore the design space, quantify the uncertainty of KPI or to optimize the design, simulations have to be performed many times. However, despite such a progress in high performance calculation, performing thousands of simulations is not always affordable in limited time. As the study carried out in this thesis, the surrogate models, e.g., PC expansion method, was applied to avoid the computational burden. As a matter of fact, our studies are mainly dedicated to build a surrogate model for a

deterministic simulator, e.g., 3G radio network planning tool. However, the simulator can also be stochastic. E.g., the stochastic geometry simulator used in Chapter 5 to build the random city models. In contrast to the deterministic one, which generate a unique output for each set of input parameters, the stochastic simulator contains the sources which are randomness, that is to say, the same input parameters create different outputs. In this case, at a given input (e.g., building height), the output of the stochastic geometry simulator, is not one value but a probability density function that need to be characterized. As a consequence, it is not feasible to execute thousands of simulations by this stochastic simulator. To overcome this limitation, surrogating an stochastic simulator is an emerging question to be solved.

Another perceptive lies in the assessment of RF-EMF exposure induced by the emerging systems and networks. As shown in this thesis, the technology, usage, proximity to the antenna, etc. have a strong influence to the exposure. Nowadays, the usages have evolved. 3G and 4G networks have been massively deployed to enable and improve data transmissions and QoS. Network infrastructures are evolving towards closer access points with variable densities, self-organized or movable capacity. The upcoming 5th generation mobile networks (5G) will change the usage: wireless communications of connected objects including machine to machine communications. In this case, the RF emissions will become massive and more sporadic (both in time and space) at the same time. There is therefore the need to characterize the day-to-day exposure by such a network through the approach of the LEXNET EI metric. The EI should thus be further extended to the emerging systems and networks.

Appendices

A

Supplementary figures and tables

Contents

A.1 Spearman correlation matrix for system's output

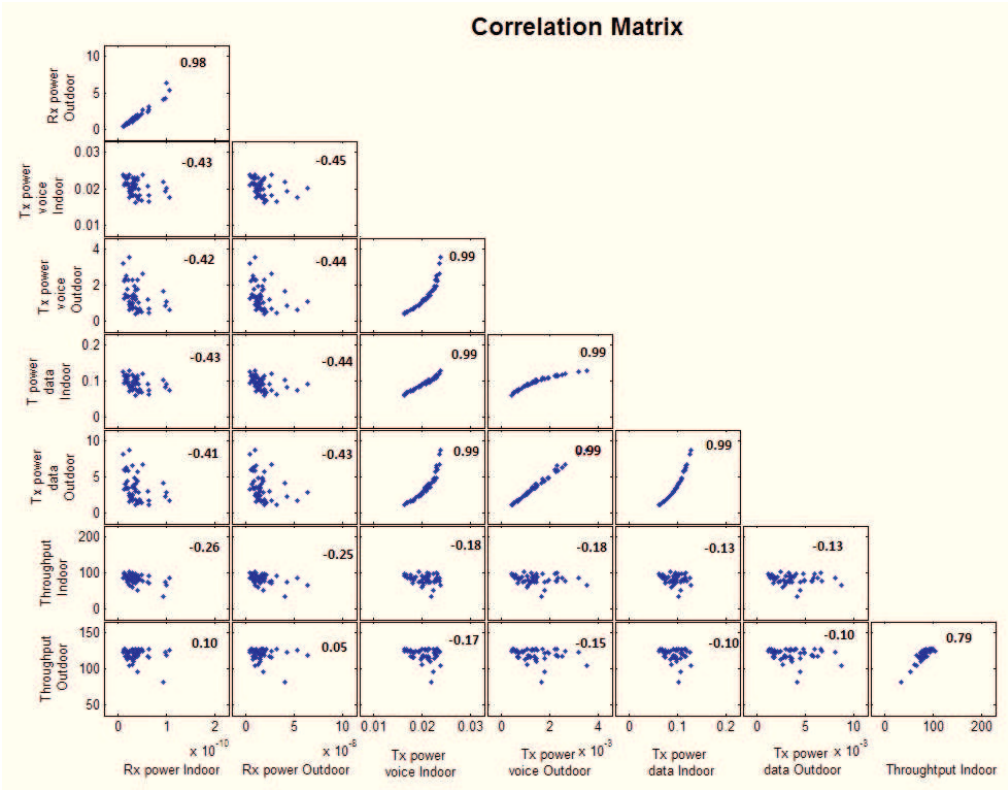

Figure A.1: A exelpme of Spearman correlation matrix for system's output variables in day time case

A.2 Statistical characteristic comparison between system's output observations and surrogate model's executions

Table A.1: Statistical characteristic comparison between 50 observations (obtained by simulations) and 10^4 executions (generated by meta-model) for each variable and its corresponding statistical model

During day time from 8 a.m. to 6 p.m.					
	50 observations	10^4 executions	Statistical model selection		
	Rx power Indoor		GEV(μ, σ, ξ)		
Mean (W)	3.6449×10^{-11}	3.4990×10^{-11}	$\mu(10^{-11})$	$\sigma(10^{-11})$	$\xi(10^{-2})$
Standard deviation	2.2742×10^{-11}	1.4602×10^{-11}	2.88	1.26	-5.21
Variation coefficient	62%	42%	$R^2 = 96\%$		

	Rx power Outdoor		GEV(μ, σ, ξ)		
Mean (W)	1.6491×10^{-8}	1.4145×10^{-8}	$\mu(10^{-8})$	$\sigma(10^{-9})$	$\xi(10^{-2})$
Standard deviation	1.1853×10^{-8}	0.7378×10^{-8}	1.09	6.03	-3.85
Variation coefficient	72%	52%	$R^2 = 97\%$		
	Tx power voice Indoor		$\mathcal{N}(\mu, \sigma)$		
Mean (W)	0.0206	0.0207	$\mu(10^{-2})$	$\sigma(10^{-3})$	
Standard deviation	0.0021	0.0015	2.07	1.45	
Variation coefficient	10%	7%	$R^2 = 95\%$		
	Tx power voice Outdoor		GEV(μ, σ, ξ)		
Mean (W)	0.0014	0.0014	$\mu(10^{-3})$	$\sigma(10^{-4})$	$\xi(10^{-2})$
Standard deviation	7.1585×10^{-4}	5.1792×10^{-4}	1.16	4.57	-4.41
Variation coefficient	51%	38%	$R^2 = 93\%$		
	Tx power data Indoor		$\mathcal{N}(\mu, \sigma)$		
Mean (W)	0.0944	0.0942	$\mu(10^{-2})$	$\sigma(10^{-2})$	
Standard deviation	0.0169	0.0112	9.42	1.12	
Variation coefficient	18%	12%	$R^2 = 93\%$		
	Tx power data Outdoor		GEV(μ, σ, ξ)		
Mean (W)	0.0036	0.0034	$\mu(10^{-3})$	$\sigma(10^{-3})$	$\xi(10^{-2})$
Standard deviation	0.0018	0.0014	2.83	1.17	-4.09
Variation coefficient	50%	42%	$R^2 = 93\%$		
	Throughput Indoor		$\mathcal{N}(\mu, \sigma)$		
Mean ($kbps$)	81.9536	83.0227	μ	σ	
Standard deviation	12.6753	9.1778	83.02	9.18	
Variation coefficient	15%	11%	$R^2 = 93\%$		
	Throughput Outdoor		$\mathcal{N}(\mu, \sigma)$		
Mean ($kbps$)	119.6785	120.2268	μ	σ	
Standard deviation	8.7212	8.5949	120.23	8.59	
Variation coefficient	7%	7%	$R^2 = 89\%$		
During night time from 6 p.m. to 8 a.m.					
	50 observations	10^4 executions	Statistical model selection		
	Rx power Indoor		GEV(μ, σ, ξ)		
Mean (W)	3.7230×10^{-11}	3.8535×10^{-11}	$\mu(10^{-11})$	$\sigma(10^{-11})$	$\xi(10^{-2})$
Standard deviation	2.0790×10^{-11}	1.6856×10^{-11}	3.14	1.40	-4.04
Variation coefficient	56%	44%	$R^2 = 95\%$		
	Rx power Outdoor		GEV(μ, σ, ξ)		
Mean (W)	1.6443×10^{-8}	1.6519×10^{-8}	$\mu(10^{-8})$	$\sigma(10^{-9})$	$\xi(10^{-2})$
Standard deviation	8.9903×10^{-9}	7.1533×10^{-9}	1.35	5.82	-2.37
Variation coefficient	55%	43%	$R^2 = 92\%$		
	Tx power voice Indoor		$\mathcal{N}(\mu, \sigma)$		
Mean (W)	0.0203	0.0204	$\mu(10^{-2})$	$\sigma(10^{-3})$	
Standard deviation	0.0022	0.0023	2.04	2.27	
Variation coefficient	11%	11%	$R^2 = 94\%$		
	Tx power voice Outdoor		GEV(μ, σ, ξ)		

Mean (W)	0.0013	0.0013	$\mu(10^{-3})$	$\sigma(10^{-4})$	$\xi(10^{-2})$
Standard deviation	6.5137×10^{-4}	4.6319×10^{-4}	1.05	4.21	-4.29
Variation coefficient	50%	37%	$R^2 = 95\%$		
	Tx power data Indoor		$\mathcal{N}(\mu, \sigma)$		
Mean (W)	0.0928	0.0931	$\mu(10^{-2})$	$\sigma(10^{-2})$	
Standard deviation	0.0173	0.0170	9.31	1.70	
Variation coefficient	19%	18%	$R^2 = 93\%$		
	Tx power data Outdoor		GEV(μ, σ, ξ)		
Mean (W)	0.0034	0.0035	$\mu(10^{-3})$	$\sigma(10^{-3})$	$\xi(10^{-2})$
Standard deviation	0.0017	0.0014	2.89	1.25	-6.04
Variation coefficient	51%	41%	$R^2 = 97\%$		
	Throughput Indoor		$\mathcal{N}(\mu, \sigma)$		
Mean ($kbps$)	84.6185	87.2121	μ	σ	
Standard deviation	10.8570	10.1933	87.21	10.19	
Variation coefficient	13%	12%	$R^2 = 95\%$		
	Throughput Outdoor		$\mathcal{N}(\mu, \sigma)$		
Mean ($kbps$)	121.8796	123.2316	μ	σ	
Standard deviation	6.2121	5.6544	123.23	5.65	
Variation coefficient	6%	6%	$R^2 = 87\%$		

Bibliography

[Abdelati, 2015] Abdelati, M. M. (2015). Electromagnetic radiation from mobile phone base stations at Gaza. *IUG Journal of Natural Studies*, 13(2).

[Aerts et al., 2014] Aerts, S., Plets, D., Verloock, L., Martens, L., and Joseph, W. (2014). Assessment and comparison of total RF-EMF exposure in femtocell and macrocell base station scenarios. *Radiation protection dosimetry*, 162(3):236–243.

[Alanko et al., 2008] Alanko, T., Hietanen, M., and von Nandelstadh, P. (2008). Occupational exposure to RF fields from base station antennas on rooftops. *annals of telecommunications-annales des télécommunications*, 63(1-2):125–132.

[Aliaga, 2006] Aliaga, C. (2006). How is the time of women and men distributed in europe. *Statistics in focus*, 4:1–11.

[Allegretti et al., 2005] Allegretti, M., Colaneri, M., Notarpietro, R., Gabella, M., and Perona, G. (2005). Simulation in urban environment of a 3D ray tracing propagation model based on building database preprocessing. *Rep. Torino: Politecnico di Torino*.

[Baste et al., 2010] Baste, V., Mild, K. H., and Moen, B. E. (2010). Radiofrequency exposure on fast patrol boats in the royal norwegian navy—an approach to a dose assessment. *Bioelectromagnetics*, 31(5):350–360.

[Benkler et al., 2009] Benkler, S., Chavannes, N., and Kuster, N. (2009). New powerful fdtd source based on huygens surface: Highly complex em simulations performed on an ordinary pc. In *Poster at the 31th Annual Meeting of the Bioelectromagnetics Society (BEMS 2009), Davos, Switzerland*.

[Bigot et al., 2013] Bigot, R., CRoUttE, P., and DAUDEY, E. (2013). La diffusion des technologies de l'information et de la communication dans la société française (2013). *CREDOC report*.

[Blatman, 2009] Blatman, G. (2009). *Adaptive sparse polynomial chaos expansions for uncertainty propagation and sensitivity analysis*. PhD thesis, Clermont-Ferrand 2.

[Blatman and Sudret, 2010] Blatman, G. and Sudret, B. (2010). An adaptive algorithm to build up sparse polynomial chaos expansions for stochastic finite element analysis. *Probabilistic Engineering Mechanics*, 25(2):183–197.

[Blatman and Sudret, 2011] Blatman, G. and Sudret, B. (2011). Adaptive sparse polynomial chaos expansion based on least angle regression. *Journal of Computational Physics*, 230(6):2345–2367.

[Bolte et al., 2011] Bolte, J. F., van der Zande, G., and Kamer, J. (2011). Calibration and uncertainties in personal exposure measurements of radiofrequency electromagnetic fields. *Bioelectromagnetics*, 32(8):652–663.

[Bornkessel et al., 2007] Bornkessel, C., Schubert, M., Wuschek, M., and Schmidt, P. (2007). Measurement and calculation of general public electromagnetic exposure around GSM and UMTS cellular base stations. *ITG-Fachbericht-INICA 2007*.

[Bortkiewicz et al., 1996] Bortkiewicz, A., Gadzicka, E., and Zmyślony, M. (1996). Heart rate variability in workers exposed to medium-frequency electromagnetic fields. *Journal of the autonomic nervous system*, 59(3):91–97.

[Castellanos et al., 2008] Castellanos, C. U., Villa, D. L., Rosa, C., Pedersen, K. I., Calabrese, F. D., Michaelsen, P.-H., and Michel, J. (2008). Performance of uplink fractional power control in UTRAN LTE. In *Vehicular Technology Conference, 2008. VTC Spring 2008. IEEE*, pages 2517–2521. IEEE.

[CENELEC, 2001] CENELEC (2001). Basic standard for the measurement of Specific Absorption Rate related to human exposure to electromagnetic fields from mobile phones. *European Committee for Electrotechnical Standardization, Brussels, EN-50361*, 35:1050.

[CENELEC, 2008] CENELEC (2008). Basic standard for the in situ measurement of electromagnetic field strength related to human exposure in the vicinity of base stations. *European Committee for Electrotechnical Standardisation, Brussels, EN-50492*.

[Chaigneaud et al., 2001] Chaigneaud, L., Guillet, V., and Vauzelle, R. (2001). A 3D ray-tracing tool for broadband wireless systems. In *Vehicular Technology Conference, 2001. VTC 2001 Fall. IEEE VTS 54th*, volume 4, pages 2043–2047. IEEE.

[Christ et al., 2010] Christ, A., Gosselin, M.-C., Christopoulou, M., Kühn, S., and Kuster, N. (2010). Age-dependent tissue-specific exposure of cell phone users. *Physics in medicine and biology*, 55(7):1767.

[Christ et al., 2009] Christ, A., Kainz, W., Hahn, E. G., Honegger, K., Zefferer, M., Neufeld, E., Rascher, W., Janka, R., Bautz, W., Chen, J., et al. (2009). The virtual family—development of surface-based anatomical models of two adults and two children for dosimetric simulations. *Physics in medicine and biology*, 55(2):N23.

[Cisco, 2016] Cisco (2016). Cisco visual networking index: Global mobile data traffic forecast update 2015–2020 white paper.

[Conil et al., 2008] Conil, E., Hadjem, A., Lacroux, F., Wong, M., and Wiart, J. (2008). Variability analysis of sar from 20 mhz to 2.4 ghz for different adult and child models using finite-difference time-domain. *Physics in medicine and biology*, 53(6):1511.

[Corre and Lostanlen, 2007] Corre, Y. and Lostanlen, Y. (2007). 3D urban propagation model for large ray-tracing computation. In *Electromagnetics in Advanced Applications, 2007. ICEAA 2007. International Conference on*, pages 399–402. IEEE.

[COST Action, 1999] COST Action (1999). COST 231-Digital mobile radio towards future generation systems. final report. Technical report, tech. rep., European Communities, EUR 18957.

[Courtat et al., 2016] Courtat, T., Decreusefond, L., and Martins, P. (2016). Stochastic simulation of urban environments. application to path-loss in wireless systems. *arXiv preprint arXiv:1604.00688*.

[De Marco and Maggi, 2006] De Marco, M. and Maggi, S. (2006). Evaluation of stray radiofrequency radiation emitted by electrosurgical devices. *Physics in medicine and biology*, 51(14):3347.

[Efron and Stein, 1981] Efron, B. and Stein, C. (1981). The jackknife estimate of variance. *The Annals of Statistics*, pages 586–596.

[FCC, 2001] FCC (2001). Evaluating compliance with FCC guidelines for human exposure to radiofrequency electromagnetic fields. Washington, DC: Federal Communications Commission. Technical report, Tech. Rep. Suppl. C to OET Bulletin 65.

[Frederic et al., 2016] Frederic, S., Huang, Y., and Wiart, J. (2016). *Programme GeoStat : Fiche technique*.

[Frei et al., 2009] Frei, P., Mohler, E., Neubauer, G., Theis, G., Bürgi, A., Fröhlich, J., Braun-Fahrländer, C., Bolte, J., Egger, M., and Röösli, M. (2009). Temporal and spatial variability of personal exposure to radio frequency electromagnetic fields. *Environmental research*, 109(6):779–785.

[Freudenstein et al., 2014] Freudenstein, F., Wiedemann, P. M., Pejanović-Djurišić, M., Koprivica, M., and Nešković, A. (2014). Intuitive exposure and risk perception of RF EMF: Case studies serbia and montenegro. In *Telecommunications Forum Telfor (TELFOR), 2014 22nd*, pages 1–4. IEEE.

[Gabriel et al., 1996] Gabriel, S., Lau, R., and Gabriel, C. (1996). The dielectric properties of biological tissues: Ii. measurements in the frequency range 10 Hz to 20 GHz. *Physics in medicine and biology*, 41(11):2251.

[Gajšek et al., 2015] Gajšek, P., Ravazzani, P., Wiart, J., Grellier, J., Samaras, T., and Thuróczy, G. (2015). Electromagnetic field exposure assessment in europe radiofrequency fields (10 MHz–6 GHz). *Journal of exposure science and environmental epidemiology*, 25(1):37–44.

[Gallastegi et al., 2016] Gallastegi, M., Guxens, M., Jiménez-Zabala, A., Calvente, I., Fernández, M., Birks, L., Struchen, B., Vrijheid, M., Estarlich, M., Fernández, M. F., et al. (2016). Characterisation of exposure to non-ionising electromagnetic fields in the spanish inma birth cohort: study protocol. *BMC public health*, 16(1):1.

[Gati et al., 2010] Gati, A., Conil, E., Wong, M.-F., and Wiart, J. (2010). Duality between uplink local and downlink whole-body exposures in operating networks. *IEEE transactions on electromagnetic compatibility*, 52(4):829–836.

[Gati et al., 2009] Gati, A., Hadjem, A., Wong, M.-F., and Wiart, J. (2009). Exposure induced by wcdma mobiles phones in operating networks. *IEEE Transactions on wireless communications*, 8(12):5723–5727.

[Ghanmi et al., 2014] Ghanmi, A., Varsier, N., Hadjem, A., Conil, E., Picon, O., and Wiart, J. (2014). Analysis of the influence of handset phone position on RF exposure of brain tissue. *Bioelectromagnetics*, 35(8):568–579.

[Gibson, 2012] Gibson, J. D. (2012). *Mobile communications handbook*. CRC press.

[Góra et al., 2010] Góra, J., Pedersen, K. I., Szufarska, A., and Strzyz, S. (2010). Cell-specific uplink power control for heterogeneous networks in LTE. In *Vehicular Technology Conference Fall (VTC 2010-Fall), 2010 IEEE 72nd*, pages 1–5. IEEE.

[Governmental Industrial Hygienists, 1995] Governmental Industrial Hygienists, A. C. (1995). Threshold limit values for chemical substances and physical agents and biological exposure indices. American Conference of Governmental Industrial Hygienists.

[Guideline, 1998] Guideline, I. (1998). Guidelines for limiting exposure to time-varying electric, magnetic, and electromagnetic fields (up to 300 GHz). *Health Phys*, 74(4):494–522.

[Guy et al., 1975] Guy, A. W., Lin, J. C., Kramar, P. O., and Emery, A. F. (1975). Effect of 2450-MHz radiation on the rabbit eye. *IEEE transactions on microwave theory and techniques*, 23(6):492–498.

[Hadjem et al., 2010] Hadjem, A., Conil, E., Gati, A., Wong, M.-F., and Wiart, J. (2010). Analysis of power absorbed by children's head as a result of new usages of mobile phone. *IEEE Transactions on Electromagnetic Compatibility*, 52(4):812–819.

[Hagness and Taflove, 2000] Hagness, S. and Taflove, A. (2000). Computational electrodynamics: The finite-difference time-domain method. *Norwood, MA: Artech House*.

[Hata, 1980] Hata, M. (1980). Empirical formula for propagation loss in land mobile radio services. *IEEE transactions on Vehicular Technology*, 29(3):317–325.

[Hirata et al., 2007] Hirata, A., Asano, T., and Fujiwara, O. (2007). FDTD analysis of human body-core temperature elevation due to RF far-field energy prescribed in the icnirp guidelines. *Physics in medicine and biology*, 52(16):5013.

[Holland and Williams, 1983] Holland, R. and Williams, J. W. (1983). Total-field versus scattered-field finite-difference codes: A comparative assessment. *IEEE Transactions on Nuclear Science*, 30(6):4583–4588.

[Homma and Saltelli, 1996] Homma, T. and Saltelli, A. (1996). Importance measures in global sensitivity analysis of nonlinear models. *Reliability Engineering & System Safety*, 52(1):1–17.

[Huang et al., 2014] Huang, Y., Wiart, J., Person, C., and Varsier, N. (2014). Sensitivity analysis of downlink received and uplink emitted powers in a geographical area to ict usage parameters. In *Proceedings of The Annual Meeting of BEMS and EBEA, Capetown, South Africa*, pages 8–13.

[Ibrani et al., 2016] Ibrani, M., Hamiti, E., Ahma, L., Halili, R., Shala, V., and Berisha, D. (2016). Narrowband frequency-selective up-link and down-link evaluation of daily personal-exposure induced by wireless operating networks. *Wireless Networks*, pages 1–10.

[IEC, 2001] IEC (2001). Procedure to measure the Specific Absorption Rate (SAR) in the frequency range of 300 MHz to 3 GHz – Part 1: hand-held mobile wireless communication devices. *International Electrotechnical Commission, committee draft for vote, IEC 62209*.

[IEC, 2011] IEC (2011). Determination of RF field strength and SAR in the vicinity of radiocommunication base stations for the purpose of evaluating human exposure (IEC 62232:2011). *Geneva, Switzerland: International Electrotechnical Commission*.

[IEEE, 2003] IEEE (2003). Ieee recommended practice for determining the peak spatial-average Specific Absorption Rate (SAR) in the human head from wireless communications devices: Measurement techniques. *IEEE, New York*.

[IEEE Standards Coordinating Committee 28, 1992] IEEE Standards Coordinating Committee 28, o. N.-I. R. H. (1992). *IEEE Standard for Safety Levels with Respect to Human Exposure to Radio Frequency Electromagnetic Fields, 3kHz to 300 GHz*. Institute of Electrical and Electonics Engineers, Incorporated.

[INSEE, 2011] INSEE (2011). Enquête emploi du temps 2009-2010 (france). *Institut National de la Statistique et des Études Économiques Première n° 1377*.

[Joseph et al., 2010] Joseph, W., Frei, P., Roösli, M., Thuróczy, G., Gajsek, P., Trcek, T., Bolte, J., Vermeeren, G., Mohler, E., Juhasz, P., et al. (2010). Comparison of personal radio frequency electromagnetic field exposure in different urban areas across europe. *Environmental Research*, 110(7):658–663.

[Joseph et al., 2002] Joseph, W., Olivier, C., and Martens, L. (2002). A robust, fast, and accurate deconvolution algorithm for em-field measurements around GSM and UMTS base stations with a spectrum analyzer. *IEEE Transactions on Instrumentation and Measurement*, 51(6):1163–1169.

[Joseph et al., 2006a] Joseph, W., Olivier, C., and Martens, L. (2006a). Assessment of exposure from wimax signals using a spectrum analyzer. In *Proceedings of the 27th Annual Meeting of the Bioelectromagnetics Society. Cancun, Mexico: BEMS*.

[Joseph et al., 2012] Joseph, W., Verloock, L., Goeminne, F., Vermeeren, G., and Martens, L. (2012). Assessment of RF exposures from emerging wireless communication technologies in different environments. *Health Physics*, 102(2):161–172.

[Joseph et al., 2006b] Joseph, W., Verloock, L., and Martens, L. (2006b). Reconstruction of the polarization ellipse of the em field of telecommunication and broadcast antennas by a fast and low-cost measurement method. *IEEE transactions on electromagnetic compatibility*, 48(2):385–396.

[Joseph et al., 2009] Joseph, W., Verloock, L., Tanghe, E., and Martens, L. (2009). In-situ measurement procedures for temporal RF electromagnetic field exposure of the general public. *Health physics*, 96(5):529–542.

[Kamo et al., 2011] Kamo, B., Miho, R., Kolici, V., Cela, S., and Lala, A. (2011). Estimation of peak power density in the vicinity of cellular base stations, fm, uhf and wimax antennas. *International Journal of Engineering & Technology IJET-IJENS*, 11(02).

[Kersaudy et al., 2014] Kersaudy, P., Mostarshedi, S., Sudret, B., Picon, O., and Wiart, J. (2014). Stochastic analysis of scattered field by building facades using polynomial chaos. *IEEE Transactions on Antennas and Propagation*, 62(12):6382–6393.

[Knafl et al., 2008] Knafl, U., Lehmann, H., and Riederer, M. (2008). Electromagnetic field measurements using personal exposimeters. *Bioelectromagnetics*, 29(2):160–162.

[Korowajcznk, 2014] Korowajcznk, L. (2014). How to dimension user traffic in LTE. Presentation.

[Krayni et al., 2016] Krayni, A., Hadjem, A., Sibille, A., Roblin, C., and Wiart, J. (2016). A novel methodology to evaluate uplink exposure by personal devices in wireless networks. *IEEE Transactions on Electromagnetic Compatibility*, 58(3):896–906.

[Kucherenko et al., 2012] Kucherenko, S., Tarantola, S., and Annoni, P. (2012). Estimation of global sensitivity indices for models with dependent variables. *Computer Physics Communications*, 183(4):937–946.

[Kwate et al., 2016] Kwate, R. K., Elmagroud, B., Taybi, C., Moutaouekkil, M. A., Picard, D., and Ziyyat, A. (2016). Interaction between human body and RF-dosimeter: Impact on the downlink E-field assessment. In *Proceedings of the Mediterranean Conference on Information & Communication Technologies 2015*, pages 187–196. Springer.

[Lai et al., 2011] Lai, Z., Bessis, N., De La Roche, G., Zhang, J., Clapworthy, G., Kuonen, P., and Zhou, D. (2011). Intelligent ray launching algorithm for indoor scenarios. *Radioengineering*.

[Lai et al., 2012] Lai, Z., Song, H., Wang, P., Mu, H., Wu, L., and Zhang, J. (2012). Implementation and validation of a 2.5 d intelligent ray launching algorithm for large urban scenarios. In *2012 6th European Conference on Antennas and Propagation (EUCAP)*, pages 2396–2400. IEEE.

[Lauer et al., 2013] Lauer, O., Frei, P., Gosselin, M.-C., Joseph, W., Röösli, M., and Fröhlich, J. (2013). Combining near-and far-field exposure for an organ-specific and whole-body RF-EMF proxy for epidemiological research: A reference case. *Bioelectromagnetics*, 34(5):366–374.

[Long et al., 2003] Long, N., Mestayer, P., and Kergomard, C. (2003). Urban database analysis for mapping morphology and aerodynamic parameters: The case of st jerome sub-urban area, in marseille during escompte. In *CD Proceedings, 5th International Conference on Urban Climate*.

[Lostanlen and Gougeon, 2007] Lostanlen, Y. and Gougeon, G. (2007). Introduction of diffuse scattering to enhance ray-tracing methods for the analysis of deterministic indoor uwb radio channels. In *2007 International Conference on Electromagnetics in Advanced Applications*.

[Magin et al., 1992] Magin, R. L., Liburdy, R. P., and Persson, B. (1992). *Biological effects and safety aspects of nuclear magnetic resonance imaging and spectroscopy*. New York Academy of Sciences.

[Mann, 2010] Mann, S. (2010). Assessing personal exposures to environmental radiofrequency electromagnetic fields. *Comptes rendus physique*, 11(9):541–555.

[Matheron, 1969] Matheron, G. (1969). Le krigeage universel.

[Merewether et al., 1980] Merewether, D., Fisher, R., and Smith, F. (1980). On implementing a numeric huygen's source scheme in a finite difference program to illuminate scattering bodies. *IEEE Transactions on Nuclear Science*, 27(6):1829–1833.

[Nataf, 1962] Nataf, A. (1962). Détermination des distributions de probabilites dont les marges sont données. *Comptes Rendus de l'Académie des Sciences de Paris*, 255(1):42.

[Nelsen, 1999] Nelsen, R. B. (1999). An introduction to copulas, volume 139 of lecture notes in statistics.

[Nouir et al., 2006] Nouir, Z., Sayrac, B., Fourestié, B., Tabbara, W., and Brouaye, F. (2006). Independent component analysis for radio network prediction enhancement. In *Proc. 20th European Conference on Modelling and Simulation*, pages 51–55.

[Nouir et al., 2007] Nouir, Z., Sayrac, B., Fourestié, B., Tabbara, W., and Brouaye, F. (2007). Comparison of neural network learning algorithms for prediction enhancement of a planning tool. In *13th European Wireless Conference, Paris, France*.

[Nouir et al., 2008] Nouir, Z., Sayrac, B., Fourestié, B., Tabbara, W., and Brouaye, F. (2008). Distribution learning for radio network planning tool simulation. *International Journal of Communication Systems*, 21(12):1307–1323.

[Okumura et al., 1968] Okumura, Y., Ohmori, E., Kawano, T., and Fukuda, K. (1968). Field strength and its variability in VHF and UHF land-mobile radio service. *Rev. Elec. Commun. Lab*, 16(9):825–73.

[Paniagua et al., 2014] Paniagua, J. M., Rufo, M., Jiménez, A., Pachón, F. T., and Carrero, J. (2014). Exposure estimates based on broadband elf magnetic field measurements versus the icnirp multiple frequency rule. *Radiation protection dosimetry*, page ncu175.

[Park, 1994] Park, J.-S. (1994). Optimal Latin-hypercube designs for computer experiments. *Journal of statistical planning and inference*, 39(1):95–111.

[Peyman and Gabriel, 2010] Peyman, A. and Gabriel, C. (2010). Cole–cole parameters for the dielectric properties of porcine tissues as a function of age at microwave frequencies. *Physics in medicine and biology*, 55(15):N413.

[Pinto et al., 2011] Pinto, Y., Ghanmi, A., Hadjem, A., Conil, E., Namur, T., Person, C., and Wiart, J. (2011). Numerical mobile phone models validated by SAR measurements. In *Proceedings of the 5th European Conference on Antennas and Propagation (EUCAP)*.

[Plets et al., 2015] Plets, D., Joseph, W., Vanhecke, K., Vermeeren, G., Wiart, J., Aerts, S., Varsier, N., and Martens, L. (2015). Joint minimization of uplink and downlink whole-body exposure dose in indoor wireless networks. *BioMed research international*, 2015.

[Rappaport et al., 1996] Rappaport, T. S. et al. (1996). *Wireless communications: principles and practice*, volume 2. Prentice Hall PTR New Jersey.

[Röösli et al., 2010] Röösli, M., Frei, P., Bolte, J., Neubauer, G., Cardis, E., Feychting, M., Gajsek, P., Heinrich, S., Joseph, W., Mann, S., et al. (2010). Conduct of a personal radiofrequency electromagnetic field measurement study: proposed study protocol. *Environmental health*, 9(1):1.

[Sadetzki et al., 2014] Sadetzki, S., Langer, C. E., Bruchim, R., Kundi, M., Merletti, F., Vermeulen, R., Kromhout, H., Lee, A.-K., Maslanyj, M., Sim, M. R., et al. (2014). The mobi-kids study protocol: challenges in assessing childhood and adolescent exposure to electromagnetic fields from wireless telecommunication technologies and possible association with brain tumor risk. *Frontiers in public health*, 2:124.

[Saker et al., 2012] Saker, L., Elayoubi, S.-E., Combes, R., and Chahed, T. (2012). Optimal control of wake up mechanisms of femtocells in heterogeneous networks. *IEEE journal on selected areas in communications*, 30(3):664–672.

[Saltelli, 2002] Saltelli, A. (2002). Making best use of model evaluations to compute sensitivity indices. *Computer Physics Communications*, 145(2):280–297.

[Saltelli et al., 2000] Saltelli, A., Chan, K., Scott, E. M., et al. (2000). *Sensitivity analysis*, volume 1. Wiley New York.

[Schmid et al., 2007] Schmid, G., Überbacher, R., Samaras, T., Tschabitscher, M., and Mazal, P. R. (2007). The dielectric properties of human pineal gland tissue and RF absorption due to wireless communication devices in the frequency range 400–1850 MHz. *Physics in medicine and biology*, 52(17):5457.

[Shellock and Crues, 1987] Shellock, F. G. and Crues, J. V. (1987). Temperature, heart rate, and blood pressure changes associated with clinical mr imaging at 1.5 t. *Radiology*, 163(1):259–262.

[Sidi et al., 2014] Sidi, H. B., Altman, Z., and Tall, A. (2014). Self-optimizing mechanisms for emf reduction in heterogeneous networks. In *Modeling and Optimization in Mobile, Ad Hoc, and Wireless Networks (WiOpt), 2014 12th International Symposium on*, pages 341–348. IEEE.

[Silly-Carette, 2008] Silly-Carette, J. (2008). *Modélisation avancée de l'absorption des ondes électromagnétiques dans les tissus biologiques: schémas en temps, approches adjointe et stochastique*. PhD thesis, Paris 6.

[Simonsson and Furuskar, 2008] Simonsson, A. and Furuskar, A. (2008). Uplink power control in LTE-overview and performance, subtitle: principles and benefits of utilizing rather than compensating for SINR variations. In *Vehicular Technology Conference, 2008. VTC 2008-Fall. IEEE 68th*, pages 1–5. IEEE.

[Sklar, 1959] Sklar, M. (1959). *Fonctions de répartition à n dimensions et leurs marges*. Université Paris 8.

[Sobol, 2001] Sobol, I. M. (2001). Global sensitivity indices for nonlinear mathematical models and their monte carlo estimates. *Mathematics and computers in simulation*, 55(1):271–280.

[Sudret, 2007] Sudret, B. (2007). Uncertainty propagation and sensitivity analysis in mechanical models–contributions to structural reliability and stochastic spectral methods. *Habilitationa diriger des recherches, Université Blaise Pascal, Clermont-Ferrand, France*.

[Sudret, 2008] Sudret, B. (2008). Global sensitivity analysis using polynomial chaos expansions. *Reliability Engineering & System Safety*, 93(7):964–979.

[Tesanovic et al., 2014] Tesanovic, M., Conil, E., De Domenico, A., Aguero, R., Freudenstein, F., Correia, L. M., Bories, S., Martens, L., Wiedemann, P. M., and Wiart, J. (2014). The lexnet project: wireless networks and EMF: paving the way for low-EMF networks of the future. *IEEE Vehicular Technology Magazine*, 9(2):20–28.

[Thuróczy et al., 2010] Thuróczy, G., Bakos, J., Ravazzani, P., and Wiart, J. (2010). Report on the level of exposure (frequency, patterns and modulation) in the european union; part 2: Extremely low frequency (elf) fields. *Deliverable Report D4 of EHFRAN project*.

[TNS, 2010] TNS (2010). Mobile et société. *Journal of Expertise of the French Association of Mobile Operators (AFOM) n° 12*.

[Varsier et al., 2015a] Varsier, N., Huang, Y., Krayni, A., Hadjem, A., Wiart, J., Vermeeren, G., Plets, D., Joseph, W., Martens, L., Corre, Y., Oliveira, C., Sebastião, D., Correia, L., Koprivica, M., Popović, M., Wiedemann, P., and Freudenstein, F. (2015a). LEXNET (Low-EMF Exposure Future Networks) project Deliverable D2.8: Global wireless exposure metric definition. *Avaiable online*.

[Varsier et al., 2015b] Varsier, N., Plets, D., Corre, Y., Vermeeren, G., Joseph, W., Aerts, S., Martens, L., and Wiart, J. (2015b). A novel method to assess human population exposure induced by a wireless cellular network. *Bioelectromagnetics*, 36(6):451–463.

[Vukmirovic, 2012] Vukmirovic, D. (2012). *Age and sex: 2011 Census of Population, Households and Dwellings in the Republic of Serbia*.

[Website Accomplir.asso.fr, 2011] Website Accomplir.asso.fr (2011). Paris : les trottoirs seront-ils rendus aux piétons? Retrived from: http://www.accomplir.asso.fr/ [Last accessed 19 July 2016].

[Website Beograd.rs, 2015] Website Beograd.rs (2015). Urban municipalities. Retrived from: http://www.beograd.rs/cms/view.php?id=201906 [Last accessed 19 July 2016].

[Website Cartesfrance.fr, 2015a] Website Cartesfrance.fr (2015a). Lyon and cergy city information. Retrived from: http://www.cartesfrance.fr/ [Last accessed 19 July 2016].

[Website Cartesfrance.fr, 2015b] Website Cartesfrance.fr (2015b). Paris city information. Retrived from: http://www.cartesfrance.fr/ [Last accessed 19 July 2016].

[Website Journaldunet.com, 2015] Website Journaldunet.com (2015). Parts de marché des opérateurs mobile en france. Retrived from http://www.journaldunet.com/ebusiness/telecoms-fai/parts-de-marche-du-mobile-en-france.shtml [Last accessed 19 July 2016].

[Website Maschek.de, 2016] Website Maschek.de (2016). Product introduction about the maschek esm. Retrived from: http://www.maschek.de/uk/frameset.php?p=produkte [Last accessed 19 July 2016].

[Website Narda.us, 2016] Website Narda.us (2016). Product introduction about the narda frequency-selective radiation and broadband field meter. Retrived from: http://www.narda-sts.us/literature_datasheets.php [Last accessed 19 July 2016].

[Website Satimo.com, 2016] Website Satimo.com (2016). Product introduction about the satimo eme spy. Retrived from: http://satimo.com/search/node/EME spy [Last accessed 19 July 2016].

[Website Wikipedia.org, 2016] Website Wikipedia.org (2016). Règlements d'urbanisme de paris. Retrived from: https://fr.wikipedia.org/wiki/Raccessed 19 July 2016].

[Website Worldlibrary.org, 2015] Website Worldlibrary.org (2015). List of mobile network operators of europe. Retrived from: http://www.worldlibrary.org/Article.aspx?Title =List of mobile network operators of Europe [Last accessed 19 July 2016].

[WHO, 2011] WHO, W. H. O. (2011). International agency for research on cancer: Press release nř 208. Retrived from: http://www.iarc.fr/en/media-centre/pr/2011/pdfs/pr208_E.pdf [Last accessed 19 July 2016].

[Wiart, 1996] Wiart, J. (1996). *Propagation des ondes radioélectriques en milieu urbain dans un contexte microcellulaire. Analyse par la GTD et validation expérimentale*. PhD thesis.

[Wiart et al., 2000] Wiart, J., Dale, C., Bosisio, A. V., and Le Cornec, A. (2000). Analysis of the influence of the power control and discontinuous transmission on RF exposure with GSM mobile phones. *IEEE Transactions on electromagnetic compatibility*, 42(4):376–385.

[Wilen et al., 2004] Wilen, J., Hoernsten, R., Sandström, M., Bjerle, P., Wiklund, U., Stensson, O., Lyskov, E., and Mild, K. H. (2004). Electromagnetic field exposure and health among RF plastic sealer operators. *Bioelectromagnetics*, 25(1):5–15.

[Xiu and Karniadakis, 2002] Xiu, D. and Karniadakis, G. E. (2002). The wiener–askey polynomial chaos for stochastic differential equations. *SIAM journal on scientific computing*, 24(2):619–644.

[Xu and Gertner, 2008] Xu, C. and Gertner, G. Z. (2008). Uncertainty and sensitivity analysis for models with correlated parameters. *Reliability Engineering & System Safety*, 93(10):1563–1573.

Publication

Journal

- Huang, Y., Varsier, N., Niksic, S., Kocan, E., Pejanovic- Djurisic, M., Popovic, M., Koprivica, M., Neskovic, A., Milinkovic, J., Gati, A., Person, C., and Wiart, J. (2016). Comparison of average global exposure of population induced by a macro 3G network in different areas in France and Serbia. Bioelectromagnetics, 37(6):382–390.

International conference

- Huang, Y., Wiart, J., Person, C., and Varsier, N. (2014). Sensitivity analysis of downlink received and uplink emitted powers in a geographical area to ICT usage parameters. In Proceedings of The Annual Meeting of BEMS and EBEA, Capetown, South Africa, pages 8–13.

- Huang, Y., Krayni, A., Hadjem, A., Wiart, J., Person, C., and Varsier, N. (2015). Comparison of the average global exposure of a population induced by a macro 3G network in urban, suburban and rural areas. In Radio Science Conference (URSI AT-RASC), 2015 1st URSI Atlantic, pages 1–1. IEEE.

- Huang, Y., Person, C., Wiart, J., and Varsier, N. (2015). Caractérisation de l'exposition d'une population aux ondes électromagnétiques RF: mise en place d'une métrique simplifiée. In JNM 2015: 19èmes Journées Nationales Microondes.

- Huang, Y., Varsier, N., Altman, Z., Courtat, T., Martins, P., Decreusefond, L., Person, C., and Wiart, J. (2017). Advanced statistical methods applied to a simplifed assessment of population exposure induced by a LTE network. Accepted by 11th European Conference on Antennas and Propagation (EUCAP 2017). IEEE.

Résumé

Cette thèse propose une nouvelle méthode, via les outils de dosimétrie et de statistiques, pour l'évaluation de l'exposition globale d'une population aux champs électromagnétiques (EMFs) radiofréquences en prenant en compte les différentes technologies, usages et environnements... Nous avons analysé pour la première fois l'exposition moyenne d'une population induite par un réseau 3G, tout en considérant à la fois les émissions EMFs montantes et descendantes dans des différents pays, dans des différentes zones géographiques et pour les différents usages des mobiles. Les résultats montrent une forte hétérogénéité de l'exposition dans le temps et dans l'espace. Contrairement à la croyance populaire, l'exposition aux ondes EMFs 3G est dominée par les émissions montantes, résultant de l'usage voix et data.

En outre, l'exposition moyenne de la population diffère d'une zone géographique à une autre, ainsi que d'un pays à un autre, en raison des différentes architectures de réseau cellulaire et de la variabilité de l'usage des mobiles.

Ensuite, la variabilité et les incertitudes liées à ces facteurs ont été caractérisées. Une analyse de sensibilité basée sur la variance de l'exposition globale a été effectuée dans le but de simplifier son évaluation.

Enfin, une méthodologie simplifiée basée sur des outils statistiques avancés a été proposée pour évaluer l'exposition réelle de la population en tenant compte de la variabilité liée à l'environnement de propagation, à l'usage, ainsi qu'aux émissions EMFs provenant des mobiles et des stations de base (BTS). Les résultats ont souligné l'importance de la densité de puissance reçue depuis les BTS pour l'exposition globale induite par un réseau macro LTE.

Mots clés : Analyse des données d'usage; profils d'utilisateurs; puissance émise et reçue; exposition aux EMF; exposition humaine; modèle de substitution; analyse de sensibilité

Abstract

Wireless communication technologies, since their introduction, have evolved very quickly and people have been brought in 30 years into a much closer world. In parallel radiofrequency (RF) electromagnetic fields (EMF) are more and more used. As a consequence, people's attentions around health risks of exposure to RF EMFs have grown just as much as their usages of wireless communication technologies.

Exposure to RF EMFs can be characterized using different exposure metrics (e.g., incident field metrics, absorption metrics…). However, the existing methodologies are well suited to the maximum exposure assessment for the individual under the worst-case condition. Moreover in most cases, when dealing with exposure issues, exposures linked to RF EMF emitted from base stations (BTS) and by wireless devices (e.g, mobile phones and tablets) are generally treated separately. This thesis has been dedicated to construct and validate a new method for assessing the real day-to-day RF EMF exposure to a wireless network as a whole, exploring the people's daily life, including both downlink and uplink exposures and taking into account different technologies, usages, environments, etc.

Towards these objectives, we analyzed for the first time the average population exposure linked to third generation network (3G) induced EMFs, from both uplink and downlink radio emissions in different countries, geographical areas, and for different wireless device usages. Results, derived from device usage statistics, show a strong heterogeneity of exposure, both in time and space. We show that, contrary to popular belief, exposure to 3G EMFs is dominated by uplink radio emissions, resulting from voice and data traffic, and average population EMF exposure differs from one geographical area to another, as well as from one country to another, due to the different cellular network architectures and variability of mobile usage. Thus the variability and uncertainties linked to these influencing factors were characterized. And a variance-based sensitivity analysis of the global exposure was performed for the purpose of simplifying its evaluation.

Finally, a substitution model was built to evaluate the day-to-day global LTE induced EMFs exposure of a population taking into account the variability linked to propagation environment, usage, as well as EMFs from personal wireless devices and BTS. Results have highlighted the importance of received power density from BTS to the issue of global exposure induced by a macro LTE network. This substitution model can be further used to analyze the evolution of the wireless network in terms of EMF exposure.

Keywords: analysis of ICT usage data; user profiles; emitted and received power; EMF exposure; human exposure; surrogate model; sensitivity analysis

N° d'ordre : 2017IMTA0009

IMT Atlantique Bretagne-Pays de la Loire - www.imt-atlantique.fr

IMT Atlantique
Bretagne-Pays de la Loire
École Mines-Télécom

Campus de Brest
Technopôle Brest-Iroise
CS 83818
29238 Brest Cedex 03
T +33 (0)2 29 00 11 11
F +33 (0)2 29 00 10 00

Campus de Nantes
4, rue Alfred Kastler - La Chantrerie
CS 20722
44307 Nantes Cedex 3
T +33 (0)2 51 85 81 00
F +33 (0)2 51 85 81 99

Campus de Rennes
2, rue de la Châtaigneraie
CS 17607
35576 Cesson Sévigné Cedex
T +33 (0)2 99 12 70 00
F +33 (0)2 99 12 70 08